TUM School of Natural Sciences

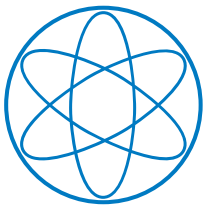

DNA origami as a molecular scaffold for directed membrane budding

Dissertation by

Michael Thomas Pinner

Technische Universität München

Technical University of Munich
TUM School of Natural Sciences

DNA origami as a molecular scaffold for directed membrane budding

Michael Thomas Pinner

Complete reprint of the dissertation approved by the TUM School of Natural Sciences of the Technical University of Munich for the awarding of the degree of

Doktor der Naturwissenschaften
(Dr. rer. nat.)

Chair: Prof. Dr. Martin Zacharias

Examiners:

1. Prof. Dr. Hendrik Dietz
2. Prof. Dr. Friedrich C. Simmel

This dissertation was submitted to the Technical University of Munich on 23 May 2025 and accepted by the TUM School of Natural Sciences on 3 July 2025.

Publication note

The research data presented and discussed in this dissertation was in parts published as a preprint on bioRxiv.org (Cold Spring Harbor Laboratory) [1]. Publication in a peer-reviewed journal is in preparation.

Michael T. Pinner and Hendrik Dietz*
Programmable DNA shell scaffolds for directional membrane budding
bioRxiv (2024)
doi: https://doi.org/10.1101/2024.01.18.576181

*Corresponding author

Abstract

Lipid membranes are ubiquitously found in nature across all three domains of life. They organise cellular life and act as a barrier to the outside world. For nutrient uptake and other transport processes across membrane-enclosed compartments, cells have developed sophisticated budding machineries which induce curvature on a lipid bilayer, culminating in the formation of a lipid vesicle separated from its parent membrane. Interestingly, components of these machineries can induce membrane curvature by imprinting their own curved structure onto an otherwise flat lipid bilayer, acting as a "molecular scaffold". This dissertation examines the principle of molecular scaffolding by establishing a synthetic budding machinery using DNA origami techniques. Three-dimensional triangles constructed using DNA as a building material were bound to giant lipid vesicles and oligomerised into polyhedral shells on the membrane, inducing curvature by imposing their polyhedral geometry upon the bilayer and culminating in the formation of small daughter vesicles with a polyhedral DNA exo- or endoskeleton. Strategic positioning of membrane-interacting moieties on the triangle determines the directionality of the budding process and thus the overall structure of the formed particles. By combining both budding directions into a 2-step experiment, complex bivesicular structures with DNA shells wedged in between two vesicles are created. Detailed characterisation of the outward-directed budding process reveals a preference of hyperosmotic conditions, compatibility with a large variety of lipids, and rapid kinetics. This work offers fundamental insights into the biophysics of membrane budding by showcasing that molecular scaffolding is not limited to the realm of proteins. In the future, this platform may be developed to direct budding of DNA nanostructures into living cells akin to viruses for the delivery of therapeutic payloads.

Contents

Chapter 1

Introduction

Lipid membranes are dynamic structures ubiquitously found in nature owing to their interesting and advantageous biophysical properties. They form fluid barriers that separate critical biological molecules into distinct enclosures whose morphology can be altered in response to changing environmental cues. An important membrane remodelling process is membrane budding in which new vesicles are formed from a pre-existing parent membrane. One natural example is the shedding of enveloped viruses from cells. Here, protein and nucleic acid components will pre-assemble into capsids within the cell, and bud off from it whilst retaining a part of the cell's membrane as an envelope. In many cases, this is achieved by hijacking the host cell's own budding machinery [2]. Cells possess a complex vesicular trafficking system that would not be possible without the ability to form lipid membrane vesicles in a tightly controlled manner.

Active membrane budding systems are interesting for both the underlying biophysical principles, and their potential applications in synthetic biology. By constructing an artificial membrane budding system inspired by natural examples, the underlying mechanisms could be studied in a controlled environment, potentially offering a deeper understanding of cellular processes and inspiring technological innovations. Scaffolded DNA origami is an ideal method for the development of such a system given the relative ease at which three dimensional nanostructures can be generated. Molecular scaffolds such as clathrin showcase the impact of protein shape on inducing membrane curvature and bud formation. Carefully designed DNA nanostructures may thus be suitable tools to gain insights into membrane dynamics and budding. This chapter explores the applicability and potential of DNA origami structures for membrane budding.

1.1 Model membranes

Budding is a key process within cells, but the sheer complexity of cells renders them unattractive for the isolated study of biophysical processes. A commonly employed alternative for the study of membranes is artificial lipid vesicles of defined composition [3]. Although exact size ranges differ between sources, vesicles are loosely categorised into small (20–100 nm), large (10–1000 nm) or giant ($\geq$ 1000 nm) vesicles according to their diameter. Vesicles are further classified according to the count of lipid bilayers composing them. Vesicles consisting of just a single bilayer are termed "unilamellar", whereas vesicles resembling onion-like stacks of bilayers are called "multilamellar". Another important factor to consider is the lipid composition of model membranes. Cell membranes are composed of a variety of mostly phospholipids intermixed with membrane-bound proteins and smaller molecules such as cholesterol and carbohydrates [4]. Chemical differences between lipid types result in altered properties and may thus influence the overall function of the membrane beyond being just a barrier. One particularly interesting aspect is the generation of spontaneous curvature by lipid geometry, as alterations in local curvature have been linked to membrane fusion and fission processes in vitro and in cells. Giant unilamellar vesicles (GUVs) are commonly used in place of cells to study membrane processes. Their large size allows for light microscopical analysis and facilitates distinction between parent and daughter vesicles following a budding event. In addition, the overall curvature of a GUV is negligible on the nanoscale and thus best resembles a near-planar bilayer. Small unilamellar vesicles (SUVs) and large unilamellar vesicles (LUVs), in contrast, better represent the size of vesicles found within cells. Furthermore, their small size facilitates analysis by electron microscopy techniques to resolve nanoscopic events. The choice of vesicle model will depend on the target application or research question.

1.2 Curvature generation and budding in nature

1.2.1 Curvature induction by lipid geometry

As reviewed by Casares et al., the various membranes of a eukaryotic cell are each composed of distinctive lipid species [5]. Even within a bilayer the composition of its two leaflets may be asymmetric as observed in the Golgi apparatus or the plasma membrane. Compositional heterogeneity between different organelles or bilayer leaflets alters the functional properties of the membrane. The lipid phosphatidylinositol 4,5-bisphosphate (PIP_2), for example, recruits a myriad of proteins involved in clathrin-mediated endocytosis (CME) including the heterotetrameric AP2 complex, which itself serves as an adapter protein for clathrin [6]. On its own PIP_2 cannot induce budding, but the mixture of lipid species in a bilayer may still alter the biophysical properties to facilitate it, as reviewed by McMahon

et al. [7]. Lipids with a near-cylindrical shape such as phosphatidylcholine (PC) will favour the formation of a planar monolayer. In contrast, lipids with a smaller polar headgroup than PC, such as phosphatidylethanolamine (PE) are more conically shaped and thus impose a negative curvature (i.e.: a monolayer by these lipids bends such that the headgroups come closer together). The opposite holds true for lipids with larger headgroups, e.g. lysophosphatidylcholine (LPC), which impose positive curvatures (i.e. the membrane bends such that the fatty acid tails come closer together). The saturation of a lipid's fatty acid tails also plays into the overall lipid geometry since double bonds cause a kink in the fatty acid's acyl chain, thereby increasing the space it occupies. Aside from geometrical considerations, asymmetric lipid quantities between the two leaflets of a bilayer may also induce spontaneous curvature to aid with budding processes [8]. An example for this is the membranes of the Golgi apparatus which use ATP-dependent aminophospholipid transporters (many of which belong to the family of P4-ATPases) to actively translocate target lipids from one leaflet of a bilayer to the other, establishing asymmetric lipid composition between the two leaflets. Deletion of these lipid translocators inhibits vesicular traffic and thereby suggests a role of lipid asymmetry for budding processes in the Golgi apparatus. The reverse has been found true for budding of extracellular vesicles in *caenorhabditis elegans* embryos [9]. Here, the transmembrane P4-ATPase TAT-5 maintains PE asymmetry by translocating PE from the exoplasmic (outer) leaflet of the plasma membrane to the cytosolic (inner) leaflet. Mutation of *tat-5* resulted in loss of cytoplasmic PE asymmetry along with increased extracellular vesicle (EV) budding. The authors of this study propose that loss of PE asymmetry induces overproduction of EVs either by changes to the density of charged lipids on the cytoplasmic leaflet leading to the formation of charged microdomains, or by induction of spontaneous curvature by PE microdomains on the exoplasmic leaflet. While these examples showcase the role individual lipid species may play in a cellular context, membrane budding does not necessarily have strict lipid requirements. In a study published by Bremser et al., COPI-coated vesicle budding was independent of lipid composition and was even possible in pure PC membranes [10]. Instead of relying on lipid species for curvature generation, COPI vesicles are formed by the interplay of several proteins. The GTPase Arf1 is of particular interest as it is an essential component of this system with the power to generate positive membrane curvature [11].

1.2.2 Clathrin-mediated endocytosis

Clathrin-mediated endocytosis (CME) is one of the best-studied budding mechanisms within cells that plays a vital role in cellular function. This process orchestrates the formation of clathrin-coated vesicles for the efficient uptake of diverse extracellular cargoes [12]. Its universal importance is highlighted by being used by all eukaryotic cells. At the heart of CME is clathrin, a protein complex made up of three identical subunits which

assume a characteristic triskelion shape [13,14]. The endocytic process can be broken down into five key stages: initiation, cargo selection, coat assembly, scission, and uncoating [12]. This section provides an overview of how these stages lead to the formation of coated buds and vesicle release, focusing on the most relevant and essential concepts to stay within the scope of this thesis.

The endocytic process is initiated by the clustering of coat proteins into what is termed the 'pioneer module' [6]. This pioneer module is primarily comprised of adaptor proteins and scaffold proteins. Adaptor proteins kickstart the process by binding to the plasma membrane and subsequently recruiting scaffold proteins. These scaffold proteins, in turn, facilitate the clustering of adaptors, thereby establishing the endocytic site. Many of these proteins can bind to the cytosolic domain of transmembrane cargo to guide it to the endocytic site. Among these cargo adaptor proteins, integral to the pioneer module, is AP2. Upon binding cargo and the lipid PIP_2, AP2 undergoes a conformational change, revealing its clathrin-binding site. PIP_2 is a plasma-membrane specific lipid and thus the pioneer module is thought to assemble only at the plasma membrane [12]. However, clathrin-coated vesicles can also originate from other membranous compartments.

Clathrin is recruited to the cell membrane from the cytosol by AP2 and accessory adaptor proteins [12]. Individual clathrin triskelia then self-assemble into a well-defined spherical cage-like structure, forcing the cell membrane underneath to bend by imposing its own curved shape onto the membrane in a process called scaffolding [6, 15]. However, controversy arose over the mechanism by which it acts. Some of the adaptor proteins with clathrin binding sites have been shown to induce curvature by themselves, and further complicating the matter is the observation that clathrin binds to the flexible regions of most adaptor proteins which would make transmission of the potential force generated by polymerisation inefficient [6, 12]. The variety of actors participating in CME raises the question whether clathrin is indeed actively involved in membrane bending. In favour of its role as membrane bender is a study by Dannhauser and Ungewickell who demonstrated budding in vitro using a minimal system that reduces the process to just clathrin bound to liposomes via a fragment of the adaptor protein epsin [16]. The authors found that the self-assembly of clathrin was sufficient to trigger bud formation in vitro. A similar study confirmed these results in cells, concluding that clathrin's role in CME is that of a membrane bender as opposed to only stabilising the curvature induced by other components [17]. Here, CME was inhibited by knocking down clathrin, but CME could be restored when cells were cultivated on engineered surfaces with nanoscopic ridges inducing curvature in the cell membrane. These results show that molecular scaffolds like clathrin can indeed shape membrane buds, but in a cellular context it is not the only contributor. Another known bender is actin filaments, which are associated with the later stages of CME when considerable membrane bending is present [6]. Inhibition of actin polymerisation can block

late stage membrane shaping in mammalian cells, but this inhibition is cell type dependent, suggesting that actin filaments play more of an accessory role [18].

In the final step of CME, the bud neck is severed to separate the vesicle from the cell membrane. This process is catalysed by the large GTPase dynamin and is facilitated by the enzyme forming tight, helical oligomers with an internal radius of 10 nm [6]. The neck is then constricted further by GTP hydrolysis until the neck is cut spontaneously through thermal fluctuations of the membrane. Dynamin is recruited to the bud neck by BAR-domain proteins, which can act as curvature sensors as well as scaffold proteins inducing curvature. As the curvature of the bud neck increases, BAR proteins with increasing curvatures are recruited to it. However, some BAR proteins posses an N-terminal amphipathic helix which was shown to be enough by itself to constrict and break membrane necks. Similarly, BAR domains may aid in constriction by acting as scaffolds, imposing their own curvature upon the neck.

1.2.3 The ESCRT pathway

Another noteworthy example is budding via the 'endosomal sorting complex required for transport' (ESCRT) pathway [19]. The ESCRT machinery is involved in the formation of intraluminal vesicles within endosomes (multivesicular bodies), cytokinesis, and also the release of budding viruses, among other functions [2, 20]. A distinctive difference between CME and the ESCRT machinery is the directionality of budding events. Whereas the components involved in CME generally shape buds from the outside, the proteins of the ESCRT machinery act from within the bud. As a result, buds formed by the CME machinery grow towards the cytosol, but buds formed by ESCRT proteins grow away from it.

Central to the ESCRT pathway is a number of ESCRT protein complexes [21]. They were named after their first identified function as ubiquitin-dependent protein sorters and several known ESCRT complexes contain ubiquitin-binding domains. However, ESCRT complexes are known to have more than one role. ESCRT-III, for example, does not have a ubiquitin-binding domain at all, but it is involved in viral budding. Budding processes mediated by ESCRT are distinct by bending the membrane away from the cytoplasm. Notably, ESCRT complexes have not been found inside the vesicles they produce, indicating that the budding mechanism does not involve polymerisation of ESCRT complexes into cages similar to clathrin [22]. ESCRT-III subunits are instead known to self-assemble into many shapes, including spirals, tubes, coils and cones [20]. In a study examining the ESCRT-III subunit Snf7, its polymerisation into spirals was found to deform lipid vesicles [23]. An amphipathic helix at its N-terminus serves as a curvature-sensitive lipid membrane anchor which by itself does not seem to induce curvature [24]. Membrane deforming properties have also been discovered for the ESCRT-III subunit CHMP2B, underlining the

central role ESCRT-III plays in the budding process [25].

ESCRT proteins are also active in the scission of membrane buds, even if the bud itself formed without ESCRT contribution, e.g. in viral budding [20]. Experimentally, ESCRT-III alone could sever membrane buds from giant unilamellar vesicles upon polymerisation.

1.3 Concept for a synthetic membrane budding system

The energetic penalty for spontaneous bud formation on a lipid bilayer (approx. 250–500 k_BT) is too large to occur spontaneously, and thus active membrane processes are required [26]. Cells reduce this penalty with sophisticated systems such as scaffold proteins (e.g. clathrin, COPII, BAR-domain proteins etc.) or cytoskeletal components to allow for budding to occur. CME, for example, involves many proteins with membrane-bending properties whose interplay finally causes budding [27, 28]. This data raises the question of whether the self-assembly of any membrane-bound object into inherently curved structures can serve as a molecular scaffold, inducing curvature that ultimately leads to budding. A suitable technique to produce such an object is scaffolded DNA origami.

1.3.1 DNA as a construction material

DNA is a biopolymer with a double helical structure typically composed of two complementary strands [29]. The backbone of these strands consists of deoxyriboses linked together by phosphodiester bonds, and extending from the deoxyriboses is one of four purine (adenine (A) & guanine (G)) or pyrimidine (thymine (T) & cytosine (C)) bases. A DNA double helix is held together by hydrogen bonds formed between a purine base on one strand, and a complementary pyrimidine base on the opposing strand. These pairs are specific: A pairs only with T, and G pairs only with C.

As the carrier of genetic information, DNA and its biological function have been heavily studied. An important discovery in understanding genetic recombination events was made by Robin Holliday who proposed that the strands of homologous chromatids can form cross-overs [30]. As a result, the two chromatids are temporarily connected by a junction known as the Holliday junction. This concept was developed further by Ned Seeman who founded the field of DNA nanotechnology with the idea of rationally designing arrays of Holliday junctions to construct three-dimensional lattices using DNA as a building material [31]. However, this concept was deemed sensitive to stoichiometry and complex structures assembled only at low yields. As an evolution to the original idea by Ned Seeman, in 2006 Paul Rothemund described the folding of long, single stranded DNA in a method he termed 'scaffolded DNA origami' [32].

1.3.2 Fundamentals of DNA origami

Scaffolded DNA origami offers a distinctive approach to spontaneously construct three-dimensional nanostructures using DNA as a construction material [32–34]. A single-stranded 'scaffold' DNA strand several kilobases in length is mixed with an array of shorter 'staple' oligonucleotides. By choosing the sequence of each staple to be complementary to multiple sections of the scaffold strand but located in different regions, the staples can 'fold' the scaffold into different shapes by forming Holliday junctions using Watson-Crick base pairing interactions. The same scaffold strand may be folded into many different structures depending on the staple mixture used. The self-assembly process is guided by a thermal annealing ramp. In the first step, unstructured coils formed by scaffold strands and staples are denatured at high temperatures. Then, the mixture is gradually cooled to promote correct folding of the structure. As the stability of a DNA duplex depends on its length (among other factors), staples whose sequence only partially matches any given scaffold segment are more easily displaced by staples with perfect sequence complementarity. This is helped by elevated temperatures which denature weak duplexes and thereby select for only the strongest scaffold-staple pairs. Folding of a DNA origami is a complex process with signs of cooperativity [35]. The routing of each staple through the final structure must be chosen carefully as otherwise structures may not fold as desired or form aggregates. For the same reason, cations need to be added to a folding reaction in sufficient quantities to overcome electrostatic repulsion between individual DNA helices. Typically Mg^{2+} is used for this purpose, but even monovalent cations like Na^{+} will aid with origami folding if used at sufficiently high concentrations [36].

The original structures presented by Rothemund were limited to two dimensions. However, the method was soon after expanded to the third dimension by arranging individual helices along a honeycomb lattice [34]. This concept is based on the geometrical parameters of B-form double helices where two turns of the helix correspond to approx. 21 base pairs (bp). As a result, each helix can connect to a total of three neighbouring helices every 7 bp (or after two thirds of a turn).

A tighter packing of helices can be achieved when helices are arranged along a square lattice [37]. Here, each helix can form crossovers with up to four neighbouring helices every 8 bp, assuming a twist of 33.75°/bp or 10.67 bp/turn (3 full turns per 32 bp). This twist is smaller than the preferred 34.3°/bp in B-DNA, resulting in a slight underwinding of the helix that is relaxed by a compensatory global right-handed twist of the structure). To reduce this twist, individual bases can be skipped in the design (i.e. periodically allowing crossovers every 7 bp to establish an average closer to the preferred 10.5 bp/turn). Of note, even though honeycomb structures are designed to match the geometrical parameters of B-DNA more closely, slight twist may also be observed in them [38].

As was shown in the original publication, three-dimensional DNA origami allows for the construction of a large variety of shapes [34]. Design possibilities were furthermore enriched by adding or removing bp in the 7 bp segments of honeycomb structures, resulting in curved structures [39]. This approach uses under- and overwinding of the helix as a design feature to specifically add twist and curvature to the structure. Despite these advances in enriching the shape diversity of origami structures, their size is always restricted by the length of the scaffold strand. This issue can be addressed by linking multiple structures together by shape-complementary protrusions and recesses [40]. Here, individual structures can form higher-order assemblies by making use of base-stacking interactions. Base-stacking interactions are attractive forces acting between the aromatic rings of neighbouring nucleobases that have been identified to be the biggest contributor to the stability of a DNA duplex [41,42]. They don't only act between the nucleobases of the same strand, but also act across a nick in a DNA duplex. A consequence of these attractive forces in origami design is that blunt ended helices need to be passivated, e.g. by single-stranded overhangs, as structures may otherwise aggregate. For controlled self-assembly of origami structures, however, blunt-ended helices are introduced as a design feature to guide the controlled assembly of origami structures [40]. Shape-complementary in this context means adding a bundle of protruding, blunt-ended helices to the structure whose overall shape matches the shape of a recess lined with blunt ended helices of the same or a different structure. As this typically requires two DNA nanostructures to come into close proximity for base-stacking connections between blunt-ended protrusions and recesses to form, attractive base-stacking interactions compete against electrostatic repulsion of the negatively charged DNA origami. The concentration of cations, typically in the form of Mg^{2+}, may act as a switch such that assembly will only occur above a threshold concentration. The threshold concentration can be influenced by the number of helices involved in a stacking contact, where more helices equal a more stable connection and thus a lower cation concentration threshold to stabilise a dimer against disassembly through electrostatic repulsion. Physically, this behaviour is explained by the repulsive term of the DLVO-theory [43]. As a negatively charged particle, DNA origami attract cations, forming a "double layer" around the particle. The ion concentration around the origami is thus higher in respect to the bulk of the solution, which screens the negative charges of the origami in dependence of the salt concentration. When two charged particles approach each other at low salt concentrations, their overlapping double layers exert a repulsive force which guarantees colloidal stability. The extent of the repulsive force is influenced by the charge density of the particle, and its length scale is given by the Debye screening length λ_D:

$$\lambda_D = \sqrt{\frac{1}{8\pi\lambda_B n_S}} \tag{1.1}$$

where λ_B is the Bjerrum length and n_S is the salt number density. For aqueous solutions at room temperature, this equation can be simplified to

$$\lambda_D = \frac{f}{\sqrt{c_S}} \tag{1.2}$$

where f is a salt-dependent factor, c_S is the salt concentration in M and λ_D is in nm [44]. For 1:1 salts like NaCl, the factor is 0.304, while for 2:1 salts like $MgCl_2$, it is 0.176. The double-layer interaction energy between spherical particles can be approximated as

$$W_{DL}(d) = \frac{2\pi R\sigma^2}{\kappa\epsilon\epsilon_0} e^{-\kappa d} \tag{1.3}$$

where R is the radius of the spherical particle, σ is the charge density of the particle, κ is the inverse of the Debye length, ϵ and ϵ_0 are the relative permittivity of the medium and the permittivity of vacuum, respectively, and d is the distance [44, 45]. This approximation is well suited for particles with low surface potentials, but as DNA origami solutions typically contain divalent cations, this condition can be assumed to be fulfilled due to ion binding, particularly at elevated $MgCl_2$ concentrations [44]. Despite inaccuracies related to particle shape and surface potential, this equation illustrates how the energy is influenced by the surface charge of the particle, and how it decays with the Debye length. Increasing the ionic strength of the medium lowers the thickness of the repulsive double layer (individual particles can come closer to one another) and reduces the strength of repulsive forces such that attractive interactions, e.g., van der Waals-forces or base-stacking interactions, become increasingly longer-lived and more stable. Because of the high charge density of DNA, a sufficiently high concentration of counter ions is necessary to screen the charges and lower repulsive forces for DNA origami dimerisation by base-stacking interactions to occur. This is reflected also by the much higher concentrations of monovalent cations needed for base-stacking interactions to form as opposed to bivalent cations [40].

Finally, temperature is another factor governing assembly, where low temperatures stabilise stacking connections, and higher temperatures disrupt them. The influence of temperature is more complex as higher temperatures also result in faster diffusion which increases collision events between two nanostructures in a given time frame. Because of this, assembly of separate DNA origami structures is often performed at elevated temperatures and thus assembly of many subunits into large higher-order structures has been achieved [40, 46, 47].

1.3.3 DNA nanotechnology applied on lipid membranes

In recent years, DNA nanotechnology has witnessed a remarkable convergence with membrane biophysics, particularly in the realm of lipid membrane engineering. Prior work

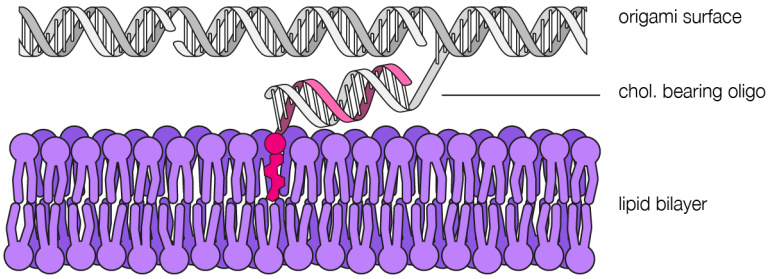

Fig. 1.1: ***Anchoring of DNA nanostructures to lipid bilayers.*** *By hybridising DNA oligos coupled to a hydrophobic moiety such as cholesterol to a DNA origami structure, the origami can be tethered to the lipid bilayer. Illustration by Volodymyr Mykhailiuk.*

showcases the versatility of DNA nanostructures for use in synthetic biology applications and its value as a tool to learn more about membrane remodelling processes. Due to the programmability of DNA origami structures, they can easily be bound to lipid membranes to orchestrate diverse functionalities at the membrane interface. Furthermore, DNA oligonucleotides ("oligos") are available at low cost and with a growing number of modifications that facilitate membrane research with DNA origami and make the technology very accessible. Due to the hydrophobic core of a lipid bilayer, DNA origami is most commonly tethered to the bilayer using hydrophobic moieties chemically coupled to a DNA oligo extending from the origami surface (fig. 1.1). The most commonly employed membrane anchor is probably cholesterol, with other examples including tocopherol, poly(propylene oxide) (PPO), or porphyrin [48]. Non-specific attachment of origami structures to lipid membranes can be achieved by electrostatic interactions such as inclusion of positively charged lipids in the membrane, or also zwitterionic lipids in the presence of Mg^{2+} or Ca^{2+}. Of particular interest is the observation that cholesteryl-modified DNA origami tethered to lipid membranes retains diffusive mobility, the degree of which is dependent on factors such as linker oligo length, linker count, or the size of the structure [49, 50]. This is similar to membrane proteins inserted into biological membranes which are also known to retain lateral diffusivity [51]. As a consequence, DNA nanostructures could self-assemble on the membrane into multimeric lattices resembling clathrin networks in cells [50, 52]. Kocabey et al. observed deformation of SUVs in response to 2D lattice formation and suggested that 'it will be possible to build DNA objects that mimic biological building blocks such as clathrin or caveolin that play a crucial role in endocytotic processes' [50]. Similar observations have been made by other groups who observed tubulation of GUVs using both curved [53–55] and planar [54] DNA origami. For the curved structures, this was not completely unexpected as the structures were designed to act as scaffolds for vesicle deformation. However, the tubulation in response to a planar ring structure lacking ordered organisation on the membrane suggests that tubulation may be driven by introducing a large number of membrane anchors into the bilayer and a high density of DNA origami on

the membrane [54]. The aforementioned examples use origami structures anchored to the membrane via linker moieties. As a result, the origami is not inserted into the membrane itself but instead hovers above it. However, membrane spanning DNA structures have also been realised. Several groups have reported the creation of membrane pores of various sizes mimicking their protein counterparts in biological membranes [56–66]. Two main design approaches have been pursued: The first reported nanopore design later replicated by other groups encompasses a vertically protruding segment with a hollow core serving as the body of the pore [61, 62, 64]. It is anchored to the membrane by hydrophobic moieties extending from a second segment perpendicular to the pore in the shape of a stand or platform on the membrane. In the second design approach, the membrane spanning element of the pore body itself is decorated with hydrophobic moieties for membrane penetration [56–60, 65, 66]. Both approaches appear to be equally effective, with one study successfully combining both a hydrophobic platform and a hydrophobic belt around the pore body [63]. Nanopore function has been demonstrated in various experiments, including DNA and protein translocation and sensing experiments [59, 61, 62, 64, 65], small molecular dye in- and efflux across vesicle membranes [56, 61, 63] and transmembrane conduction studies reminiscent of ion channels [56–58, 60]. Interestingly, a simple nanopore consisting of four helices reportedly enhances lipid mixing between both leaflets of the bilayer, thereby functionally mimicking the cellular enzyme scramblase [66].

The work discussed thus far aimed to manipulate existing membranes, but DNA origami has also been used as a scaffold to guide the self-assembly of new membranes. This was achieved using a spherical wireframe DNA nanostructure decorated with DNA handles chemically conjugated to a lipid molecule [67]. By adding a mixture of lipids and surfactant followed by a dialysis step to slowly and selectively remove the surfactant from the sample, a lipid bilayer self-assembled around the DNA origami guided by the lipid-functionalised handles. The resulting DNA-lipid hybrid structure harnessed the advantages of both materials, with the lipid coat providing protection against DNase I digestion, preventing activation of innate immune functions, and increasing the half-life in mouse models. Using a similar strategy, cuboid and dumbbell-shaped DNA origami were coated with vesicles composed of amphiphilic polymers and surfactants [68]. While these studies have shown that vesicles could be grown around a DNA nanostructure, the reverse is also true where vesicles are grown within it. Here, instead of using a spherical DNA origami, a ring was employed whose inner face was decorated with hydrophobic moieties. Addition of a lipid-surfactant mixture follow by dialysis now resulted in a vesicle grown within the ring [69]. The diameter of the ring determined the size of the resulting vesicles, and lead to an overall narrower size distribution than vesicles prepared in the same way but without the rings. The same structure could also be used to capture preformed SUVs using complementary ssDNA handles on both components. By including a cellular vesicle snap

receptor protein (v-SNARE) onto the DNA origami structure, the captured vesicle could be fused with a supported lipid bilayer containing target SNARE (t-SNARE) proteins. The DNA origami along with ssDNA handles on the target membrane and the origami served to facilitate the fusion process triggered by the cellular SNARE proteins.

This section illustrated how DNA origami could be used to mimic selected cellular processes. Membrane-assisted lattice formation, vesicle deformation and tubulation, the formation of functional nanopores, and the templated growth and fusion of SUVs are all examples that are in one way or another inspired by natural membrane processes. An important biological process that has thus far not been replicated using engineered DNA nanostructures is membrane budding.

1.4 Electron microscopy

Electron microscopy is an advanced imaging technique which resolves sample materials using electrons instead of light. The resolution limit of light is given by the Rayleigh criterion as

$$\delta = \frac{0.61\lambda}{\mu \sin \beta} \tag{1.4}$$

where λ is the wavelength of light, μ is the refractive index of the medium and β is the semi-angle of collection of the magnifying lens [70]. A commonly employed approximation of the resolution limit is half of the wavelength of the incident light. For visible light, this limits the smallest resolution to approximately 200 nm, which is well above the typical size of a DNA nanostructure. In fact, the DNA origami triangles that were used in the present study have an approximate size of 50 nm, emphasising the need for an alternative imaging technique. Louis de Broglie laid the foundation for the use of electrons for imaging purposes in his doctoral thesis, in which he postulated that all matter can be assigned a wavelength [71]. Applying this principle, the wavelength of electrons can be approximated as

$$\lambda = \frac{1.22}{\sqrt{E}} \tag{1.5}$$

where E is the electron's energy in eV [70] and λ is its wavelength in nm. By accelerating electrons with a 120 kV electron microscope (thereby increasing its energy), the theoretical resolution limit drops into the picometre range and thus well below the size of DNA origami structures (or DNA itself). It also becomes evident that the resolution limit can be adjusted by altering the energy of the electron using higher accelerations.

Among the subtypes of electron microscopes available, the type most relevant for the present work is the transmission electron microscope (TEM). In this type of microscope, electrons are accelerated through the sample specimen towards a fluorescent screen or camera, creating a measurable signal [70]. As the electrons pass through the specimen, some of

them are scattered, which alters the number of electrons detected per unit area, forming a visual representation of the illuminated sample. An important concept to remember is that the resulting image is a 2D-projection of the sample, where three-dimensional spheres or cylinders will appear as circles. The fewer electrons are detected per unit area, the darker the respective area in the image becomes. Scattering events are necessary to generate a contrast-rich image, and increasing the extent of it is used to enhance image contrast. The probability of scattering and the scattering angle both depend on the atomic number, and thicker samples likewise increase the chance of scattering events. Because of this, TEM samples are prepared by incubating the sample solution on a thin grid that is optionally coated with a thin film to support sample particles. The "holes" of the grid can be imaged, while the copper grid itself is impenetrable for the electron beam. Electron microscopy is a very complex technique, and a detailed description of its fundamental physics is outside the scope of this thesis. Nevertheless, for a better understanding of the applied methods in this thesis, the following section provides a brief overview from a practical point of view with a focus on aspects particularly relevant for this work.

1.4.1 Negative staining transmission electron microscopy

Elastic scattering of electrons is a major source of contrast in TEM images [70]. Here, electrons are scattered either by interacting with the electron cloud of an atom (low-angle scattering), or with its nucleus (high-angle scattering). According to the Rutherford cross section, the nuclear scattering cross section (and thus the scattering probability) scales with the square of the atomic number squared. In other words, the probability of high-angle scattering is much larger for heavy elements at the bottom of the periodic table than for lighter ones at the top. This has an important consequence for studying DNA-lipid hybrid particles in the present work. As biological molecules are mostly composed of atoms with low atomic numbers, they generally do not generate a lot of contrast in TEM micrographs. While increasing the thickness of the sample can help with improving the contrast, this is often not feasible. Instead, biological samples are commonly stained with heavy metal salts to provide amplitude contrast. The high atomic number of heavy metals increases the number of high-angle scattering events and facilitates the removal of electrons scattered in this way by an aperture. In principle any heavy metal could be used, but among the most commonly used ones are uranyl salts, including uranyl formate (the staining reagent used in this thesis). With an atomic number of 92, Uranium is one of the heaviest naturally occurring elements and thus exceptionally well suited as a contrasting agent. Heavy metal stains tend to accumulate in certain regions of a particle which then appear darker in a micrograph. In the case of DNA origami, uranyl formate accumulates around the structure and in-between the individual helices (Fig. 1.2). In the resulting micrographs, the contrast stems mainly from the heavy metal stain surrounding sample particles, but not from the

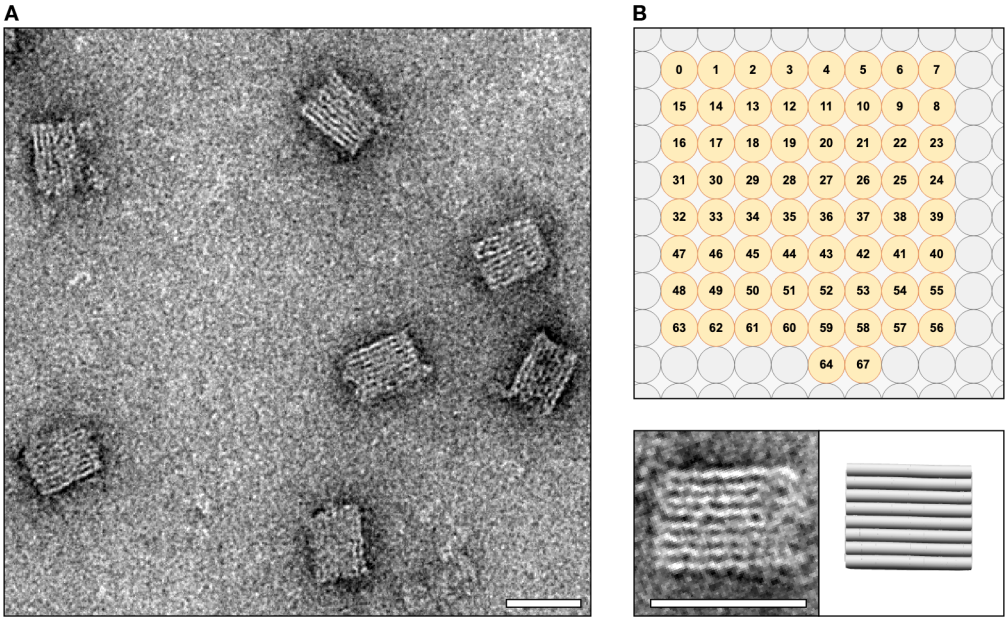

Fig. 1.2: ***Negatively-stained DNA origami cubes.*** ***(A)*** *TEM micrograph of cube-shaped DNA origami structures negatively stained using uranyl formate. Because micrographs are 2D projections of the sample specimen, the origami structures appear as flat sheets despite being cuboid-shaped.* ***(B)*** *Top: Cross-section of the origami structure as designed using caDNAno, showing its three-dimensional 8x8 helix structure [72]. Bottom left: Close-up of a single origami cube showing the accumulation of stain (dark) around the structure and in between the DNA helices. As stain accumulates not on the helices but in-between them, the DNA helices themselves appear as white stripes. The number of helices visible (eight) matches the number of helices on each side as designed. Bottom right: Structure prediction by CanDo based on the original caDNAno design file [73, 74]. The computational model matches the appearance of the structure under the TEM. Scale bars: 25 nm*

sample particles themselves. This type of staining, where objects appear brighter than the empty space around them, is called negative staining. To distinguish TEM of negatively stained samples from that of vitrified samples (discussed in the following section), it will be referred to as negative staining TEM (or ns-TEM) throughout this thesis. Negative staining has the advantage of being a relatively simple and quick method to obtain contrast rich micrographs from biological samples [75]. However, staining and subsequent drying are known to alter the structure of lipid vesicles. Moreover, insertion of the sample grid into the high vacuum inside a TEM column further dehydrates and damages vesicle samples. In the context of this thesis, negatively stained samples can be used to study the overall structure of DNA-shell coated vesicles (DCVs, the products of outward-budding reactions), but ns-TEM is unsuitable for detailed structural analyses of vesicles.

1.4.2 Cryogenic electron microscopy

Cryogenic electron microscopy (cryoEM) is a powerful technique to analyse samples in their native environment, resulting in fewer artifacts than by conventional ns-TEM. Herein, the sample solution is applied onto a TEM grid, and, after blotting off the bulk of the solution (leaving only a thin film of sample solution on the grid), plunge frozen using liquid ethane [76]. This results in rapid freezing of the remaining sample solution without the formation of ordered water crystals (vitrification [77]). An important difference between ns-TEM and cryoEM is that damage by staining and/or dehydration is avoided in the latter, making the method a lot more suitable for imaging delicate biological samples such as vesicles. The lack of heavy metal stain results in a stark reduction of amplitude contrast in comparison to ns-TEM so that cryoEM relies mostly on phase contrast [78]. This type of contrast is improved by imaging the specimen out-of-focus, but it comes at the cost of reduced resolution. Another drawback of vitrified samples is their high susceptibility to radiation damage, due to which imaging is usually conducted under low-dose conditions.

As particles for analysis by cryoEM are embedded in a film of vitreous ice, the overall thickness of the sample must be considered. Using higher acceleration voltages reduces the probability of elastic scattering events (which generate amplitude contrast) and thus allows for penetration of thicker samples at the cost of more radiation damage [70]. Areas on the TEM grid with very thick ice reduce the image quality or may even be impenetrable to the electron beam [78]. Because of this, the size of particles that can be studied by cryoEM is limited, with the giant mimivirus being among the largest reported objects measured by cryoEM with a diameter of 750 nm [79]. This limitation influenced the vesicle sizes used for budding assays of samples to be analysed by cryoEM.

Chapter 2

Membrane-interacting DNA nanostructures

Nature has developed sophisticated molecular machineries to facilitate membrane remodelling processes. These machineries typically involve the coordinated action of various proteins that can induce and stabilise membrane curvature, as well as catalyse the final scission event. Budding processes require energy input and do not occur spontaneously without external triggers. The biological budding systems discussed in the introductory chapter provide insights into biological membrane remodelling processes. In this chapter, I will describe the design and analysis of a synthetic budding machinery inspired by natural examples. A primary objective behind this work is to enrich our current understanding of the matter by putting basic principles and hypotheses to the test. It also offers opportunities to explore and pinpoint critical design principles for iterative improvement of the system which may also aid in the development of related membrane-active technologies.

2.1 DNA origami as a molecular scaffold

Clathrin-mediated endocytosis (CME) is a well-studied budding machinery that exemplifies the concept of molecular scaffolding. By self-assembling into cage-like structures, clathrin imposes its shape upon the cell membrane to generate and stabilise membrane curvature [6,15]. While this process is helped by many other proteins, clathrin has been identified as a key component in a minimal CME-based budding system [16]. Molecular scaffolding is thus an attractive concept that I considered worth exploring in my endeavour of creating a synthetic budding system. Candidate molecular scaffolds can easily be designed and folded using the DNA origami technique [32]. As DNA is chemically distinct from proteins like clathrin, this approach puts further emphasis on particle shape as the main driver of membrane deformation.

In a DNA origami-based membrane budding system, the origami components must generate sufficiently strong molecular forces to remodel a flat membrane and stabilise the induced curvature. Opposing bud formation by molecular scaffolds such as clathrin is membrane tension, which if too high could inhibit deformation of the membrane as simulations have shown [80]. At intermediate, physiologically relevant tensions, U-shaped (open) buds undergo a 'snap-through instability' into omega-shaped (closed) buds upon expansion of the bud-shaping coat. However, this transition becomes smoother with higher bending rigidity of the structural coat. Thus, shaping and closure of a bud is directly dependent on the polymerisation of the structural coat.

The principle of a bud-shaping membrane coat is not unique to CME. Vesicle trafficking between the endoplasmic reticulum and the Golgi apparatus are mainly governed by two other machineries relying on cytoplasmic coat proteins, namely coat protein complexes 1 and 2 (COPI & COPII) [81, 82]. Clathrin, COPI and COPII share structural design features and the ability to self-assemble into ordered protein cages [15,82–84]. Because of this, the DNA origami-based scaffold should likewise be designed as monomers with the ability to self-assemble into closed cages. The energy necessary to induce membrane curvature is derived from the polymerisation process [85]. The subunit itself does not need to be curved if polymerisation of subunits by design occurs at an angle. This approach has the advantages of avoiding steric hindrance where the cavity of a too highly curved structure cannot interact with the membrane [53], simplifying the design of polymerisable subunits, and the opportunity to include a trigger for polymerisation to improve control over the system. A DNA origami satisfying these conditions is three-dimensional triangles as published by Sigl et al. (Fig 2.1) [47]. The triangles feature bevelled sides with shape-complementary protrusions and recesses for assembly via base-stacking interactions (stacking contacts) [40]. By adjusting the bevel angle on a triangle's side, the dihedral angle between two triangles in an assembly is likewise changed. In their publication, Sigl et al. demonstrate that by carefully adjusting the bevel angle, triangles can be made to assemble into octahedra and icosahedra. For this, the bevel angle α is calculated by subtracting the dihedral angle ϕ from an angle of 180°and halving the result.

$$\alpha = \frac{180 - \phi}{2} \tag{2.1}$$

Of the five shells described by Sigl et al., I decided to proceed with the smallest icosahedral shell-forming triangle with three identical sides. Although octahedra require fewer triangles to form a complete shell and have been shown to assemble faster than icosahedra [47], the dihedral angle of an octahedron (109.47°) is steeper than that of an icosahedron (138.19°) which may in turn slow down or even prevent assembly of membrane-bound triangles due to steric hindrance. Another advantage of icosahedra is their larger inner cavity which

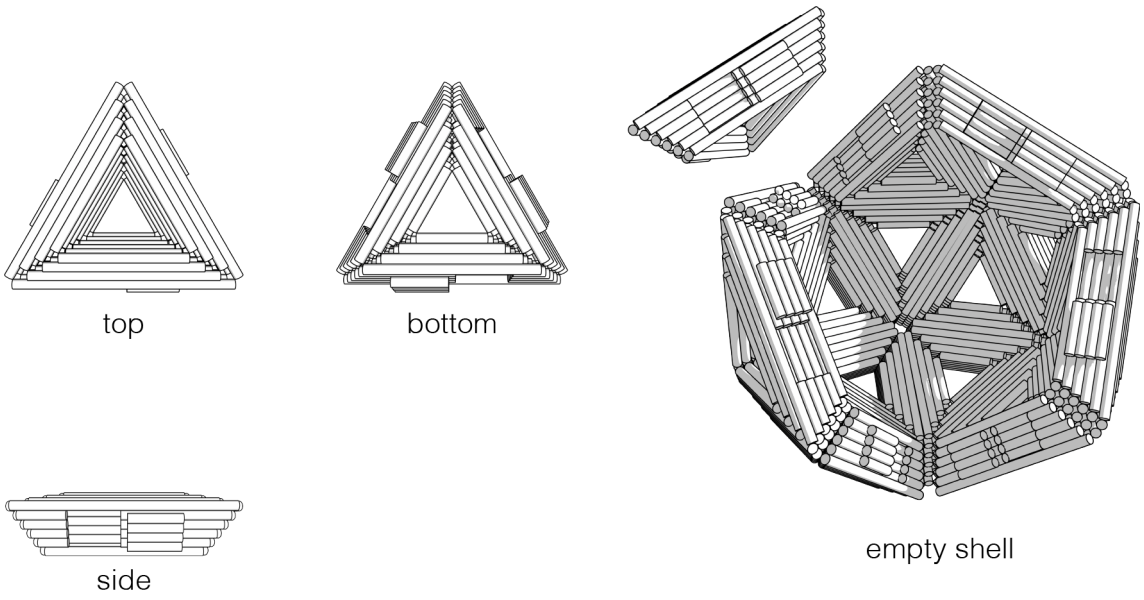

Fig. 2.1: ***DNA origami triangles.*** *Illustration of DNA origami triangles as published by Sigl et al. The three-dimensional structure with bevelled edges and shape-complementary protrusions and recesses enables self-assembly of triangles into hollow shells. Pictured is an incomplete icosahedral shell with another triangle about to join the assembly.*

is particularly interesting for potential applications of this budding system. The sizes of octahedra (90 nm) and icosahedra (110 nm) as reported by Sigl et al. are both within the size range of clathrin-coated vesicles, which are typically reported to be in the range of 50–150 nm [86,87]. Finally, assembly by shape-complementary base-stacking contacts requires a sufficiently high concentration of cations to overcome electrostatic repulsion otherwise exhibited by two DNA origami objects in close proximity. Assembly and thus budding may therefore be triggered and controlled by adjusting the Mg^{2+} concentration.

The DNA triangles were chosen for sharing certain properties with natural coat proteins. As discussed in the introduction chapter, biological budding machineries consist of dozens of components with various functions. Importantly, biological budding machineries typically involve active constriction and scission of the bud neck. In CME, this role is carried out by the GTPase dynamin [6], but membrane insertions have been reported to be able to destabilise and sever the bud neck independent of dynamin [88,89]. The forces generated by origami assembly along with membrane anchors inserted into the membrane to tether the origami to it may therefore suffice to destabilise and sever the bud neck.

2.2 Cholesterol as a membrane anchor

Just how clathrin does not bind lipid membrane by itself but requires the help of adaptor proteins, a hydrophobic membrane anchor is commonly employed to tether the origami

to the lipid membrane. Alternatively, the strong interaction between DNA and positively charged lipid could be used to bind origami to the bilayer [48], but a disadvantage of this approach is the loss of control over the orientation in which the origami binds to the membrane. This is particularly problematic in the context of membrane budding as the triangles studied here need to be aligned for assembly. As a consequence of the structure's non-zero thickness and due to its bevelled sides, the two triangular faces of the structure differ in size, with the shell-inner face being smaller than the shell-outer face. For assembly to occur around the membrane bud (in similarity to clathrin), the smaller, shell-inner face needs to interact with the membrane. The opposite is true for budding towards the membrane analogous to buds formed by the ESCRT machinery. Here, the shell-outer face needs to interact with the membrane for it to wrap around the growing shell. Unless stated otherwise, the main focus of the work described here is on buds growing away from the bilayer with an origami exoskeleton.

The most commonly used hydrophobic membrane anchor to connect DNA origami to lipid membranes probably is cholesterol. It not only occurs naturally in biological membranes, but is also sold commercially as a terminal oligonucleotide ('oligo') modification. As it has been used in many studies in the past, its properties as a membrane anchor for DNA nanostructures are well studied and characterised. I therefore decided to integrate oligos chemically linked to cholesterol moieties into the origami triangles for membrane anchoring. However, as hydrophobic moieties may cause DNA origami structures to aggregate [90], cholesterol-modified oligos (chol-oligos) should not be included in origami folding reactions. A simple compromise is adjusting the design of the structure to include staples with unpaired bases extending away from the origami surface. Chol-oligos complementary to these linker handles can then be added at a later stage to reduce the time origami structures are incubated with chol-oligos without a lipid membrane. Among the parameters to consider in linker handle design is the number and positioning thereof on the structure. The sequence of the chol-oligo should allow for stable dimer formation, and the orientation of the cholesterol after hybridisation must be considered. In proximal configurations, the cholesterol is oriented towards the surface of the origami. In a distal configuration, the reverse is true and the cholesterol is facing away from the origami surface. Finally, the ratio of chol-oligo in respect to the available linker handles may also influence the results.

2.2.1 Excess chol-oligo reduces aggregation

In an initial experiment, 9 linker handles were distributed over the bottom (shell-inner) face of a triangle (Fig. 2.2A). The positioning of the linker handles was kept equal across the three sides of the triangle such that each side featured three linker handles. These triangles were then mixed with chol-oligo at different ratios in respect to the available linker handles. In this scenario, a 1:1 ratio means that all of the added chol-oligos can

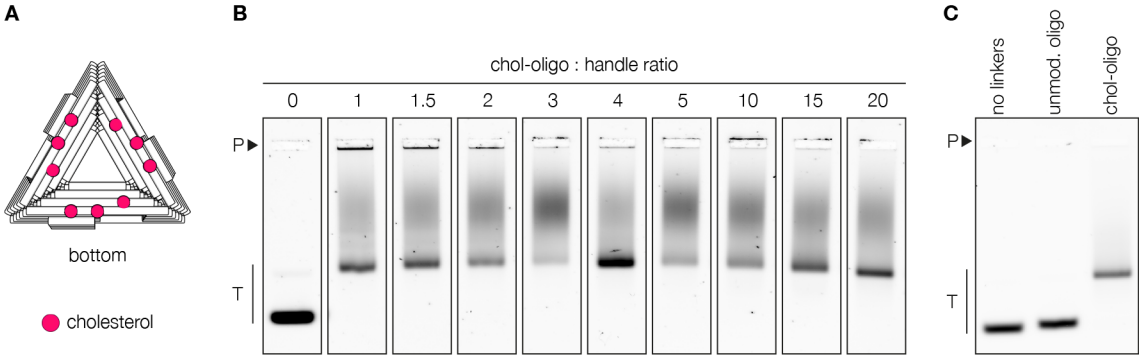

Fig. 2.2: ***Cholesterol alters the gel migration behaviour of triangles.*** ***(A)*** *Scheme of the bottom face of a triangle hybridised to 9 chol-oligos.* ***(B)*** *Agarose gel of triangles hybridised to various chol-oligo : linker handle ratios. Cholesterol causes triangle aggregation, smearing and a migratory shift. If added at large excess, aggregation can be prevented while smearing and band shifts remain. (P - pocket; T - triangles)* ***(C)*** *Band shifts are only observed when the linker handles on triangles are hybridised to cholesterol-bearing oligos. Hybridisation to unmodified control oligos only results in a minor band shift. (P - pocket; T - triangles)*

hybridise to a linker handle, while a 10:1 ratio means that 9 out of 10 chol-oligos will not have a hybridisation partner (i.e. they are in excess). As shown in Fig. 2.2B, addition of chol-oligo results in a significant smearing in agarose gel electrophoresis, likely due to hydrophobic interactions between the triangles resulting in transient clusters with slower migration speeds. Interestingly, aggregation is mostly present at lower ratios but is absent in the highest tested ratios. This result suggests that excess cholesterol may interact with chol-oligos hybridised to the structure, weakening the interactions between triangles. Even though the most pronounced leading band was obtained for the 4:1 ratio sample, excess cholesterol may negatively influence membrane insertion or the budding reaction. A pipetting error may also explain the unexpected prominence of this band. Slight aggregation as observed in the 1.5:1 ratio sample is likely to be further reduced in the presence of lipid membranes, and thus I decided to proceed with this ratio as a compromise between complete hybridisation of all available linkers at only a small excess of cholesterol and evident hydrophobic effect.

The leading band of structures hybridised to chol-oligos appeared significantly shifted in respect to the unhybridised control sample. One way to explain this shift is the much larger persistence length of dsDNA (hybridised linkers) versus ssDNA (unhybridised linkers) [91, 92]. The greater flexibility of ssDNA linkers may facilitate migration through the gel compared to linkers hybridised to an oligo. However, when comparing triangles without any linker handles to triangles hybridised to either unmodified control oligos or chol-oligos, a large shift is only observed in triangles hybridised to chol-oligos (Fig. 2.2C). The shift observed due to DNA-DNA hybridisation itself is minimal (unmodified control oligo). Thus, cholesterol itself appears to be behind the large shift, possibly by the same

mechanism that also causes smearing.

2.2.2 Surfactants act like chol-oligos in excess

A cholesterol-to-linker-handle ratio of 1.5:1 sacrifices gel aesthetics to reduce the occurrence of unexpected side-effects that may occur at a large excess of chol-oligos. Nevertheless, it is worth exploring whether or not hydrophobic interactions between triangles can be reduced or suppressed. A better understanding of the mechanism behind aggregation and smearing is useful to further optimise linker handle placement and design. As a large excess of chol-oligos can suppress aggregation of triangles (as was shown in Fig. 2.2B), it is likely that interactions between chol-hybridised triangles are simply replaced by interactions between triangles and excess chol-oligos. If true, the same results should be obtainable using additives with similar properties to chol-oligos. As a conjugate of both cholesterol (as an overall hydrophobic molecule) and DNA (as an overall hydrophilic molecule at physiological pH), chol-oligos can be considered amphiphiles. Therefore, addition of other amphiphiles such as surfactants may have similar effects to chol-oligos in excess. I tested this hypothesis by hybridising triangles to a 1.5 x excess of chol-oligo at different concentrations of the mild surfactant octyl glucoside (OG, Fig. 2.3A). As before, unhybridised triangles migrated significantly faster than chol-hybridised ones. Increasing amounts of OG resulted in decreased aggregation and smearing. In fact, the aggregates and smear above the leading band condensed into distinct bands likely representing oligomers (dimers, trimers etc.). However, at the highest OG concentration of 20 mM, most aggregates, oligomers and the smear disappeared. As the material no longer is distributed across the length of the lane, the resulting leading band is much brighter than in the other lands, coming close to the brightness of unhybridised triangles. Similar results were obtained when the experiment was repeated with the detergent Tween20 (Fig. 2.3B). Without addition of detergent, both smearing and aggregated structures in the gel pocket were lower in the sample with a chol-oligo to handle (C:H) ratio of 20 compared to a C:H ratio of 1.5. Tween20 could reduce smearing and aggregation further, with just 10 µM completely disbanding any aggregates in the C:H = 20 sample. More detergent was needed in the sample containing less chol-oligo.

An interesting observation is that Tween20 was effective at much lower concentrations than OG. This can easily be explained by the different critical micelle concentrations (CMC) of both detergents (approx. 50 µM for Tween20 [93] and 25 mM for OG [94]), above which surfactants aggregate into micelles. At a C:H ratio of 20, the concentration of chol-oligo in the sample is around 2 µM, which is well above the CMC for pure cholesterol (approx. 25–40 nM [95]). Based on this, one can assume that excess cholesterol forms micelles around chol-oligos hybridised to the origami. The dose-dependency can also be explained in this way, as low ratios equal nanomolar concentrations just above the CMC of cholesterol. It is likely that higher ratios are required for complete formation of micelles

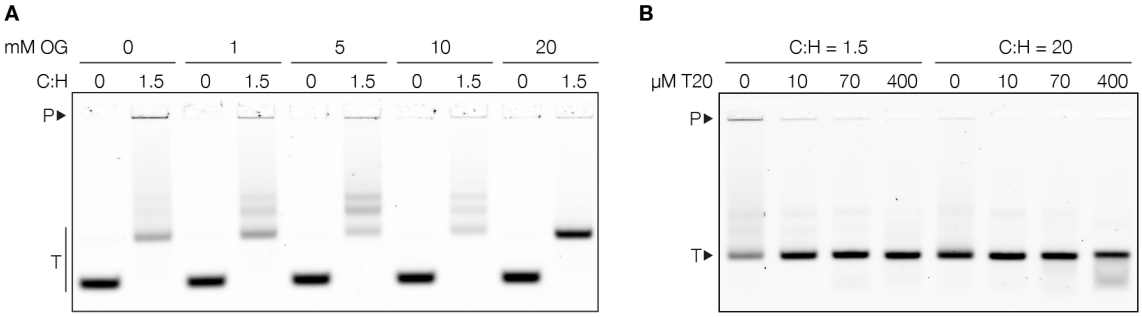

Fig. 2.3: ***Detergents counteract cholesterol-driven aggregation and smearing in agarose gel electrophoresis. (A)*** *Agarose gel of triangles hybridised to chol-oligos in the presence of increasing concentrations of the mild detergent octyl glucoside (OG). Chol-oligos were added at a 1.5 excess in respect to the available linker handles. With increasing detergent concentrations, smearing and aggregation diminish until only a band shift in chol-hybridised triangles remains. The detergent had no visible effect on triangles not hybridised to chol-oligos. (P - pocket; T - triangles)* ***(B)*** *Agarose gel of triangles hybridised to chol-oligos in the presence of increasing concentrations of the detergent Tween20 (T20). Chol-oligos were added at either 1.5 or 20-fold excess in respect to available linker handles. Addition of detergent resolved most aggregation and smearing issues caused by cholesterol. Aggregation and smearing were more significantly more pronounced in samples incubated with only a small excess of chol-oligos. (P - pocket; T - triangles)*

around linker-bound chol-oligos, and to reduce the risk of chol-oligo micelles crosslinking two or more triangles. The addition of surfactants can circumvent this issue by breaking up chol-oligo micelles and covering free chol-oligos.

2.2.3 Cholesterol shifts assembly from icosahedra towards octahedra

Although surfactants largely suppress the negative effects caused by cholesterol, they also disrupt lipid membranes and alter their physical properties [96]. Inclusion of surfactants in budding assays may therefore interfere with the experiment and distort results. However, it is questionable if additives to prevent aggregation are even necessary. By mixing chol-decorated triangles with lipid vesicles, free cholesterol moieties will integrate into the hydrophobic core of the lipid bilayer and may thus no longer interact with cholesterols on other triangles. The data presented thus far was acquired at relatively low Mg^{2+} concentrations (typically 5 mM) where self-assembly into icosahedral shells does not occur due to electrostatic repulsion of individual triangles. This raises the question of whether elevating the Mg^{2+} concentration above the assembly threshold (typically above 20 mM) would worsen chol-mediated aggregation by reducing electrostatic repulsion. To lower the risk of aggregation, the C:H ratio was kept at 20 which previously resulted in less aggregation (see Fig. 2.3). However, when chol-hybridised triangles were incubated at assembly conditions (22.5 mM $MgCl_2$, 70 h, 40 °C), analysis by agarose gel electrophoresis revealed noticeable aggregation visible by material stuck in the gel pocket (Fig. 2.4). Interestingly, chol-hybridised triangles assembled into octahedral shells which, due to their smaller size,

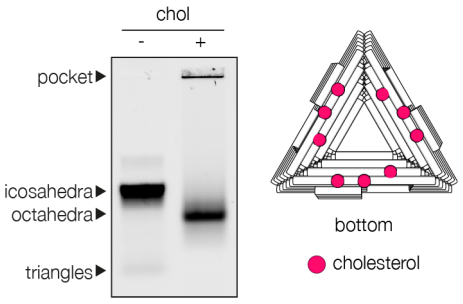

Fig. 2.4: ***Cholesterol alters the assembly behaviour of triangles.*** *Upon increasing the concentration of $MgCl_2$, triangles self-assemble into hollow shells. By design, icosahedral shells composed of 20 triangles will form. However, when chol-oligos are hybridised to the linker handles distributed on the bottom face of the triangles, octahedral shells (composed of just 8 triangles) will form. Due to the smaller size of octahedral shells, they will migrate faster during agarose gel electrophoresis than icosahedral shells, but slower than monomeric triangles. The scheme shows the distribution of cholesterols on the triangles used in this experiment.*

migrate faster through the gel than their icosahedral counterparts. This result complicates the matter further as cholesterol not only promotes aggregation and noticeable gel shifts of monomeric triangles, but it also interferes with assembly. Since the dihedral angle of octahedra (109.47°) is steeper than that of icosahedra (138.19°), I hypothesised that induction of membrane curvature by triangle self-assembly would be less efficient or not possible at all for steric reasons. The formation of icosahedra in triangles not hybridised to chol-oligos confirmed that the problem was not due to flaws in the origami design, but resulted mostly from the interference of cholesterol with the assembly process. The reduction of the dihedral angle by 30° suggests chol-oligos of neighbouring triangles may prevent further opening the angle by interacting with one another.

2.2.4 Reduced handle reach mitigates negative effects of cholesterol

While chol-mediated aggregation of triangles does not depend on their precise alignment, self-assembly into shells does. The observed shift of assembled species from icosahedra towards octahedra in chol-decorated triangles implies a comparably defined mechanism behind this phenomenon such as interaction of cholesterols on neighbouring triangles. In this scenario, linker handles might act as a leash preventing further opening of the dihedral angle, with cholesterols connecting them. A simple solution could be to limit the reach of each linker handle, e.g. by shortening linker handles, so that neighbouring cholesterols cannot interact anymore. In practice, shortened DNA sequences result in lowered melting temperatures and thus duplexes may fall apart at elevated temperatures such as the assembly temperature of 37–40 °C. An alternative approach would be extending linker handle lengths. Herein, cholesterol interaction could still occur, but the oligonucleotide would provide enough leeway for the dihedral angle to fully open. The disadvantage of

this approach is that oligonucleotide costs go up with length whilst the quality goes down, requiring expensive purification strategies that also lower the final yield. A more practical and economical solution would be to either change the position of linker handles, shifting them towards the centre of the triangle, or to change the configuration of cholesterol in respect to the linker handle. The triangle variant discussed so far features three linker handles per side, which are positioned at the outermost helices of the structure (Fig. 2.5A, variant A). After forming a duplex with the linker handle, the cholesterol on the chol-oligo is positioned at the end of the linker handle (distal configuration). By chemically linking cholesterol to the other end of the oligo, the cholesterol can be positioned closer to the surface of the origami structure (proximal configuration). This approach requires only minimal changes to the current design. Alternatively, by shifting linker handles away from the edges towards the centre of the structure, no changes to the chol-oligo itself are required (Fig. 2.5A, variant B). In Fig. 2.5A, structure A represents the triangle variant used in the experiments discussed until now, whereas structure B has its linker handles shifted towards the central hole of the triangle. Both variants feature a total of 9 linker handles for hybridisation to chol-oligos. As discussed previously, distal cholesterol on structure A results in slower migration through the gel compared to the unhybridised control. However, when this structure is hybridised to a chol-oligo with reversed chol positioning (proximal cholesterol), the migration shift relative to the control is minimal (Fig. 2.5B, sample A_P). Similar results were obtained with distal cholesterol on structure B, but the leading band appears more smeared out which implies that proximal configurations reduce interactions between triangles more effectively than distal configurations regardless of linker handle positioning (sample B_D). The migratory shift between hybridised and unhybridised samples appear to be influenced strongly by the positioning of the linker handles. Combinations of both linker handle designs into triangles featuring a total of 18 linker handles yielded gel patterns that look like combinations of the individual configurations (sample A+B).

These results demonstrate that the negative effects of chol-decorated origami structures can be mitigated by optimising the design of linker handles and chol-oligos. Gel migration behaviour appears to be influenced by the horizontal reach of cholesterol away from the structure, whereas smearing appears to be more strongly influenced by the vertical reach of cholesterol. More data using different origami structures is required to test the general applicability of these design principles. Nevertheless, the present data suggests that aggregation and related issues can be circumvented by positioning linker handles away from the edges, and using proximal chol configurations. These effects likely reflect the competition between hydrophobic attraction and electrostatic repulsion of individual origami structures. Proximal chol configurations require structures to be in closer proximity for cholesterols to interact, which also means stronger repulsion of the structures. The overall effect is thus expected to be weaker than in structures using distal cholesterols. Simi-

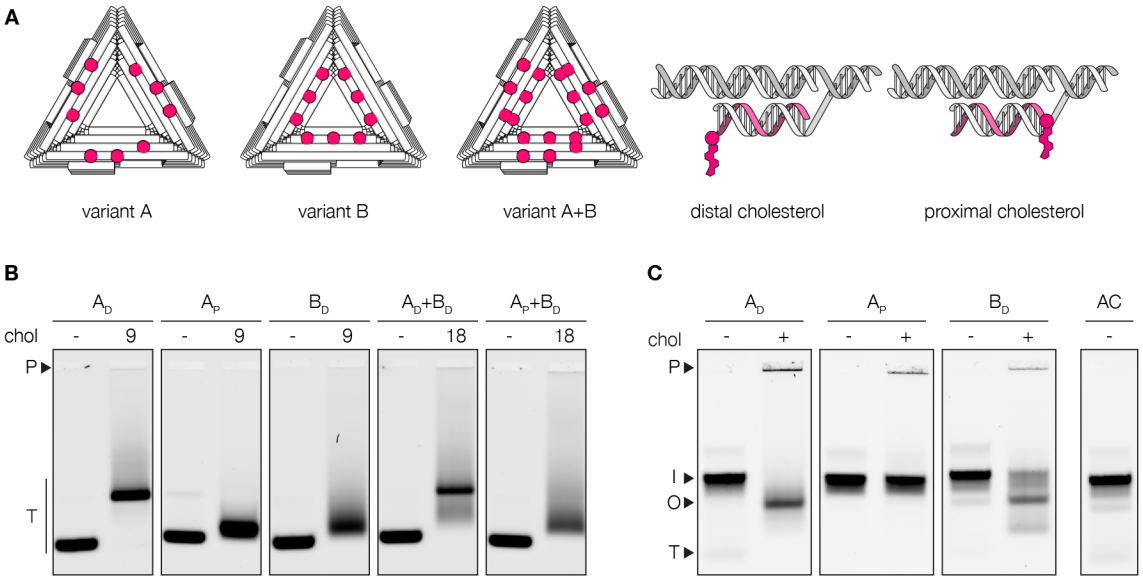

Fig. 2.5: ***Cholesterol-mediated assembly interference depends on the position of linker handles on the triangle.*** ***(A)*** *Linker handle positions on three different variants, and scheme of distal and proximal cholesterol configurations. The upper, white helix represents the triangle surface (side view), the pink strand represents the chol-oligo. Cholesterol may be oriented facing away (distal) or towards (proximal) the origami surface.* ***(B)*** *Agarose gel of triangle variants carrying distal (X_D) or proximal (X_P) cholesterol. Limiting the reach of cholesterol by using proximal configurations or placing linker handles closer to the centre of the triangle (variant B) reduces smearing and band shifts in respect to unhybridised controls. (P - pocket; T - triangles)* ***(C)*** *The principles discussed in (B) also translate to assembled species, where the abundance of octahedral shells depends on the reach of cholesterol. (P - pocket; I - icosahedra; O - octahedra; T - triangles; AC - assembly control (no linker handles on triangle))*

larly, the influence of linker handle position may reflect the difference in charge densities at different positions on the structure. As charge density is expected to be lowest at the outermost edge of the triangle, cholesterols on different triangles positioned here can interact more easily. This hypothesis helps to explain and optimise the migration behaviour of chol-hybridised origami triangles in agarose gel electrophoresis, but these design principles need to be refined for shell assembly which is triggered at elevated Mg^{2+} concentrations where electrostatic repulsion is considerably reduced. Fig. 2.5C shows structures A (with proximal and distal chol) and B (with distal chol) assembled into shells in comparison to an unhybridised assembly control (AC). As shown before, sample A_D assembled mostly into octahedra when hybridised to chol-oligos. Using proximal cholesterol (sample A_P) prevented this phenomenon such that the chol-hybridised sample looked like the unhybridised control. However, distal cholesterol hybridised to linker handles positioned around the centre of the structure (sample B_D) yielded both an icosahedral and an octahedral band. Before assembly, monomeric B_D ran like monomeric A_P, though with more smearing. This behaviour can be understood by looking at the geometry of this system. Assuming an effective DNA helix diameter of 2.6 nm in DNA origami structures [97] and perfect alignment

of linker handles between two structures, the smallest distance for linker handles to bridge is 2.6 nm in structure A (one helix), and 13.0 nm in structure B (5 helices). The length of linker handles and chol-oligos is 15 nt, which, after multiplying by the helical rise per base of 0.34 nm [29], translates into a DNA length of 5.1 nm. Cholesterol is chemically linked to this DNA oligo using a tetraethylene glycol (TEG) linker, which I estimated at about 1.75 nm based on the linker structure and reported monomer lengths of 0.35 nm/ethylene glycol unit [98]. Two chol-oligos can thus, together, span about 13.7 nm and thus interact even if linkers are positioned close to the centre of the structure. This estimate is close to the assumed minimum distance between linkers in structure B, which might explain why there is no clear shift towards octahedra as in sample B_D. These results support the idea that the shift towards octahedral species is linked to the interaction of cholesterols on neighbouring triangles. By limiting the reach of cholesterol, self-assembly into icosahedra can proceed normally.

2.2.5 Lipid membranes shift triangle assembly towards octahedra

The linker handle design principles described so far help to avoid unexpected behaviour of chol-decorated triangles in the absence of lipid membranes. Aggregation of triangles as well as changes to the assembly behaviour could all be traced back to hydrophobic interactions between cholesterols on separate triangles. The question that remains is if any of these problems are also prevalent in the presence of lipid membranes. Cholesterol spontaneously inserts itself into the bilayer, thus making it unavailable for interaction with other chol-oligos outside the bilayer. Secondly, the number of cholesterols per triangle may offer another opportunity for optimisation. A smaller number of cholesterols may further mitigate undesirable effects, but comes at the cost of weaker membrane tethering of origami structures.

Based on the aforementioned design principles, I designed new linker handles that are positioned close to the centre of the triangle and hybridise to chol-oligos with cholesterol in a proximal configuration (Fig. 2.6A). Furthermore, preceding the segment complementary to the chol-oligo is an 18 nt spacer region consisting of just thymidines (spacer Ts). These spacer Ts were included to facilitate membrane tethering and to reduce potential aggregation issues [99]. I prepared three variants carrying either 1, 3 or 9 linker handles hybridised to chol-oligos, and assembled these in the presence of GVs. As shown in Fig. 2.6B, the assembly was shifted towards octahedra in a chol-count dependent manner. I estimated the theoretical reach of cholesterol in this sample at approx. 7.9 nm (following the considerations discussed in section 2.2.4), which means cholesterols on neighbouring triangles could interact. However, the shift towards octahedra is also present in triangles carrying just a single cholesterol where chol-chol interactions are less likely than in variants carrying one or more cholesterols on each side. This result is surprising not only because

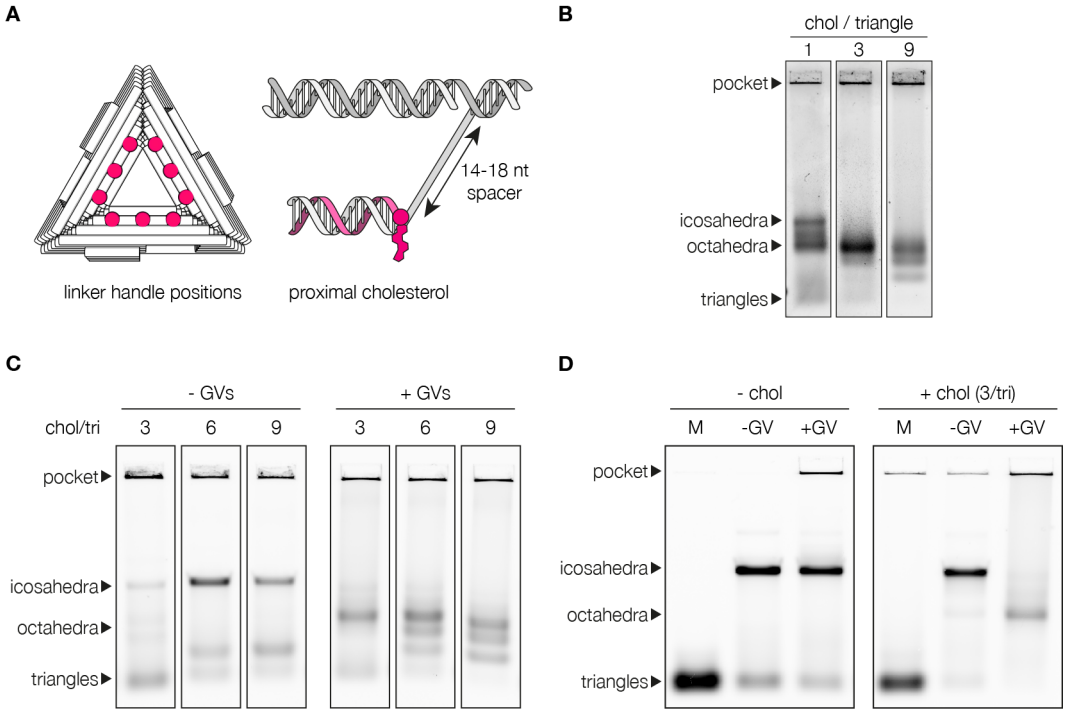

Fig. 2.6: ***Lipid membranes promote assembly of chol-decorated triangles into octahedra.*** ***(A)*** *Up to 9 linker handles positioned close to the centre extend from the bottom face of a triangle. Upon hybridisation with chol-oligos, cholesterol will assume a proximal configuration in respect to the triangle surface, separated from it by 14–18 nt spacer thymidines.* ***(B)*** *Agarose gel of triangles carrying 1, 3 or 9 cholesterols after assembly in the presence of GVs. Despite optimised linker handle configuration, triangles self-assemble into octahedra depending on the cholesterol count per triangle.* ***(C)*** *Agarose gel of triangles carrying 3, 6 or 9 cholesterols after assembly in the presence or absence of GVs. Triangles only self-assemble into octahedra in the presence of lipid vesicles. In the absence of lipid vesicles, triangles with optimised linker handle configuration self-assemble into icosahedra as originally intended.* ***(D)*** *Agarose gel of triangle assemblies. Without cholesterol, triangles self-assemble into icosahedra even in the presence of GVs, indicating that both cholesterol and vesicles are required for octahedra to form from linker handle optimised triangles. (M - unassembled monomer control sample)*

addition of lipid membranes could not prevent this phenomenon from happening, disproving previous hypotheses, but the effect was even more pronounced than in sample B_D in Fig. 2.5C with a very similar setup.

The discrepancy between the present and previous results suggests that the inclusion of spacer Ts into the linker handle design could be reintroducing aggregation problems. A significant fraction of DNA signal in the gel stems from the pockets, which could be due to chol-mediated aggregation of triangles, or triangles stuck onto GVs which, because of their size, cannot enter the gel. I repeated the former experiment with the spacer region on linker handles shortened to 14 nt. The estimated reach of cholesterol could thereby be reduced to approx. 6.5 nm, which is about half the estimated minimal distance of 13 nm between two cholesterols. In practice, full extension of linker handles is very unlikely,

and thus interaction of neighbouring cholesterols is not expected in this case. I tested assembly of triangles with these modified linker handles in the presence and absence of GVs to also probe the influence of lipid bilayers in this system (Fig. 2.6C). Surprisingly, triangles assembled into octahedra only in the presence of GVs. In samples containing no GVs, triangles assembled into icosahedra regardless of their cholesterol count. This result strongly suggests that lipid bilayers introduce another variable which shifts the assembly towards octahedral species. Furthermore, the effect occurs only in chol-hybridised triangles mixed with GVs, but not in triangles with unhybridised linker handles (Fig. 2.6D). Thus, if either cholesterol or GVs are missing, triangles will assemble into icosahedra as expected.

The mechanism behind this seems distinct from before as the previously determined linker handle design guidelines could largely prevent cholesterol-mediated issues such as promoting triangle assembly into octahedra instead of icosahedra as originally intended. The reappearance of octahedra in samples containing both cholesterol-decorated triangles and lipid vesicles initially hints that close proximity to the membrane may be required for this effect to occur. However, when triangles lacking cholesterol are mixed with GVs, they will still assemble normally despite triangles stuck in the pocket indicating electrostatic interaction between triangles and vesicles (Fig. 2.6D, -chol/+GV sample). Octahedral assembly is thus more likely to be a multifactorial process depending on variables such as triangle density on the vesicle, on-membrane diffusivity, or membrane bending in response to self-assembly of triangles.

2.2.6 Sodium chloride prevents non-specific adsorption onto vesicles

Agarose gel electrophoresis of chol-oligo hybridised and unhybridised triangles in the presence of GVs revealed that in both cases a noticeable fraction of triangles remains in the pockets (Fig. 2.6D). In the case of chol-hybridised triangles, this result is not unexpected and most likely represents membrane-tethered triangles. As the vesicles used are several microns in size, on average, they are too large to enter the gel matrix and any material stuck to them will thus likewise remain in the pockets. The retardation of unhybridised triangles, however, indicates non-specific interactions between triangles and vesicles. Indeed, previous studies revealed that bivalent cations promote the adsorption of DNA onto vesicles composed of zwitterionic lipid species [100]. To confirm magnesium-mediated adsorption of DNA triangles onto GVs, I prepared and mixed fluorescently labelled GVs and triangles for subsequent analysis by confocal microscopy. As shown in Fig. 2.7, the DNA nanostructures (grey) adsorbed to the lipid vesicles (magenta) irrespective of cholesterol. Addition of 300 mM sodium chloride prevented non-specific adsorption by displacing magnesium ions (present at 5 mM), but did not influence specific membrane binding via cholesterol. Based on these results, budding reactions were typically prepared in folding buffer (FoB) supplemented with 5 mM $MgCl_2$ and 300 mM NaCl (FoB5/N300).

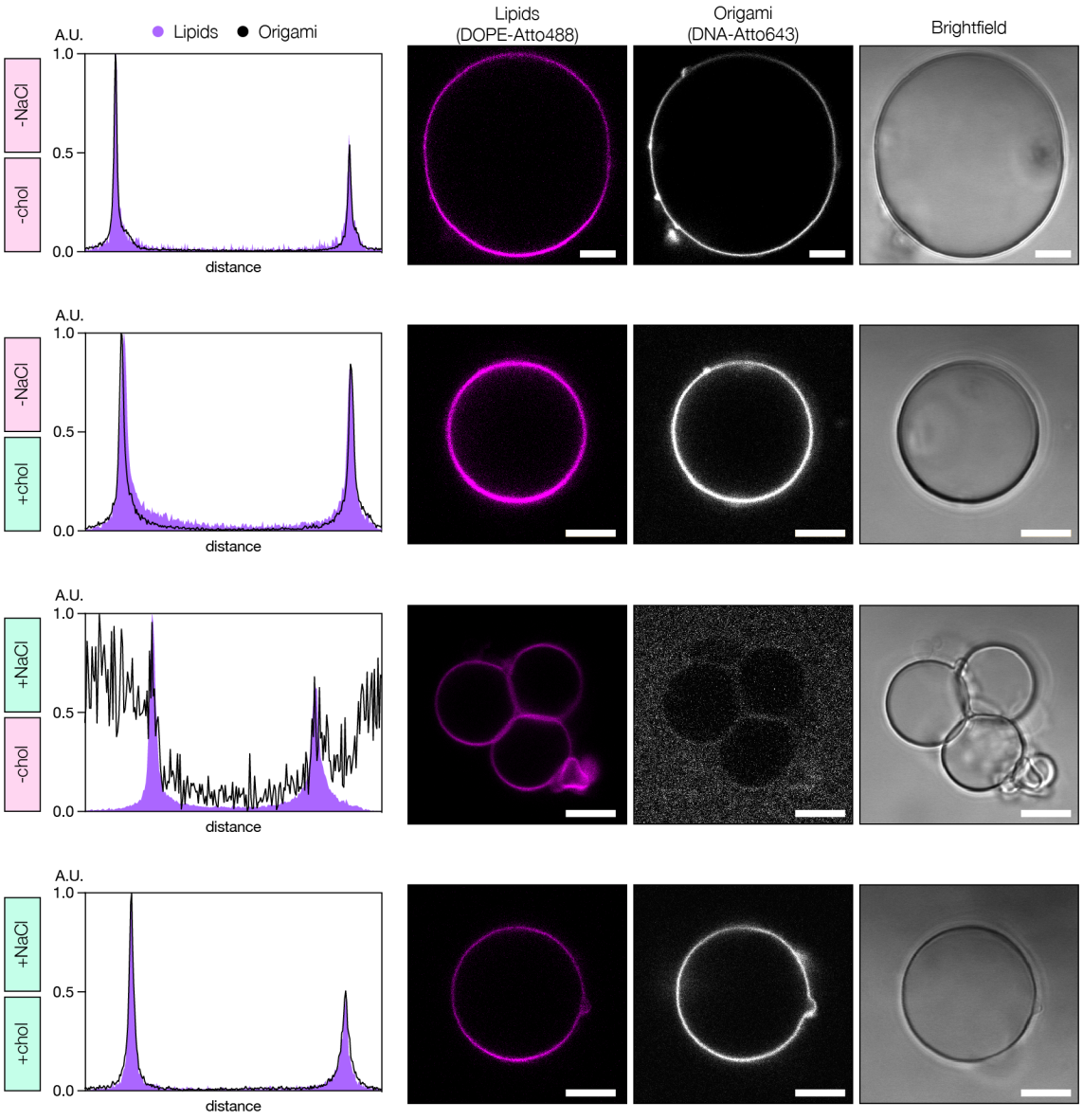

Fig. 2.7: ***Sodium chloride prevents non-specific adsorption of DNA origami onto giant vesicles.*** *Cross-sectional intensity profiles and channel-separated confocal microscopy images of giant vesicles mixed with DNA origami triangles. Conditions: +/− cholesterol-modified oligonucleotides (chol) and +/− 300 mM NaCl, as indicated. All samples contain 5 mM $MgCl_2$ to maintain origami stability. At low-salt conditions, triangles adsorb onto lipid vesicles even if not hybridised to chol-oligos. By adding 300 mM NaCl, non-specific origami-vesicle association is suppressed without interfering with cholesterol-mediated association. Scale bars: 10 µm*

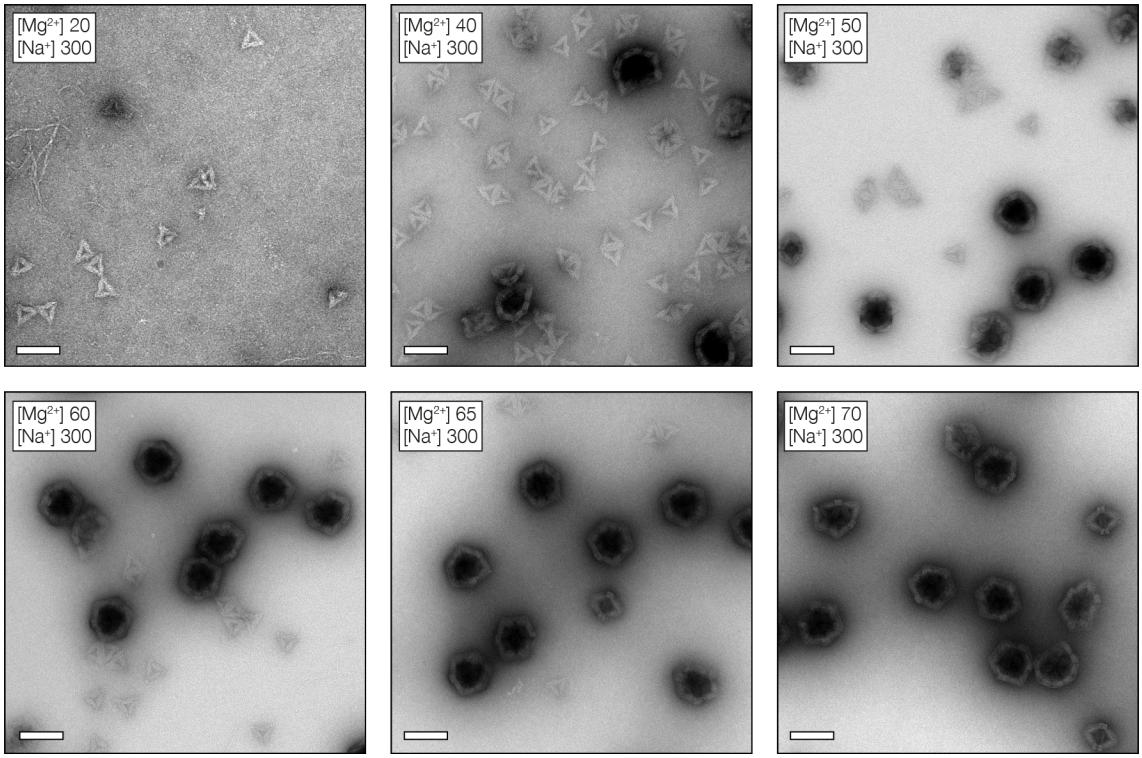

Fig. 2.8: ***Triangle assembly screen at high-salt conditions.*** *TEM micrographs of DNA origami triangles after incubation in 300 mM NaCl and increasing amounts of $MgCl_2$. NaCl increases the required concentration of magnesium ions for efficient triangle assembly from approx. 20–25 mM to 60–70 mM. Concentrations in inserts are in mM. Scale bars: 100 nm.*

2.2.7 Sodium chloride elevates the shell assembly threshold

As a side effect of NaCl supplementation, the magnesium requirement for triangle assembly changed. Assembly occurs above a $MgCl_2$ threshold concentration of approximately 20 mM, but in the presence of 300 mM NaCl this threshold is elevated. Here, although assembly begins to occur between 30–35 mM $MgCl_2$ (data not shown), reasonable quantities of complete or nearly complete shells were achieved using at least 40 mM $MgCl_2$ with a lot of monomeric triangles still present. By increasing the $MgCl_2$ concentration further, the yield of shells increased whereas the number of monomeric triangles decreased until only a small number of monomeric triangles remained at 70 mM. The presence of a small amount of monomeric triangles is necessary to fill in the gaps of nearly complete shells, and thus escalating the $MgCl_2$ concentration too much may result in mostly incomplete shells. Based on the TEM data shown in Fig. 2.8, 65 mM $MgCl_2$ appears to be a sweet spot for assembly in the presence of 300 mM NaCl, yielding a large amount of complete shells with still a few monomeric triangles remaining. It is likely that increasing the magnesium concentration 13-fold over the base concentration of 5 mM re-establishes non-specific adsorption of triangles onto vesicles. However, by mixing vesicles and chol-decorated triangles together in

FoB5/N300 for membrane tethering and adjusting the magnesium concentration to 65 mM after a brief incubation step, non-specific adsorption as well as chol-mediated aggregation of triangles can be mitigated. Chol-oligo insertion into lipid vesicles occurs at a timescale in the order of minutes, and the avidity provided by coupling multiple chol-oligos to each triangle is expected to make membrane binding irreversible [101].

2.2.8 Temperature and $MgCl_2$ influence assembly behaviour

The impact that inclusion of NaCl into the sample buffer had on the magnesium requirements for shell assembly raises the question of whether it also influences the temperature optimum. In general, elevated temperatures weaken shape-complementary base-stacking interactions holding together two DNA objects, but they also accelerate the assembly of triangles into shells [40, 47]. By including 300 mM NaCl into the sample buffer, this fine balance between binding strength and assembly kinetics may be influenced to yield high quantities of shells also at lower temperatures. I tested the assembly behaviour of triangles between 4–40 °C and 65–85 mM $MgCl_2$ to better understand the optimal assembly conditions (Fig. 2.9). While all tested conditions yielded octahedral and icosahedral shells, the yield significantly increased at and above 30 °C. Likewise, the yield of octahedral shells decreased at the same temperatures. The magnesium concentration had the opposite effect, where higher concentrations up to 85 mM yielded a larger fraction of octahedra than the optimal concentration of 65 mM discussed in section 2.2.7.

These results are surprising because they demonstrate the occurrence of octahedra even in the absence of cholesterol or lipid vesicles. The steeper dihedral angle of octahedra is in conflict with the bevel angle of the triangle structure, which suggests that triangles in octahedra may not use all available stacking contacts on each side but less to achieve the steeper angle. This hypothesis is supported by the temperature dependent assembly behaviour shown here. Elevated temperatures may promote icosahedral shell assembly by accelerating diffusion and breaking up the weaker bonds in octahedra. Assuming dimers at an icosahedral dihedral angle use all eight available helices in a stacking contact, the steeper dihedral angle needed for octahedral assembly may sterically only be achievable if the stacking contact is formed by fewer helices, weakening the bond. In either case, assembly is only possible if the cation concentration in the sample is sufficiently high to overcome electrostatic repulsion of individual DNA origami objects. The relative increase of octahedral species at elevated $MgCl_2$ concentrations may thus counteract the destabilising effect of elevated temperatures by weakening electrostatic repulsion further. One could argue that icosahedral yields and assembly kinetics could further be optimised by increasing and balancing out both temperature and $MgCl_2$ concentration, but the melting temperature of DNA duplexes poses an upper limit above which the DNA nanostructures would fall apart. Increasing the temperature above 40 °C is thus too risky. Based on this

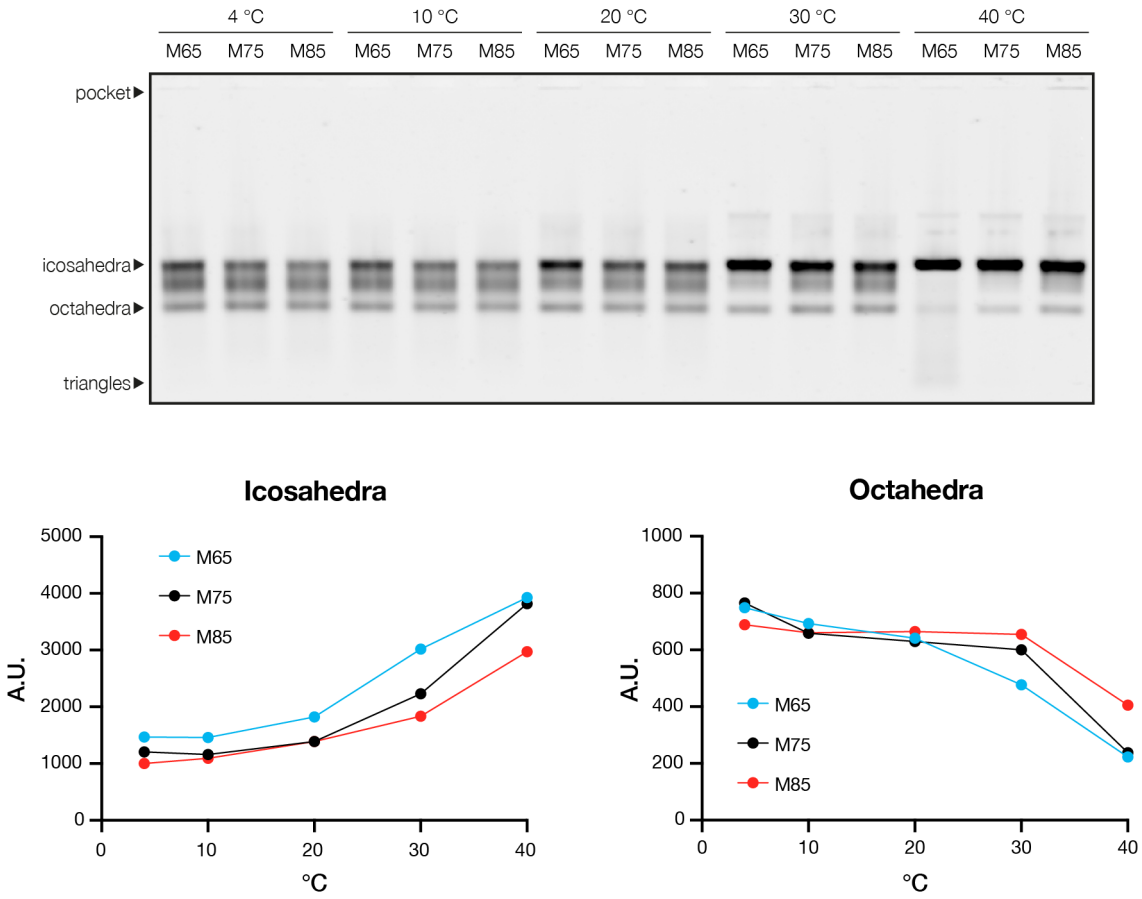

Fig. 2.9: ***Fine tuning of triangle assembly in high-salt buffer at varying temperatures and magnesium concentrations.*** *Agarose gel of triangles assembled in 300 mM NaCl and 65/75/85 mM $MgCl_2$ at temperatures ranging from 4–40 °C. The graphs below display the intensities of icosahedral and octahedral gel bands in arbitrary units. Assembly of icosahedral subspecies occurs most efficiently at elevated temperatures and moderate magnesium concentrations. The reverse is true for octahedral subspecies.*

data, the optimal shell assembly conditions are FoB65/N300 at 37–40 °C for 1–3 d.

Chapter 3

Outward Budding

Membrane budding on lipid vesicles can occur in two directions: either into the vesicle (inward budding), or out of the vesicle (outward budding). While both cases yield daughter vesicles, the mechanism by which they are generated may differ considerably. In CME, clathrin assembles on the inner leaflet of the plasma membrane and shapes a bud towards the cytoplasm. Enveloped viruses also assemble on the inner leaflet of the plasma membrane, but bend the membrane away from the cytoplasm. In cellular contexts, buds growing toward the cytoplasm are commonly defined as positively curved, whereas buds growing away from the cytoplasm are said to be negatively curved [102]. In this context, CME generates positive curvature, whereas viral budding generates negative curvature. The following chapter explores using DNA origami triangles for outward budding from lipid vesicles. The scenario investigated here is different from cells in that the triangles acting as molecular scaffolds attack the parent vesicles from the outside. While the DNA origami-based system presented here is inspired by clathrin, the curvature induced by the DNA origami, following the definition outlined above, is negative as the bud bends away from the parent vesicle. Encapsulation of the origami within the parent vesicles would closely mimic CME, but once encapsulated the triangles are no longer addressable without rupturing the parent vesicle. Hybridising chol-oligos to the triangles and increasing the magnesium concentration to assembly conditions are therefore not possible post encapsulation. Because of these technical limitations, I explored membrane budding from lipid vesicles using externally bound DNA origami triangles. This chapter covers membrane budding with buds bending away from the membrane (induction of negative curvature).

3.1 Energetics of membrane bending & choice of shell size

Membrane budding happens ubiquitously in nature, but has until now not been replicated using synthetic molecular scaffolds. Moreover, the work discussed in this thesis uses DNA

nanostructures as molecular scaffolds, whereas biological budding machineries mostly rely on protein components. As a consequence, there is a large number of influencing variables which decide whether or not budding can occur and at which yield. Among these are the design of the DNA origami triangles, the choice of membrane anchor, its positioning on the nanostructure's surface, and the assembly behaviour which have been discussed in sections 2.1 & 2.2 of the previous chapter. One of the observations was the interference of lipid vesicles with the assembly of triangles into icosahedral shells, resulting in the formation of a significant fraction of octahedral shells. I originally chose the icosahedron as the desired higher-order assembly shape due to their larger inner cavity and the shallower curvature of the structure. In 1973, Helfrich proposed that the membrane bending energy per unit area is given by

$$f = \frac{1}{2}\kappa(J - J_s)^2 + \bar{\kappa}K \tag{3.1}$$

where κ is the bending modulus of the membrane, $\bar{\kappa}$ is the bending modulus related to the Gaussian curvature, J is the total curvature, J_s is the spontaneous curvature, and K is the Gaussian curvature [103, 104]. The total curvature J and the Gaussian curvature K are both composed of the two principal curvatures c_x and c_y, where $J = c_x + c_y$ and $K = c_x \cdot c_y$. Curvature in this context is defined as $c = \frac{1}{r}$, where r is the radius of the curvature in x or y direction. Equation 3.1 is a general expression describing the bending energy per unit area for arbitrarily bent membranes. However, in budding processes spherical deformations are most frequently observed. The principal curvatures of a sphere are identical in all directions, and the total energy required to bend a planar membrane into a sphere is then given by:

$$E_{sphere} = 8\pi\kappa \tag{3.2}$$

The total elastic energy in a spherical vesicle therefore solely depends on the bending modulus of the membrane regardless of its size [103]. Given $\kappa \sim$ 10–25 k_BT, the expected energetic cost lies at around 250–600 k_BT which is too high a penalty to occur spontaneously [105]. The function of membrane benders such as clathrin is to provide enough energy to finally overcome this energetic barrier. Although equation 3.2 does not include the sphere radius as a variable, membrane benders must provide the required energy in a finite area. By dividing the total elastic energy by the surface area of a sphere, one obtains the elastic energy per unit area

$$f_{sphere} = \frac{8\pi\kappa}{4\pi r^2} \tag{3.3}$$

for a spherical vesicle [106]. It becomes clear that larger spherical deformations may be more feasible by having a lower energy requirement per unit area, even if the total energy requirement remains constant. A consequence for the rational design of a membrane budding system is that larger vesicles should be preferred over smaller ones. Octahedral shells

not only have a smaller inner cavity resulting in a larger energy per unit area requirement, but they are also composed of fewer individual triangles which are to provide the required energy. It has previously been described that the energy provided by clathrin polymerisation contributes to membrane bending in CME [6], and thus self-assembly of DNA origami triangles by base-stacking interactions may similarly provide enough energy to bend the membrane. The octahedral and icosahedral shells described by Sigl et al. are both formed by self-assembly of triangles via shape-complementary base-stacking contacts comprised of four blunt-ended DNA helices [47]. Without changes to the design, the polymerisation energy obtained from triangle self-assembly is therefore likely to be very similar (if not identical) between both designs. However, as icosahedra are comprised of 20 triangles as opposed to 8 in octahedra, the total energy obtainable from triangle self-assembly may thus be up to 2.5 times higher in icosahedra. Based on these considerations, one could argue that larger shells may be even better suited by increasing both the inner cavity size and the number of triangles per shell. On the other hand, as Sigl et al. described in their paper, larger shells have less favourable assembly kinetics due to their increased complexity. Self-assembly is further hindered when confined to a lipid vesicle due to the reduced mobility of triangles and steric hindrance. Icosahedral shells therefore offer a good compromise between size, number of subunits, assembly kinetics and structural simplicity.

These theoretical considerations finally lead to the question: can triangle assembly provide enough energy to shape a membrane bud? Using model vesicles composed of only one lipid species with a low melting temperature (e.g. DOPC) in the absence of osmotic pressure differences, and assuming no significant contribution of introducing chol-oligos into the vesicle membrane, triangle assembly through base-stacking interaction is the main source of free energy for curvature induction. Each side of a triangle features a recess spanning four helices with blunt ends on both sides, and an adjacent protrusion of the same shape and size allowing two triangles to click together like LEGO® bricks (Fig. 3.1). Triangle dimers are therefore held together by a total of 16 stacking interactions. Numerous studies have shown that the strength of a stacking interaction is dependent on the nucleobases forming it, with typical values ranging between −0.19 and −3.42 kcal/mol [107,108]. Using the median of the data presented in the two studies considered here (−1.41 kcal/mol), the free energy of triangle dimerisation amounts to −22.56 kcal/mol per edge, or −676.8 kcal/mol in a full icosahedron (30 edges). The assembly energy for an icosahedron thus corresponds to −1100 k_BT (T = 310 K), which is well above the estimated bending energy of 250–600 k_BT. Even octahedral shells lie well within this range (−440 k_BT).

In practice, budding reactions are influenced by many more factors than were discussed here. Different lipid mixtures and osmotic pressure differences may modulate membrane tension, which has been shown to influence clathrin-mediated budding [80]. Temperature modulates membrane fluidity and the assembly kinetics of origami triangles. The data

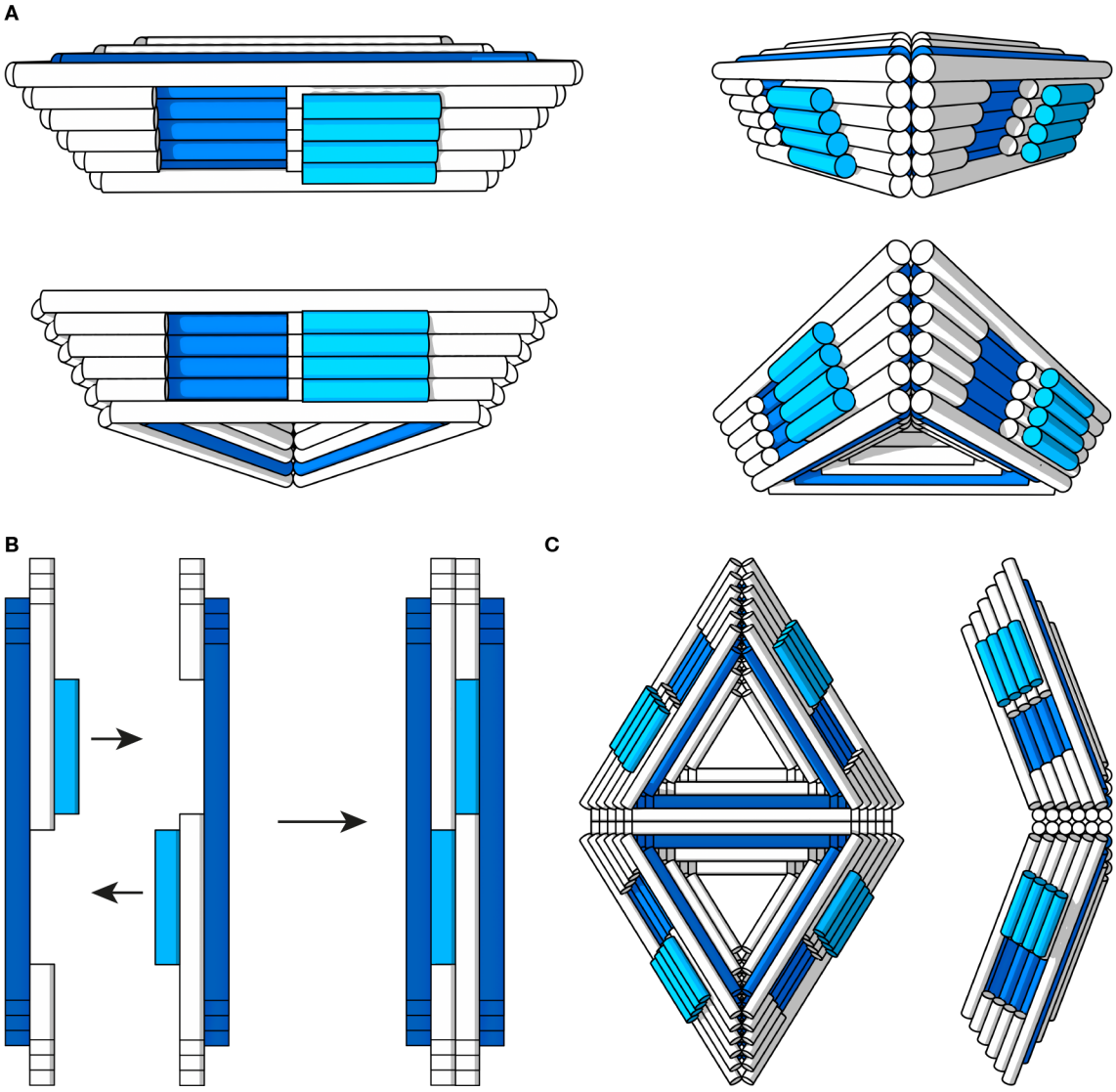

Fig. 3.1: ***Shell assembly through shape-complementary base-stacking interactions.*** *DNA helices are represented as cylinders. Helices forming the inner wall of a recess are painted dark blue, while helices forming protrusions are painted light blue.* ***(A)*** *Schemes of triangles shown from different angles.* ***(B)*** *Schematic representation of a shape-complementary base-stacking interaction viewed from the bottom. The helices above and below the stacking contact (painted white in A), as well as any helices not participating in the interaction have been removed for clarity.* ***(C)*** *Schematic representation of a triangle dimer shown from two angles. Note that the stacking interaction as shown in B is hidden underneath the helices forming the upper and lower rim of the triangle side.*

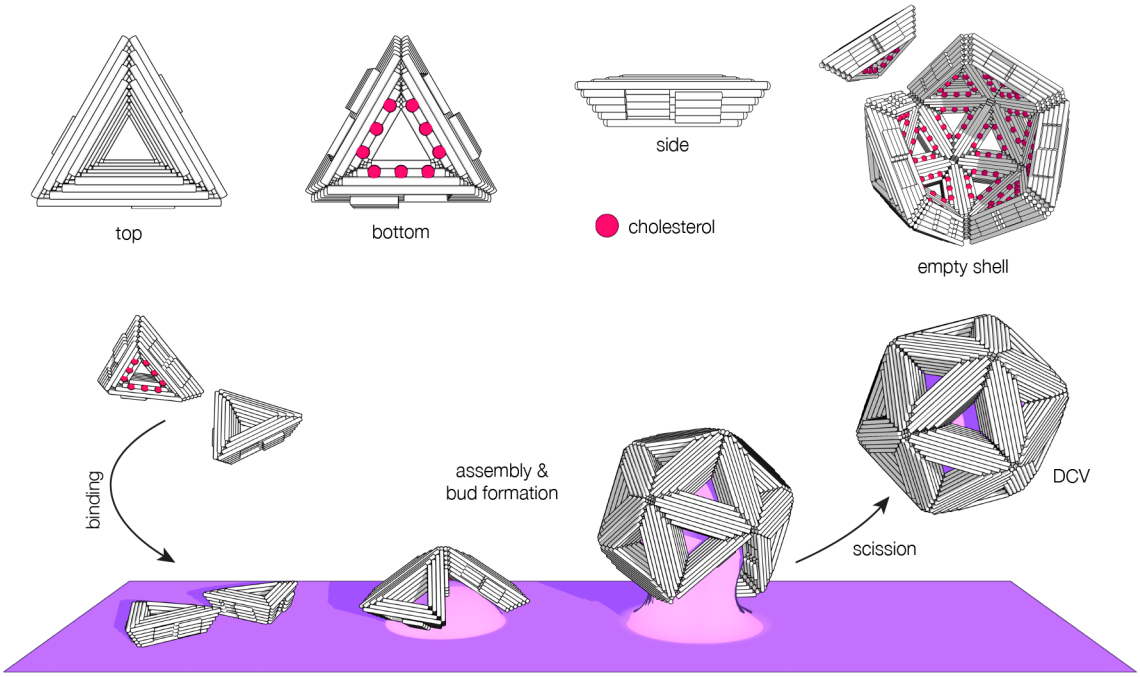

Fig. 3.2: ***Outward budding using DNA origami triangles.*** *Triangles are tethered to a liposome using a membrane anchor such as cholesterol, and then assembled into shells by increasing the cation concentration. On-membrane assembly of triangles remodels the vesicle surface giving rise to buds. Finally, the bud neck is thought to be severed spontaneously, releasing a DNA-shell-coated vesicle (DCV).*

presented in this section nevertheless demonstrates that self-assembly of triangle suffices to induce curvature on the membrane. Moreover, self-assembly into icosahedra releases almost double than the estimated energy required to bend a membrane into a vesicle which may act as a buffer to make up for any difficulties not considered here, including scission of bud necks.

3.2 Shells assembled on membranes contain vesicles

Membrane budding driven by the assembly of DNA origami triangles can be roughly divided into three steps: membrane tethering, triangle assembly, and neck scission (fig. 3.2). As was discussed in section 2.2.6, chol-oligo hybridised triangles are mixed with GVs at a high NaCl concentration to promote specific membrane anchoring. In the next step, the concentration of $MgCl_2$ is increased and the sample is incubated at 37 °C for up to three days for triangles to assemble into shells. Since assembly in this step occurs on the vesicle membrane, I assumed that the angle between two triangles (caused by their bevelled sides) might transfer directly onto the underlying membrane. The extent of this induced curvature can consequently be assumed to correlate with the number of triangles participating in the assembly. A triangle dimer may induce a mere bump on the membrane, whereas

near-complete icosahedral shells would shape a spherical bud. Once a mature bud has formed, it will persist in this state until the neck is spontaneously pinched off to release a DNA-shell-coated vesicle (DCV).

While the first step, membrane tethering, has been demonstrated in section 2.2.6, the explorative assembly experiments discussed so far did not thoroughly examine the feasibility of on-membrane assembly and spontaneous neck scission. Previous studies have demonstrated the assembly of membrane-bound DNA origami objects which resulted in vesicle deformation, but the assembly mechanism used typically involves linking two objects together using single-stranded linker handles and complementary polymerisation oligonucleotides [54]. This approach results in linked structures of undefined size that differ considerably from the closed shells comprised of 8 (octahedra) or 20 (icosahedra) triangles assembled by shape-complementary base-stacking interactions. To test if these triangles can be used as molecular scaffolds to direct membrane budding as shown in fig. 3.2, chol-oligo hybridised triangles were mixed with GVs and assembled as described above. For analysis, the sample was incubated on a TEM grid with a carbon support and stained with uranyl formate to enhance image contrast. As shown in figure 3.3 A, DCVs were identified as shells with a bright interior as opposed to the dark interior of empty shells. This difference in contrast stems from the lack of stain accumulation in DCVs where buffer-filled vesicles displace most of the contrast-giving stain. The staining and subsequent drying steps of grid preparations are known to distort and damage water-filled vesicles, which often results in vesicles appearing cracked (fig. 3.3 B). As stain accumulates in these cracks, the vesicles inside DCVs occasionally appear incomplete or like disconnected micelles. To verify the integrity of the vesicle, cryogenic electron microscopy (cryoEM) micrographs of DCVs were obtained (fig. 3.3 C). Here, the sample solution is plunge frozen in liquid ethane to avoid staining and drying artifacts. In the obtained micrographs, the inner vesicles appear as rings filling up the interior of the origami shell completely. None of the defects occasionally seen in negatively stained particles were observed using cryoEM which confirms the integrity of the vesicle inside DCVs. As TEM micrographs project three-dimensional objects in a two-dimensional image, using them to draw conclusions about the structure of three-dimensional particles may lead to false assumptions. In the case of DCVs, individual micrographs may suggest that the vesicle is positioned within the DNA shell, but they could also be above or underneath an empty DNA shell. It is also difficult to tell whether or not the DNA shell is fully assembled or if only half of the vesicle is covered by triangles. To answer these questions, I prepared a tomogram from a series of micrographs acquired at tilt angles ranging from $-50°$ to $+50°$. Each image in a tomogram represents a slice of the particle in z-direction, thus enabling analysis of the relative position of individual components. Figure 3.4 shows summed up slices of a DCV tomogram, where the three images represent summed z-slices of the top, middle and bottom sections,

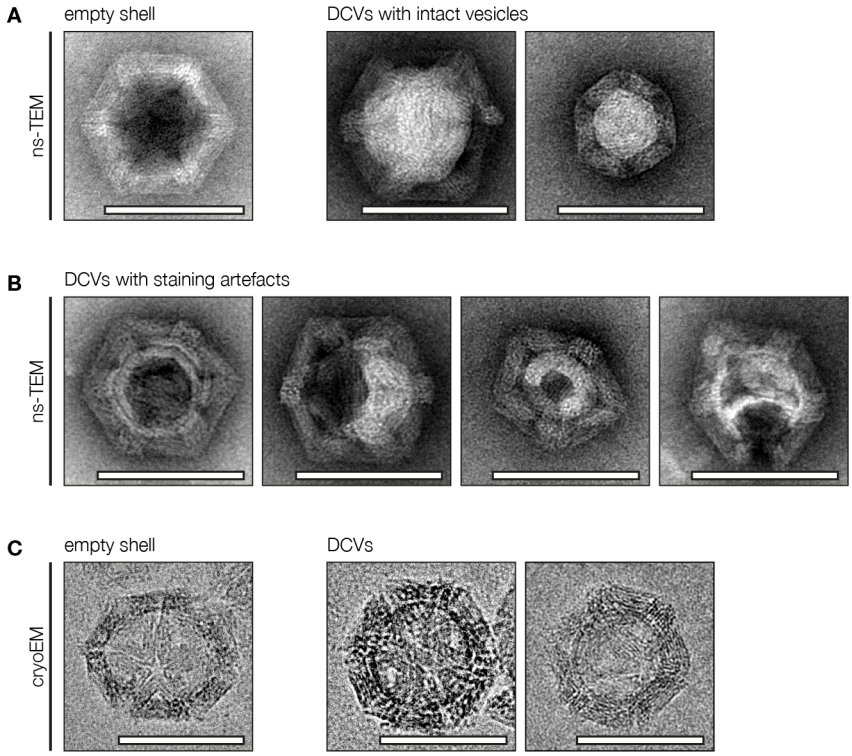

Fig. 3.3: ***TEM micrographs of DCVs.*** ***(A)*** *Negative stain TEM (ns-TEM) micrographs of an empty shell and DCVs with intact vesicles. Vesicles are visible as white material within the DNA origami shell.* ***(B)*** *ns-TEM micrographs of DCVs with staining artifacts. The staining and subsequent drying of lipid vesicles commonly damages them. As a result, vesicles appear cracked, deformed or incomplete.* ***(C)*** *Cryogenic electron microscopy (cryoEM) micrographs of an empty shell and DCVs. As cryoEM samples are not stained or dried, particles can be studied in their native state. Here, vesicles within the DCVs are visible as a dark ring within the origami shell. All scale bars: 100 nm*

respectively. The vesicle is most prominently visible in the middle section, whereas the top and bottom sections show the caps of an icosahedral DNA shell. This confirms both that the vesicle is indeed entrapped within the DNA shell, and that the DNA shell is mostly complete.

3.3 Shell assembly shapes membrane buds

On the first look the presence of DCVs following assembly of membrane-tethered triangles seems to confirm the proposed budding mechanism shown fig. 3.2. However, the mere presence of DCVs does not rule out alternative formation mechanisms such as capture of small vesicles contaminating the GV suspension. GVs are generally considered fragile and despite careful handling, repeated pipetting and mixing may damage them and promote their division into smaller sized vesicles. Rather than looking at the final product, more insights into the formation of DCVs can be obtained by observing shell assembly as it

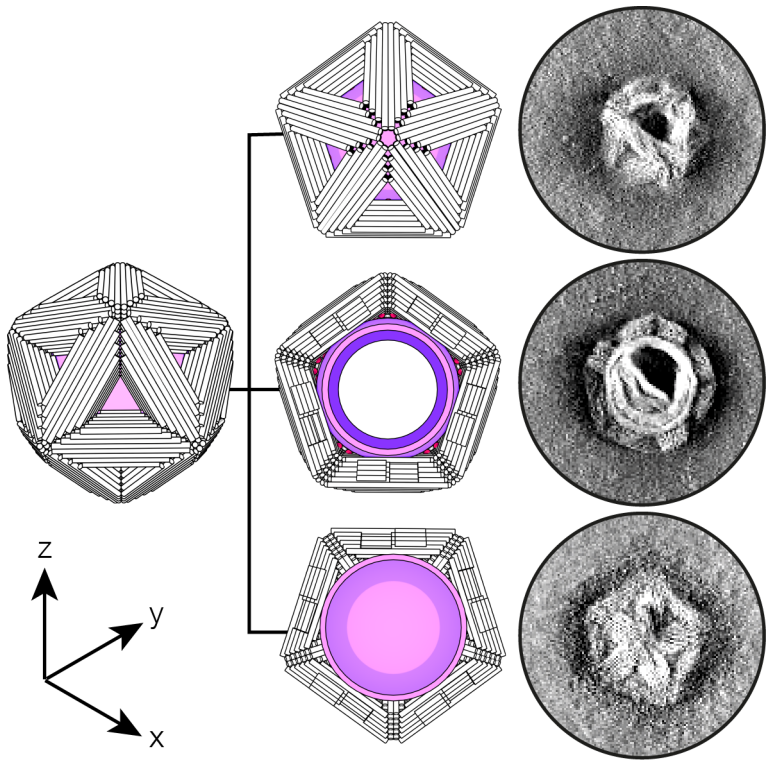

Fig. 3.4: ***Tomogram of a DCV.*** *The individual slices of a tomogram in z-direction were split up into three groups representing the top, middle and bottom section of a DCV. The slices in each group were then summed up to obtain the shown images. The vesicle is clearly visible as white material only in the middle section, indicating that the vesicle is indeed located inside the origami shell. Vesicle traces in the top and bottom sections were diluted by the other slices and are thus not as prominently visible as in the schemes.*

happens on a vesicle. The difficulty herein lies in the size difference between DCVs and GVs, which spans multiple orders of magnitude. While light microscopy can resolve GVs, the size of DCVs is below the resolution limit of visible light which is why DNA origami are typically studied using TEM. Negative staining provides good contrast for the study of biological components, but the staining and subsequent drying procedures destroy the integrity and structure of liposomes. A viable alternative is cryoEM where the sample solution is rapidly frozen on the TEM grid, leaving behind a thin film of vitrified ice. As the sample is neither stained nor dehydrated during grid preparation for cryoEM, sample components can be studied in their native state. A drawback, however, is that thick ice sheets cannot be penetrated by electrons, thus limiting the thickness of particles that can be studied [109]. This is particularly problematic for GVs, which are loosely defined as vesicles with at least 1 µm in diameter, while the largest published structure studied using cryoEM is the giant mimivirus at 750 nm [79]. Even if GVs could be successfully vitrified, resolving any details on objects so large is very challenging. For all of these reasons, I have decided to use large vesicles (LVs) with a diameter of approximately 200 nm in a

budding assay to resolve the assembly of membrane-tethered triangles into shells. These vesicles are about twice the size of a DCV and therefore do not fit within the cavity of the shell, but they are small enough to be studied by cryoEM. Furthermore, I shortened the shell assembly time to just a couple of hours (as opposed to several days) to increase the chances of finding incomplete shells still attached to their parent vesicles, and used isotonic $MgCl_2$ solution to trigger assembly without artificially altering the shape of the vesicles. Micrographs of vitrified samples prepared this way revealed intermediate states of DCV formation (Fig. 3.5 A). As predicted, oligomeric assemblies of triangles imprinted their intrinsic curvature onto the underlying vesicle, deforming it. In contrast, membrane patches void of any triangles appear undisturbed, highlighting the role of triangle assembly in generating membrane curvature. The induced curvature closely follows the curvature of the origami assembly and ranges from little bumps in the membrane to complete buds with narrow necks. Spontaneous scission of the neck finally releases the DCV, occasionally leaving behind a "scar" of missing triangles in the DNA shell (Fig. 3.5 B). These scars may represent the site of the bud neck before scission, which remains free of triangles due to steric hindrance. This data represents the missing link between membrane tethering (discussed in section 2.2.6) and DCVs (section 3.2), and strongly supports the notion of budding as the mechanism.

3.4 Osmotic conditions influence DCV yields

The effective osmotic pressure difference (tonicity) between the vesicle lumen (inner buffer) and the surrounding buffer (outer buffer) influences membrane tension by inflating or deflating the vesicle. For example, if the outer buffer is hypertonic in respect to the inner buffer, a net flow of water molecules from within the vesicle to outside it deflates the vesicle and thereby lowers the membrane tension. This effect has previously been exploited to alter the shape of vesicles using DNA origami structures similar to how the assembly of membrane-tethered triangles deforms the membrane [53]. To investigate the influence of osmotic conditions on DCV budding yields, I conducted a series of experiments at varying tonicities by adding increasing amounts of osmolytes to the samples while maintaining constant quantities of DNA origami triangles and vesicles.

Choice of osmolyte

Ideally, the osmolyte of choice should be chemically inert, uncharged, unable to pass through the membrane and highly soluble in water to not be limited in the hypertonic regime. A commonly used osmolyte to induce hypertonic stress is glucose. It has previously been used to induce origami-driven vesicle deformation and has the benefit of being electrically neutral [53]. Moreover, as the GVs used in this study were prepared in sucrose

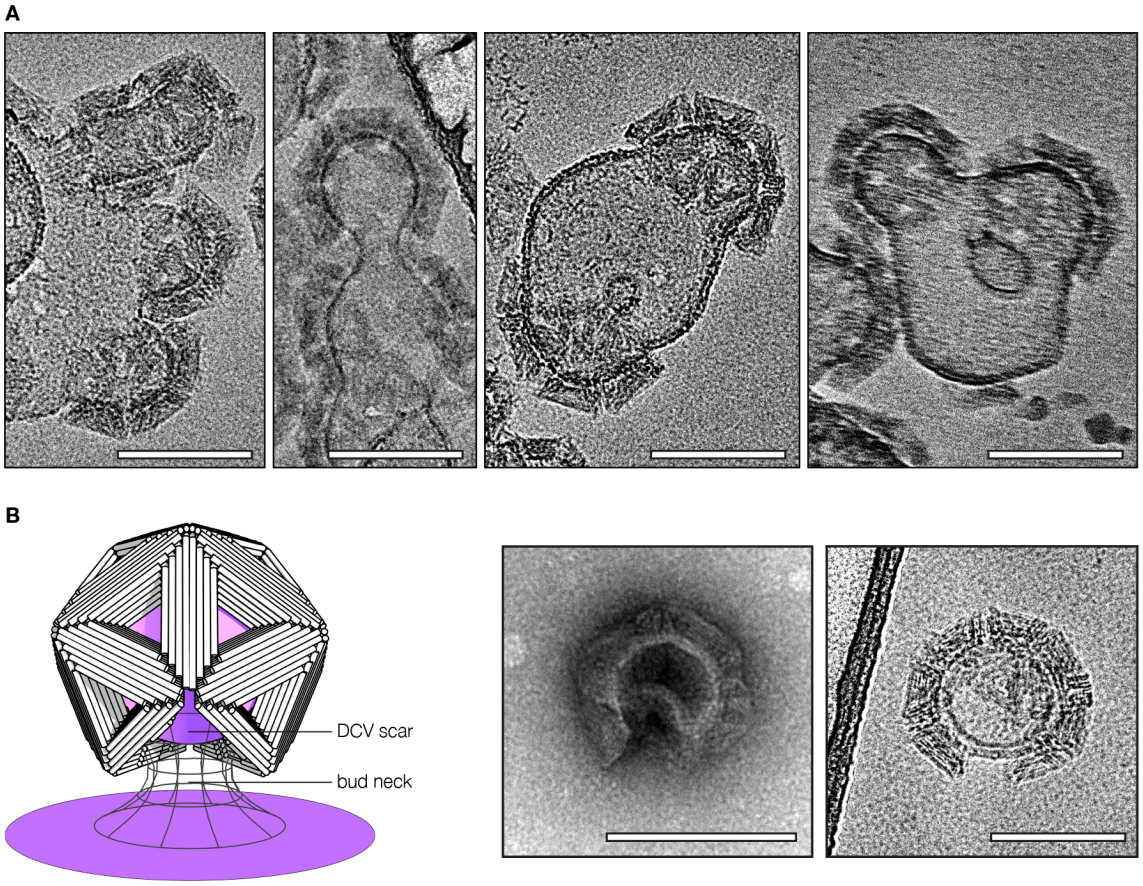

Fig. 3.5: ***Triangle assembly shapes membrane buds.*** ***(A)*** *CryoEM micrographs of large vesicle (LV) deformation upon assembly of membrane-bound DNA origami triangles. Bud curvature increases gradually and closely follows the intrinsic curvature of the assembling shells.* ***(B)*** *The origami shell of DCVs occasionally has visible holes ("scars") of missing triangles. These scars may indicate the site of the bud neck, which prevented closure of the origami shell due to steric hindrance. All scale bars: 100 nm.*

buffer, using glucose to alter the tonicity of the outer buffer seems logical considering both substances are carbohydrates. To study solely the influence of different osmotic conditions, all other interfering variables must be eliminated. In practical terms, this means that the composition of the assay buffer must be kept constant between individual samples, with only the concentration of osmolyte changing. Typically, budding was conducted in folding buffer containing $MgCl_2$ and NaCl, but no sucrose. The GVs were therefore washed and resuspended in FoB5/N300 after swelling in sucrose buffer, to ensure the stability of DNA nanostructures and re-establish standard sample conditions. Both buffers have approximately the same osmolality, and the density difference between the sucrose buffer in the vesicle lumen and FoB5/N300 on the outside causes the GVs to sink to the bottom of the tube. This density difference facilitates washing of the vesicles using low centrifugation speeds without noticeably altering the yield of DCVs. Another particular benefit of this

buffer system in the context of this experiment is that its baseline osmolality of approx. 590 mOsm/kg gives plenty of room to explore both hypo- and hypertonic conditions. By keeping the amount of origami solution, GVs, and the final sample volume constant, the difference between the final volume (V_{final}) and the volumes of the sample components ($V_{final} - V_{origami} - V_{vesicles} - V_{MgCl_2}$ (see section 1.3.2 for details on origami assembly)) is the available volume to vary the osmolality between the individual samples. An important constraint is that the $MgCl_2$ concentration before triggering assembly should be kept constant at 5 mM $MgCl_2$ to ensure the stability of the origami. Based on these considerations, the lower osmolality limit is achieved by filling up the available volume entirely with FoB5, whilst the highest possible osmolality fills it up entirely with osmolyte buffer. In this experiment, the osmolyte buffer is composed of FoB5 with additional 1000 mM Glucose (FoB5/Glu1000). I probed osmolalities in the range of +/− 15/30/60 % of the initial osmolality, and by applying the principles just discussed, the individual samples have the exact same composition differing only in the final concentration of glucose and their osmolality, as intended. Despite this, the results looked very puzzling (Fig. 3.6). Hypertonic conditions should deflate vesicles, thereby lowering membrane tension and facilitating vesicle deformation as previously described for both DNA origami-based systems and also clathrin-mediated endocytosis [53, 110]. However, the samples here formed only very weak bands, which appeared to get brighter under hypotonic conditions. One may be tempted to deduce that DCV budding peculiarly functions better under increased membrane tension, but a similar effect appeared also in assembly controls where triangles were assembled into shells in the absence of lipid vesicles. Here, triangles formed clear bands at the expected heights for icosahedral and octahedral shells, but their brightness increased at lower osmolalities. A likelier explanation is that glucose itself interfered with the assembly process, which is why assembly worked best at the lowest osmolality to which no glucose had been added. To find better alternatives to glucose, I repeated this screen with two different osmolytes: mannitol and glycine. Mannitol is a sugar alcohol with medical uses as an osmolyte [111]. It is an uncharged molecule with good solubility in water and almost identical molecular weight as glucose, but it is structurally different from glucose and has its aldehyde group replaced by another alcohol group. In contrast, glycine is an amino acid with good water solubility but a much smaller molecular weight. As an amino acid, dissolving glycine in water affects the pH of the solution. By keeping the concentration of osmolyte in the osmolyte constant at 1000 mM, adjusting the pH of the glycine stock to the typical assay pH of 8 requires addition of significant amounts of NaOH, which would alter the concentration of sodium between the individual samples with potential effects on the assembly. To avoid this, the pH of the glycine stock solution was not adjusted and kept at a final pH of 6.8. Furthermore, as glycine's isoelectric point is in the acidic regime at pH 5.97, the pH-unadjusted stock solution is closer to the perfect zwitterionic state

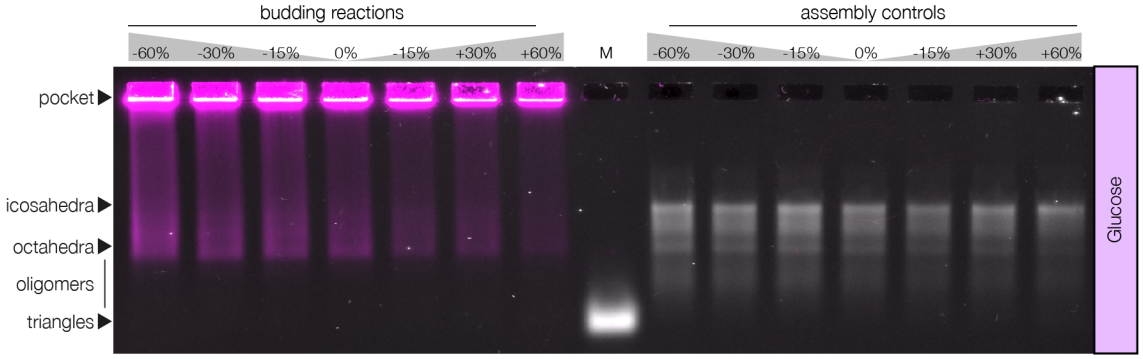

Fig. 3.6: ***Glucose interferes with DCV budding.*** *The sample osmolality was varied in respect to the osmolality inside the vesicles (+/− 0/15/30/60 % relative change) by adding increasing amounts of glucose solution to the samples. No clear DCV bands formed, and the lipid signal decreases with increasing glucose concentration. Likewise, vesicle-free assembly controls formed a mixture of icosahedral and octahedral shells, with overall yields decreasing with increasing amounts of glucose in the sample. Osmolalities are stated in relation to the osmolality of the buffer inside the vesicles (relative change). Magenta: Lipid signal (DOPE-Atto643); Grey: DNA (EtBr);*

and thus adjusting the pH is unlikely to cause any benefit [112]. Like glucose, budding assays prepared in the presence of mannitol yielded no clear bands, but the brightest signal was again received at the lowest osmolality step which did not contain any mannitol (Fig. 3.7A, top and middle). Furthermore, the gel lanes appear warped, with fuzzy bands appearing at increasingly higher levels as the concentration of mannitol in the sample goes up. In contrast, budding reactions containing glycine produced clearly visible bands that increased in intensity as the osmolality went up, confirming previous observations where osmotic deflation facilitates membrane remodelling processes (Fig. 3.7A, bottom) [53,110]. A caveat is that the assembly controls were noticeably affected by the presence of glycine. As its concentration increases, triangles increasingly assemble into icosahedral shells while gel lanes are mostly smeared out at the lowest osmolality. Interestingly, the control sample with the highest glycine concentration again appears smeared out in agarose gel electrophoresis. As both no glycine (−60 % control) and too much glycine (+60 % control) prevented the efficient assembly of icosahedral shells, I hypothesised that glycine interfered with the assembly by competing with magnesium cations in the same way that NaCl does (discussed in section 2.2.7). The inclusion of 300 mM NaCl into the assay buffer prevented the non-specific adsorption of triangles to the vesicles (see section 2.2.6), but also raised the assembly threshold from 20–25 mM to 60–70 mM $MgCl_2$. Indeed, assembly screens run at various $MgCl_2$ concentrations probing glycine concentrations from 0 to 700 mM revealed that the optimal $MgCl_2$ concentration increases with the glycine concentration (Fig. 3.7B). This does not explain the failed budding assays using glucose or mannitol as osmolytes. While the control samples with added glucose got fainter with the amount of glucose added, the mannitol control samples, though visually warped, did not seem to

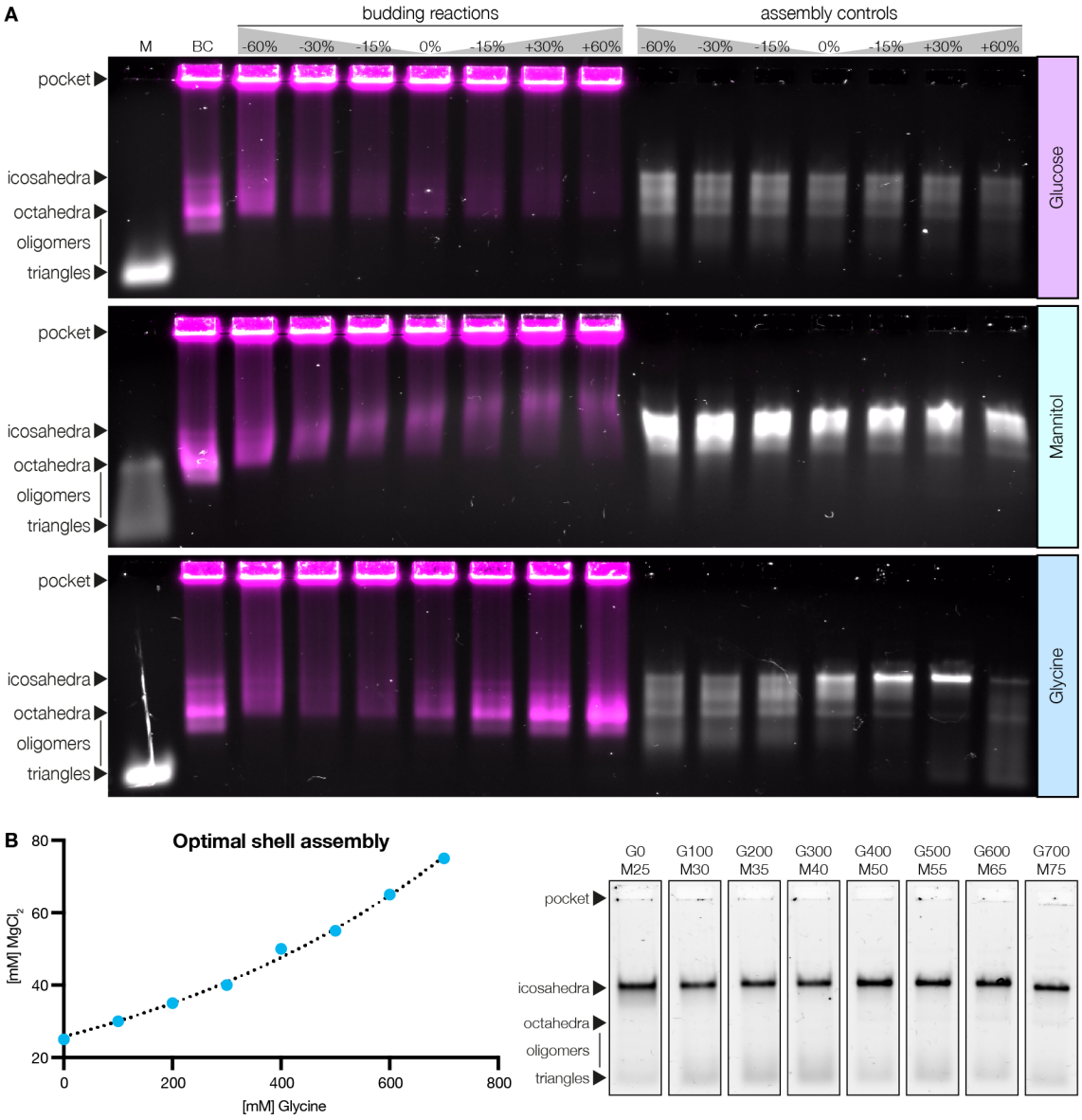

Fig. 3.7: ***Osmolyte screen.*** ***(A)*** *Agarose gel electrophoresis of budding reactions and assembly controls in the presence of glucose (top), mannitol (middle) or glycine (bottom). Glucose and mannitol both resulted in decreased lipid intensities with increasing osmolyte concentration. In contrast, glycine produced clear DCV bands whose intensity increased with the total osmolality. Osmolalities are stated in relation to the osmolality of the buffer inside the vesicles (relative change). Magenta: Lipid signal (DOPE-Atto643); Grey: DNA (EtBr)* ***(B)*** *Optimal $MgCl_2$ concentrations for shell assembly in dependence of glycine levels (left) derived from qualitative analysis by agarose gel elctrophoresis (right). $MgCl_2$ requirements increase non-linearly with the glycine concentration.*

be influenced by mannitol as much. Both osmolytes appear to, in fact, interfere with the assembly process much less than glycine, potentially by lacking charges. One could argue that the main problem was the much higher than necessary $MgCl_2$ concentration, and that glucose may therefore be a more suitable osmolyte than glycine once the optimal $MgCl_2$ concentrations have been determined. However, an important detail we have not yet discussed is the final density of the sample solutions. When mixing sucrose swelling buffer (the buffer inside the vesicles) with a dye to make a coloured solution, and pipetting it into solutions mimicking the +60 % osmolality samples, I found that the coloured solution floated up in both glucose and mannitol-containing samples, but sank in the replicate containing glycine (data not shown). The density of hypertonic samples prepared with glucose or mannitol are likely denser than the sucrose buffer, causing any GVs added to float up to the water-air interface. As a result, the vesicles may aggregate or be damaged, reducing the membrane material able to support DCV budding. Despite competing with magnesium cations, glycine remains the best osmolyte out of those three.

Discussion of results

As discussed, adding more Mg^{2+} than needed leads to the formation of mostly intermediate species and only very few shells. Therefore, the concentration of $MgCl_2$ needs to be increased in parallel to the glycine concentration to hit the right ionic conditions for triangle assembly in every sample. Samples prepared under these conditions revealed a marked increase in DCV yields under hypertonic conditions, contrasting with decreased yields in hypotonic environments (Fig. 3.8). This trend can be attributed to the deflation of vesicles in hypertonic solutions, which not only facilitates the shaping of membrane buds by DNA origami triangles but also generates excess membrane area to support the budding of a potentially large number of DCVs from the same vesicle. As each DCV removes membrane material from its parent vesicle, it is likely that each vesicle can only support a finite number of budding processes according to the amount of excess membrane area available. Conversely, the diminished yields observed under hypotonic conditions likely reflect the heightened energetic cost associated with bending membranes under tension and the scarcity of excess membrane material available for DCV budding. This is echoed in cells, where clathrin recruits actin filaments to shape buds under increased membrane tension [110]. Despite a marked reduction in yield under hypotonic conditions, the formation of some DCVs even then suggests that triangle assembly provides enough free energy to counterbalance a moderate increase in membrane tension to a small, but noticeable extent. These results underscore the critical role of osmotic pressure in modulating the efficiency of membrane budding processes.

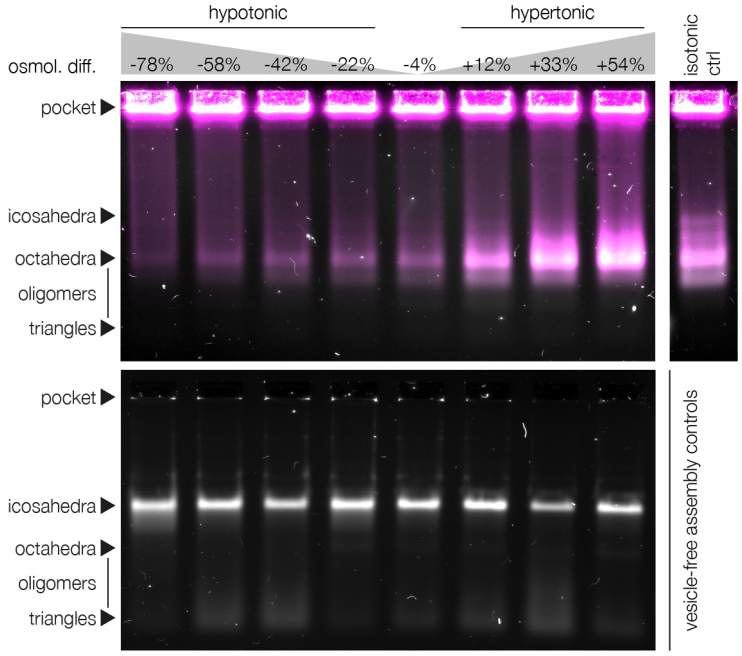

Fig. 3.8: ***Budding of DCVs is strongly influenced by buffer tonicity.*** *Top panel: Agarose gel of DCV budding at the indicated relative osmolalities (adjusted using glycine). At isotonic conditions and above, DCV yields gradually increase with the osmolality. Bottom panel: Assembly controls prepared using the same conditions as in the top gel, but without adding cholesterol or vesicles. The conditions promoted the efficient assembly of triangles into icosahedral shells. Magenta: Lipid signal (DOPE-Atto643); Grey: DNA (EtBr)*

3.5 Budding with NeutrAvidin anchors

All budding experiments discussed so far were conducted using triangles hybridised to chol-oligos serving as membrane anchors. Cholesterol is arguably the most popular membrane anchor and has been used many times to anchor DNA nanostructures onto lipid membranes (discussed in section 1.3.3). Its popularity stems from the ease and reliability with which nanostructures can be anchored to the membrane, and a number of studies have aimed to establish design rules for optimal use of cholesterol with DNA origami [53, 99, 113]. For all of these reasons it made sense to first explore membrane budding using a tried-and-tested anchor like cholesterol. Nevertheless, once I could confirm the initial hypothesis that assembly of membrane-bound triangles can induce membrane curvature and budding, I decided to revisit the topic of membrane anchor choice to elucidate the requirements and limitations of the budding process in more detail. As a hydrophobic moiety, cholesterol is practically insoluble in water and will instead self-integrate into hydrophobic environments such as the hydrophobic core of a lipid bilayer. When imagining a simple unilamellar vesicle (i.e. a spherical bilayer with a hollow core) with a homogenous lipid composition, the inner diameter (i.e. the distance between lipid head groups of the inner leaflet on opposing sides of the liposome) must inevitably be smaller than the outer diameter (the

distance between lipid head groups of the outer leaflet on opposing sides) by approximately double the thickness of the bilayer. Consequentially, the surface area of the outer leaflet is slightly larger than that of the inner leaflet. In terms of lipids, this means that the outer leaflet must contain more lipids than the inner leaflet to make up for this difference in surface area. Adding more lipids to just one of the two leaflets leads to an asymmetric area expansion of that leaflet relative to the other, which is accommodated for by altering the shape of the vesicle [114]. This hypothetical experiment bears similarity to the budding assays discussed so far. The GVs were typically composed of just a single lipid species (DOPC, occasionally supplemented with a small fraction of fluorescently labelled DOPE species) and used at isotonic or moderately hypertonic conditions. As discussed in section 3.4, hypertonic conditions significantly improved DCV yields by deflating the vesicles. This reduction in luminal volume at constant membrane area leads to an alteration of the vesicle shape similar to how asymmetric area expansion of one leaflet in respect to the other alters the vesicle shape at constant volume [114, 115]. As triangles are tethered to the vesicles by insertion of cholesterol into the outer leaflet of the vesicular bilayer, attaching a large number of triangles to a single vesicle thus introduces a large number of additional lipid species into the outer leaflet. This raises the question of whether, and to what extent, asymmetric cholesterol insertion contributes to curvature induction and budding of DCVs. Depending on the setup and experiment, DCVs were obtained from triangles carrying 3–9 cholesterols which on first glance appears to be insignificant. However, using area estimates for single DOPC species (0.67 nm^2) and origami triangles (approx. 1400 nm^2), one obtains that cholesterol would be present at a molar fraction of approx. 0.14–0.42 % [116]. Since area expansions of less than 1 % of the total leaflet area may result in significant shape changes, this amount may suffice to contribute noticeably to the budding process [117]. A membrane condensing effect has previously been ascribed to cholesterol in DOPC bilayers, in which the area per DOPC lipid decreases with increasing cholesterol content in the bilayer [116]. Interestingly, at molar fractions below 20 %, cholesterol condenses the total area of the bilayer, shrinking it. This suggests that in our case where cholesterol is only inserted into the outer leaflet of the bilayer, the outer leaflet may contract, forcing the bilayer to bend towards the vesicle lumen (negative curvature inducation). However, since we are using cholesterols chemically linked to a DNA oligo via a hydrophilic spacer, these principles may not necessarily be applicable here as the spacer and DNA oligo increase the overall size of the membrane-interacting unit in comparison to free cholesterol. Supporting this view is a previous observation where tethering DNA origami structures to lipid vesicles using chol-oligos resulted in vesicle tubulation (positive curvature) instead of invagination (negative curvature) [54]. This principle may thus promote budding by covering some of the energetic cost of membrane deformation with the remainder being covered by triangle assembly.

Experimental setup

To elucidate the role of asymmetric leaflet area expansion, I prepared a budding assay in which no foreign molecules are introduced into the bilayer after formation of the vesicles. For this, I included a fraction of 3 % biotinylated DOPE species into the lipid mixture and prepared GVs from it. Biotin is a small molecule that forms extremely strong non-covalent bonds with its protein counterpart avidin [118]. As a tetrameric protein, avidin has four binding sites for biotin and as such can act as a bridge between biotinylated molecules. Instead of hybridising chol-oligos to the single-stranded linker handles on the DNA origami triangle surface, I used DNA oligos with a different sequence coupled to a biotin molecule. Despite sequence differences, once these oligos are hybridised to their respective linker handles on the origami, any observed effects can be directly linked to the type of membrane anchor used. Cholesterol's hydrophobicity is what allows it to integrate into the bilayer and act as a membrane anchor when coupled to a DNA origami structure. However, a side-effect is that cholesterols (like any hydrophobic molecule) have the tendency to aggregate in aqueous environment and may thus likewise cause aggregation of triangles hybridised to chol-oligos. Biotin, in contrast, is a hydrophilic molecule and therefore does not aggregate in aqueous solution. Due to avidin's four binding sites, problems may still occur when four (instead of two) biotins bind to the avidin. For example, a single biotin could link two or more triangles together which would interfere with both their assembly into shells and vesicle binding. Alternatively, when avidin is added to the GV suspension before coupling it to the triangles, it would likely link all the vesicles in the sample together and lead to artefactual results. To circumvent these issues, I treated the biotinylated DNA oligos with a 500-fold excess of NeutrAvidin (a commercially available, deglycosylated avidin variant). This very large excess of NeutrAvidin increases the probability of a single NeutrAvidin binding to just one oligo to near-certainty at the cost of generating a lot of NeutrAvidin waste.

Origami purification by magnetic beads

To remove excess NeutrAvidin, I developed a simple strategy using magnetic beads coated with DNA oligos complementary to specific purification linker handles on the origami triangle surface (which are orthogonal to the linker handles for the biotinylated oligos). In this approach, NeutrAvidin is mixed with triangles already hybridised to the biotinylated oligos. Following a brief incubation step to form the biotin-NeutrAvidin bonds, the magnetic beads are added whose oligos hybridise to the purification linker handles on the triangles. By holding a magnet against the sample tube, the beads will now form a pellet on the tube wall which now allows for the solution containing excess NeutrAvidin to be removed by pipette. The beads can now be washed by adding fresh buffer solution, followed by

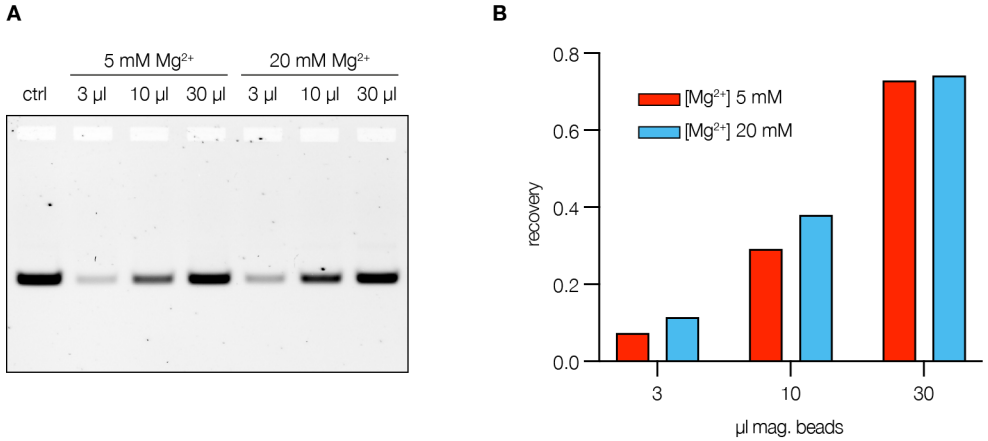

Fig. 3.9: ***Purification of DNA origami triangles using magnetic beads.*** ***(A)*** *Origami triangles are mixed with 3, 10 or 30 µl of magnetic beads coated with ssDNA oligonucleotides. These oligonucleotides are complementary to purification handles on the origami surface and therefore form a duplex. Following four washing steps in which the initial buffer (DMEM, 10 % FBS, folding buffer (FoB) with either 5 or 20 mM $MgCl_2$) was replaced for pure FoB with 5 or 20 mM $MgCl_2$, respectively, the triangles were released by strand displacement using an invader strand and ran on an agarose gel. Compared to an untreated control sample, triangle recovery was highest with the highest volume of beads added, as visualised in* ***(B)****. The Mg^{2+} concentration in the samples does not have a strong influence on the recovery yields.*

resuspension of the beads and pelleting them anew using a magnet. After 4 washing steps, the beads are resuspended in fresh buffer and mixed with an 'invader strand' to detach the origami from the beads by strand displacement. The invader strand is a DNA oligo complementary to the full length of the oligos on the magnetic beads, while the purification handles on the origami triangle are shorter and thus only hybridise to one segment of the bead oligos. As longer DNA duplexes are energetically more stable, the invader strand displaces the purification handles of the origami to form a more stable duplex with the bead oligos, releasing the triangles into solution. As shown in Fig. 3.9, this approach allows for quick purification of origami samples at high recovery yields as long as sufficiently high amounts of beads are added to the sample.

Discussion of results

As the inclusion of biotinylated lipids into the lipid mixtures used to prepare GVs may influence the results, I prepared each sample in duplicates, using triangles hybridised to either chol-oligos or biotinylated oligos coupled to NeutrAvidin (b-NAv). As described above, cholesterol insertion into the bilayer may induce curvature by asymmetric area expansion of the outer leaflet, whereas no insertion and thus no area expansion occurs in triangles bearing b-NAv. TEM and agarose gel electrophoresis both confirm the formation of DCVs using both cholesterol and b-NAv (Fig. 3.10). Interestingly, the distribution between octahedral and icosahedral DCVs was noticeably shifted towards icosahedral species

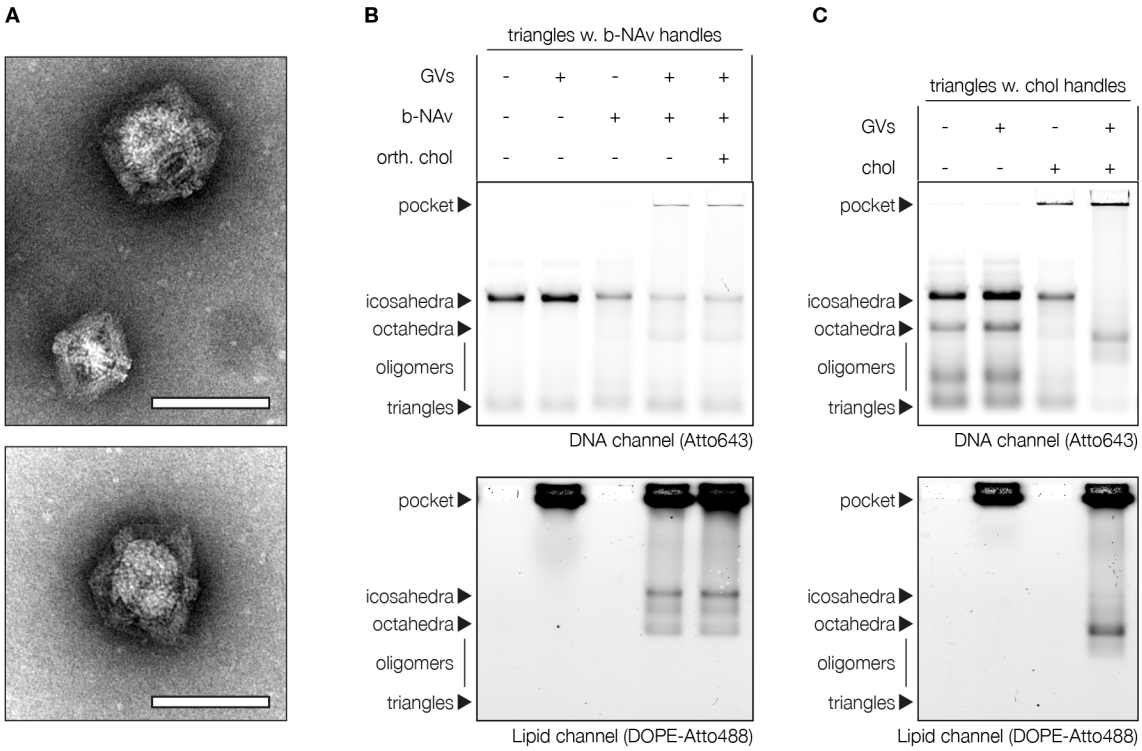

Fig. 3.10: ***DCV budding using biotin-NeutrAvidin as membrane anchor.*** ***(A)*** *TEM micrographs of DCVs obtained using biotin-NeutrAvidin (b-NAv) as membrane anchor. In comparison to the vesicles inside DCVs obtained using chol-bearing triangles, the vesicles here appear spotted due to the proteins. Scale bars: 100 nm.* ***(B)*** *Channel-separated images of an agarose gel showcasing the formation of DCVs from triangles bearing b-NAv-oligos. Addition of orthogonal chol-oligos did not influence the DCV yield.* ***(C)*** *DCVs obtained using triangles hybridised to chol-oligos under the same conditions as the samples in B. Unlike the samples in B, the majority of DCVs here have an octahedral geometry, indicating anchor-dependent differences in on-membrane triangle assembly.*

when using b-NAv, but octahedral species when using cholesterol. Assembly of triangles with unpaired linker handles for cholesterol (i.e. no chol-oligos were hybridised to the linker handles) likewise yielded a significant fraction of octahedral species, which indicates that the unpaired linker handles themselves may interfere with triangle assembly. As this was not the case for triangles with unpaired linker handles for b-NAv, this effect appears to be sequence dependent. Repeating the assembly with linker handles now hybridised to the respective modified oligo, mostly icosahedral shells were obtained regardless of the linker handle sequence. In fact, both chol- and b-NAv-decorated shells appear nearly identical in gel electrophoresis, supporting the idea that unpaired linker handles may interefer with triangle assembly in a sequence-dependent manner. While linker handle sequences used for b-NAv do not appear to influence assembly, the sequences used for chol promote octahedral assembly. However, as this effect does not occur when linker handles are hybridised to their respective modified oligos, DCV samples can still be compared. As was

thoroughly discussed in section 2.2.5, on-membrane assembly promotes formation of octahedra. In comparison to vesicle-free control samples, this observation holds true also for b-NAv decorated triangles, but to a significantly lesser extent. Once inserted into a bilayer, cholesterols themselves should no longer interfere with the assembly. Instead, cholesterol may act through altering the biophysical properties of the membrane, including leaflet area changes or condensing and stiffening effects [116, 119]. However, by being chemically linked to DNA, chol-oligos may not behave in the same way as free cholesterol. When orthogonal chol-oligos are added to a budding reaction using triangles decorated with b-NAv at 4.44 times the amount present in chol-mediated budding reactions, no differences to chol-free DCV buddings were observed. While this result suggest that octahedral DCVs primarily form from triangles hybridised to chol-oligos, it is also possible that not enough cholesterol integrated into the membrane at the budding sites. This is because in chol-hybridised triangles, the positions of all cholesterols are pre-determined by the positions of the linker handles on the origami surface. In contrast, b-NAv triangles carry no linker handles complementary to the chol-oligos, which instead diffuse freely. As a result, not only may chol-oligos aggregate among themselves to reduce exposure of cholesterol to the surrounding water, but the attached DNA oligo may prevent sufficiently high cholesterol densities at the sites of membrane deformation and budding due to electrostatic repulsion from origami triangles. Alternatively, NeutrAvidin itself may participate in curvature generation as has been observed for other membrane-bound proteins [120].

In summary, this experiment has confirmed that insertion of foreign lipid species into the bilayer to alternate its biophysical parameters is not a requirement for DCV budding. Biotin-NeutrAvidin-mediated budding reactions yield noticeably more icosahedral DCVs than those mediated by cholesterol. Unlike cholesterol, NeutrAvidin does not insert itself into the bilayer, but by binding biotinylated lipid head groups it gets very close to it and may disturb its structure locally. As a truly inert membrane anchor is unlikely to exist, anchor-mediated curvature generation or biophysical property altering effect facilitating origami-mediated curvature induction cannot be ruled out. Nevertheless, the successful formation of DCVs using two distinct membrane anchors underscores the versatility of the system, where the choice of membrane anchor can be tailored to the specific environment. This could include receptor-ligand interactions for applications in cells, or click-chemistry linkages in synthetic contexts.

3.6 Budding from vesicles of complex composition

The budding experiments discussed so far have been conducted using GVs composed of mostly DOPC, with only small amounts of chemically modified DOPE species. DOPC membranes are very fluid at physiologically relevant temperatures due to DOPC's sub-

zero °C melting temperature, which, as a consequence, results in an equally low membrane rigidity and thereby facilitates membrane deformation processes [121]. Easily malleable membranes are useful to explore the general feasibility of origami-driven membrane budding, but they do not necessarily reflect the properties of biological membranes which are typically composed of a complex mixture of lipids. The logical next step in the characterisation of DCVs is therefore trying to understand how the composition of the membrane and its biophysical properties affect budding yields. To probe this, I conducted budding assays using GVs of varying lipid compositions.

Choice of lipid mixtures

An important variable to consider when choosing lipids is the lipid geometry. The acyl chain length determines the membrane thickness, and along with its saturation it influences the overall melting temperature of the lipid, and thus the bending rigidity of the membrane [122]. Lipids with a geometry deviating from a cylinder will induce spontaneous curvature in the membrane and locally disrupt lipid packing. The large variety of lipids commercially available facilitates studying complex lipid mixtures, but requires careful selection of promising candidates. Due to the negatively charged DNA backbone, I excluded charged lipids from this study to avoid electrostatic interactions which may alter the attachment of origami triangles to the membrane and additionally cause sample aggregation. Instead, I focused on studying bending rigidity using lipids with melting temperatures above the sample incubation temperature of 37 °C, namely DSPC and DPPC. DSPC differs from DOPC solely by having fully saturated acyl chains, but is otherwise structurally identical to it. This results in a melting temperature of approx. −18 °C for DOPC, but 55 °C for DSPC [123]. DPPC differs from DSPC in its shorter acyl chains (16 vs. 18 carbons), which translates into a slightly lower melting temperature of approx. 42 °C. The melting or phase transition temperature indicates the packing behaviour of lipids in the membrane, roughly differentiating between an ordered "gel" phase below the transition temperature, and a disordered fluid phase above it. At the usual sample incubation temperature of 37 °C, DOPC membranes have fully melted into the fluid phase, whilst DSPC membranes are still within the gel phase. DPPC membranes, in contrast, enter a transitional "ripple phase", which is a special sub-class of the gel phase in which the membrane forms characteristic ripples. As membranes in the gel phase have an increased bending rigidity, these three lipids thus represent three different states of membrane rigidity to test the limitations of origami-driven budding [124].

Binary mixtures of low- and high-melting lipids can provide further insights by altering the overall properties of the bilayer in respect to single-lipid membranes. As the budding system works reasonably well on DOPC membranes, I kept DOPC as the main lipid at 70 mol % and filled up the remainder with either DSPC, DPPC or cholesterol. Unlike DSPC

and DPPC, cholesterol is a sterol which modifies membrane properties including fluidity and permeability [125]. Its effect is context dependent and varies with its concentration in the membrane and its lipid environment [124]. In DOPC membranes, cholesterol increases the packing density of lipids in the bilayer, which results in increased membrane thickness and bending rigidity [116, 119]. Supplementing DOPC membranes with 30 mol % of high-melting lipids or cholesterol may thus alter the ability of origami triangles to shape membrane buds. A special case is ternary lipid mixtures of a high-melting lipid, a low-melting lipid and cholesterol. Under the right conditions, membranes composed of such mixtures can spontaneously demix, forming liquid phases with short-range order (L_o) or disordered phases (L_d) [126]. As phase-separated vesicles combine some of the properties of individual lipid compositions discussed in this section into a single vesicle, they offer an interesting platform to confirm or expand on the data obtained from other lipid mixtures in this screen. Finally, I included lipid mixtures of natural origin into this screen. Unlike the other cases discussed so far, these mixtures are polar extracts obtained from biological sources (namely brain, soy, yeast or *E. coli*). These mixtures best represent the complex composition of biological membranes without potentially interfering components such as membrane proteins. By including these mixtures into this study, we can test the versatility of the budding system while gaining insights into whether or not biological membranes support origami-driven budding in a controlled environment.

Budding from homogenous vesicles

For the budding assays, GVs were prepared from the lipid mixtures to be tested. The swelling buffer was adapted for this experiment. While the GVs for most experiments were produced by swelling of dry lipid cakes in folding buffer with 5 mM $MgCl_2$ and 300 mM NaCl or 320 mM CsCl (FoB5/N300 or FoB5/Cs320, respectively), these buffer compositions failed to produce GVs particularly from some of the natural lipid extracts. Unlike the other mixtures in this screen, these lipid extracts contain a fraction of charged lipids which may interact with the ions in the swelling buffer. To circumvent these issues and to keep the conditions consistent, all GVs in this experiment were produced in TE buffer containing 470 mM sucrose, but no salts. Sucrose is commonly used in vesicle preparations due to its uncharged nature and high density. Because some lipids used in this study have a high melting temperature, all vesicles were prepared at 60 °C to ensure all lipids are in the L_d phase. For consistency reasons, these conditions were used even in lipid mixtures that do not contain any high-melting lipids. With these optimised conditions, GVs could be formed from all lipid mixtures, albeit at varying yields and sizes. Before use, the vesicles were washed by mixing the supension with FoB5/N300 and pelleting the vesicles. This washing step was repeated 2–3 more times.

To keep lipid quantities in the individual budding assays consistent, the lipid content

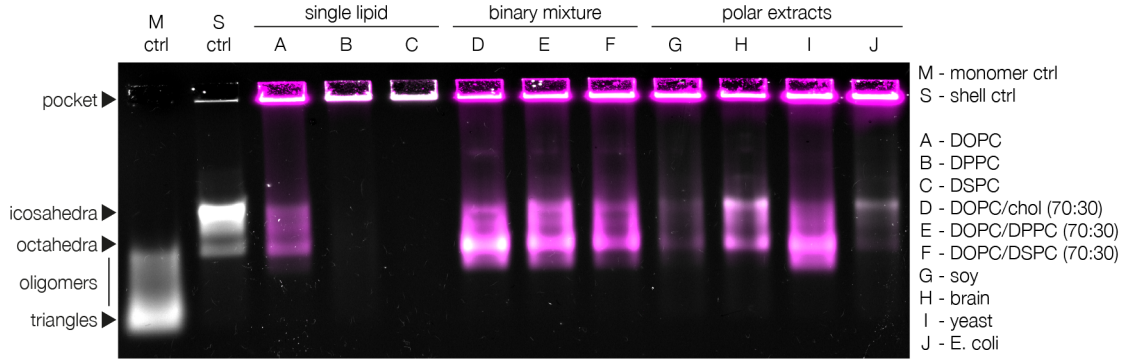

Fig. 3.11: ***DCV budding from GVs of various compositions.*** *Among the tested lipid mixtures, only GVs composed entirely of high-melting lipids prevented DCV formation. Grey: DNA (EtBr); Magenta: Lipids (DOPE-Atto643);*

of the DOPC GV preparation was quantified using a commercial assay based on lipid hydrolysis and subsequent quantification of freed choline species. As this assay cannot be used to quantify non-choline-containing lipid species, the lipid quantities of all the other GV preparations were estimated based on the quantification result for DOPC vesicles. As each lipid mixture used in this screen contained the same mol % of fluorescent Atto643-DOPE, the lipid concentration in each GV preparation was calculated by measuring the fluorescence of Atto643-DOPE in each sample and comparing it to the fluorescence of the DOPC vesicle sample. A drawback of this approach is that it relies on the assumption that the molar fraction of fluorescent lipid species in the vesicles remains unchanged during the swelling process, and that the fluorescence yield is not influenced by the lipid composition of the membrane. To mitigate some of the problems, vesicles were disintegrated by adding detergent at 60 °C before measuring the fluorescence. By dissolving the vesicles, a more even distribution of fluorophore can be achieved to avoid quenching, which would distort quantification results. The budding reaction was conducted as described before, and DCV yields were analysed by agarose gel electrophoresis. DCVs were formed from nearly all the GVs tested (Fig. 3.11). Only GVs composed entirely of DPPC or DSPC prevented DCV formation, which strongly points towards membrane bending rigidity as a major variable. At the assay temperature of 37 °C, DOPC is deep within the (fluid) L_d phase, whereas DPPC and DSPC are still in the gel phase. One might assume DCV yields would therefore be reduced in DOPC vesicles with 30 mol % of either lipid, but the contrary was the case. Similarly, 30 mol % cholesterol did not seem to decrease DCV yields, despite its stiffening effect on DOPC membranes [119]. This result is reproducible even when different amounts of vesicles are mixed with the origami triangles. A possible explanation may be the differences in lipid geometry between DOPC and cholesterol, DPPC or DSPC. With its two unsaturated acyl chains, DOPC is bulkier than any of the other lipids, and this difference in geometry may result in local changes in lipid concentration at the site of a

membrane bud to better accommodate the curvature [127].However, a definite answer to this question requires a more in-depth analysis that is beyond the scope of this work. The influence of the lipid mixture on DCV yields is also reflected in GVs composed of polar extracts of natural origin. Here, differences in lipid composition between the individual mixtures derived from soy, brain, yeast or *E. coli* appeared to allow DCV budding more or less efficiently. Unlike the vesicles of defined composition, these vesicles not only contain lipids with variations in the length and saturation of their acyl chains, but some are also likely to carry a charge. These differences may not only influence the biophysical properties of the membrane, but also the unilamellarity of the vesicles with potentially consequences for budding. Furthermore, the concentration of fluorescently labelled lipids may differ from that in GVs of defined composition. As described before, lipids in individual vesicle preparations were quantified based on the fluorescence of added Atto643-DOPE, but due to the complex nature of polar lipid extracts, the molarity of the lipid stock solutions used to prepare the vesicles is unknown. Instead, the mass concentration of the lipid extracts was equalised to that of the DOPC vesicle stock (approx. 2 mg/ml). As a result, the molarity of fluorescently labelled lipid in the polar extract solutions may deviate from that of the defined stocks (0.8 mol %). Despite these caveats, the formation of DCVs also from GVs of complex lipid composition highlights the versatility of the budding system and indicates that budding off vesicles from cells using DNA nanostructures may be feasible.

Budding from phase-separated vesicles

As discussed, membranes composed entirely of high-melting lipids did not support DCV budding, but when high-melting lipids are included as a minority fraction in an otherwise fluid membrane composed of the low-melting lipid DOPC, DCV yields appeared to increase. The results discussed so far (with the exception of polar extracts) concerned homogenous binary mixtures of DOPC mixed with either DSPC, DPPC or cholesterol at a 7:3 ratio. In the next step, I tested ternary mixtures of DOPC, cholesterol and either DSPC or DPPC. Frequently, lipid membranes composed of a low-melting lipid, a high-melting lipid and cholesterol have been shown to spontaneously phase-separate if mixed at sufficiently high ratios [126, 128]. To not favour one lipid over the other, I fixed the ratio of DOPC, DSPC/DPPC and cholesterol at 40:40:20 mol % and prepared GVs from the resulting mixtures. Phase-separated vesicles yielded noticeably more DCVs than pure DOPC vesicles, reminiscent of how binary mixtures of DOPC and either one of the other components supported budding in the same way (Fig. 3.12, left). An important difference is that due to phase-separation, the majority of high-melting lipid and cholesterol is to be found concentrated within the L_o phase. As discussed before, GVs composed entirely of high-melting lipids did not support budding (see Fig. 3.11) and thus budding is likely to occur mostly (if not exclusively) from the DOPC-rich L_d phase. This fact leads to

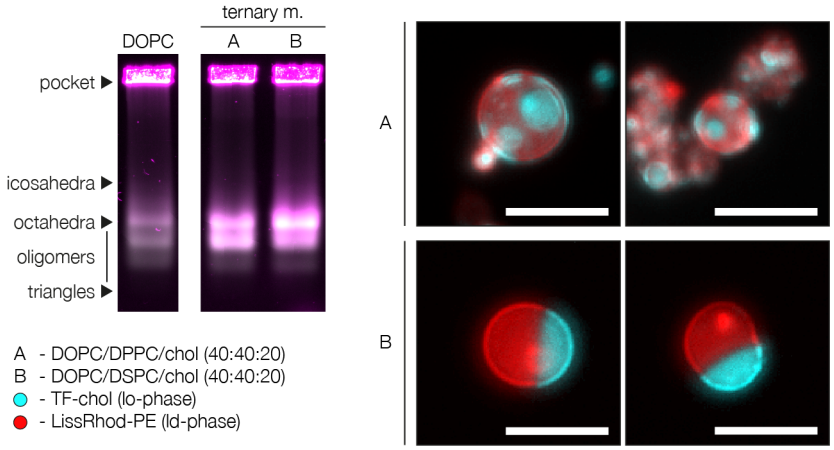

Fig. 3.12: ***Budding from phase-separated vesicles improves DCV yields.*** *Left: Agarose gel comparing DCVs obtained from GVs composed of DOPC or phase-separated ternary lipid mixtures. Phase-separated vesicles yielded more DCVs, suggesting an influence of phase boundaries on the budding mechanism. Grey: DNA (EtBr); Magenta: Lipids (LissRhod-PE); Right: Micrographs of exemplary phase-separated vesicles showing the lipid-ordered (cyan) and -disordered (red) phases. Scale bars: 20 µm.*

the question why DOPC in the L_d phase of a phase-separated vesicle yielded more DCVs than pure DOPC vesicles. According to previous studies, the ternary mixtures used here become miscible at or slightly below the sample incubation temperature of 37 °C [128]. A plausible explanation may thus be that once the samples have reached this temperature, the vesicles no longer are phase-separated. Conflicting with this explanation are fluorescence microscopy images of the vesicles at 37 °C, showing clear phase separation (Fig. 3.12, right). The proximity of the miscibility temperatures (34 °C for the mixture containing DPPC, 37 °C for DSPC) to the sample incubation temperature may, however, allow for some degree of phase-separation to persist particularly in DSPC-containing vesicles. Even so, DSPC-containing ternary mixtures do not perform worse DPPC-containing ones. In fact, they seem to yield a little bit more. As will be discussed in section 3.7, the kinetics of DCV budding are surprisingly fast, with a lot of DCVs forming within the first few minutes. What this means for budding from phase-separated vesicles is that a significant fraction of DCVs forms before the sample solution has equilibrated at 37 °C in the incubator. The line tension at the boundary between two lipid phases represents a defect in the membrane that has previously been described to facilitate fission of membrane vesicles [129]. Triangles might therefore predominantly assemble on and deform membrane patches in the DOPC-rich L_d phase, and subsequently bud off as DCVs in the vicinity of a phase boundary acting as a catalyst for neck scission.

3.7 Budding kinetics

Clathrin-mediated endocytosis exhibits rapid kinetics with previously reported internalisation times being on the order of approx. 0.5–3 min [130–132]. This not only includes the recruitment of clathrin to the cell membrane, but also its assembly to form clathrin-coated pits and neck scission. In contrast, origami triangles require 30–60 min for the first icosahedral shells to form, and up to several hours for the shell yield to plateau [47]. More rapid is the assembly into octahedral shells with good yields after 5 min, and near-completion after about 1–2 h. Although DCVs have the tendency to be octahedral instead of icosahedral as intended (discussed in sections 2.2.3–2.2.5), the triangles used in the kinetic study of octahedral assembly were specifically designed for this purpose with a matching bevel angle and thus differ from the triangles intended for icosahedral assembly used in this thesis. Nevertheless, it is possible that the strong bias towards formation of octahedral DCVs is rooted not least in more favourable kinetics. I based the incubation period of 1–3 d for budding assays on the assembly kinetics of icosahedral shells, paired with the assumption that the energetic penalties of membrane deformation and neck scission would significantly slow down the kinetics and push the yield of DCVs well below the theoretical assembly yield of unmodified triangles not confined to a lipid membrane. Without a sufficiently high number of DCVs in the sample, the fluorescence signal of DCVs in an agarose gel may be too weak for analysis. While longer incubation times may resolve this problem by allowing for more budding events to complete, this comes at the cost of a reduced experimental throughput and loss of kinetic resolution which is needed to study the budding mechanism. As has been discussed in section 3.3, the mechanism behind DCV formation was identified as budding by cryoEM analysis of samples plunge frozen after a shorter-than-usual incubation period. An interesting observation was that despite the shortened incubation period, the sample included not only deformed vesicles but also a large number of completed DCVs (data not shown). Along with the aforementioned fast assembly kinetics of octahedral shells, this raises the question of how the kinetics of DCV budding compare to the kinetics of CME.

Experimental setup

To understand the kinetics of DCV formation, I prepared budding reactions with defined incubation times. As the differences between individual samples in this kinetic sample may be small, pipetting errors may distort the results and must therefore be avoided. Moreover, the composition of each individual sample must remain constant so that the incubation time is the only difference between individual samples. To fulfil these requirements in precision and consistency, I prepared a master mix composed of the individual components of the final sample, most notably chol-hybridised triangles and GVs. The concentration of

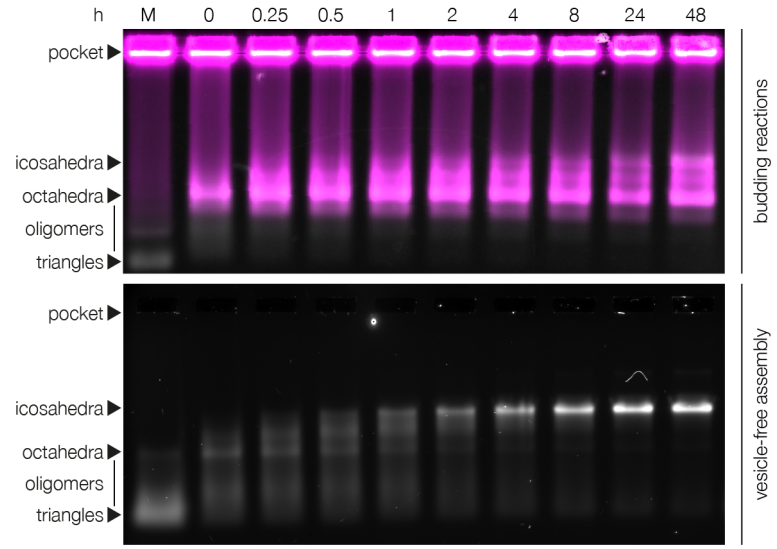

Fig. 3.13: ***DCV budding kinetics.*** *DCV budding kinetics (top) compared against vesicle-free assembly kinetics. DCV budding occurs instantly and yields mostly octahedral species, but at longer incubation times a notable fraction of icosahedral DCVs forms. Grey: DNA (EtBr); Magenta: Lipids (DOPE-Atto643);*

$MgCl_2$ was initially kept low for triangles to bind to the vesicles without triggering assembly just yet. Once the $MgCl_2$ concentration had been increased up to assembly conditions, the mixture was immediately aliquoted and incubated at 37 °C for the desired duration. When an aliquot had reached the desired incubation time, gel loading dye (supplemented with $MgCl_2$ to maintain shell stability) was added to the aliquot and the aliquot was snap frozen using liquid nitrogen. Frozen samples were stored in the freezer until conclusion of the time series. The following incubation times were probed: 0, 0.25, 0.5, 1, 2, 4, 8, 24 and 48 h.

Discussion of results

A significant fraction of octahedral DCVs appears at the 0 h time point, suggesting very rapid budding kinetics (Fig. 3.13, top). Despite the label, it is important to point out that the budding reaction was started as soon as the $MgCl_2$ concentration was increased to assembly conditions. The reaction continued to proceed during all subsequent steps in which the samples were in liquid state (including sample aliquotation, addition of loading dye, freezing in liquid nitrogen, thawing, mixing and gel loading). Despite my best efforts to handle the samples rapidly, the actual incubation time may have been up to 10 min longer than indicated (albeit at room temperature). While this is unlikely to affect samples incubated for longer than 1 h, this discrepancy between theoretical and practical incubation times puts the data obtained for the shorter incubation times into context. As mentioned in the beginning of this section, CME proceeds with rapid kinetics on the order of just 0.5–3 min [130–132]. Based on the present results, DCV budding appears to follow similarly rapid

kinetics. An interesting observation is the appearance of icosahedral DCVs after a couple of hours of incubation, reminiscent of the assembly kinetics of vesicle-free triangles (Fig. 3.13, bottom). In the shown gel of vesicle-free triangle assembly, the same triangles used for DCV budding were hybridised to an unmodified control oligo with identical sequence to the chol-oligo. Like in DCV budding, bands at the expected height of octahedra form early on, but then rapidly mature to icosahedral shells. The kinetics of DCV budding have characteristics of both octahedral and icosahedral shell assembly described in [47]. However, confinement of triangles to the lipid membrane reduces their degrees of freedom and may thus prevent many oligomers from maturing into icosahedra. Although the origami triangles take on the role of molecular scaffolds to deform the membrane, the membrane's biophysical properties are an important factor to consider when trying to understand the distribution between octahedral and icosahedral DCVs. Once DCVs have formed, the final size of the internal vesicle locks the structure in place.

Chapter 4

Inward Budding

In the previous chapter, we saw that assembling membrane-bound DNA origami triangles into polyhedral shells results in membrane deformation and budding. The assembly mechanism used in this work relies on shape-complementary base-stacking interactions, which by itself supplies sufficient amounts of free energy to bend a hypothetical planar membrane into a sphere (discussed in more detail in section 3.1) [40]. While this crude estimate does not paint the full picture, ignoring factors such as neck scission, it provides a theoretical foundation which together with the experimental data supports membrane budding as the mechanism by which DCVs are formed. DCVs bud off with rapid kinetics and from most membrane compositions, being only hindered by membranes composed exclusively of high-melting lipids (see sections 3.6 & 3.7). Nevertheless, most experiments were conducted using GVs composed entirely of the low-melting lipid DOPC to rule out lipid mixture-specific effects. In this simplified model system, both leaflets of the lipid bilayer have the exact same composition, which is not necessarily the case in biological membranes [4]. Furthermore, the induction of curvature on the membrane in response to origami assembly may alter the local distribution of lipids in complex mixtures, favouring lipids whose geometry matches the curvature of the membrane. As DCVs bud off from homogenous DOPC membranes, I hypothesised that DNA origami-induced budding in the opposite direction may have very similar energetic requirements. In this scenario, the assembling shell would shape a membrane bud growing into the lumen of the parent vesicle, resulting in vesicle-coated DNA shells (VCDs) trapped within their respective parent vesicle (Fig. 4.1). The vesicle of a VCD is larger than that of a DCV, which results in a slightly shallower curvature but a larger surface area. In terms of energy, these differences in curvature and surface area cancel each other out such that the energetic cost of bending a flat membrane into a sphere is independent of its radius [103]. Encouraged by these considerations, I explored inward budding of VCDs next.

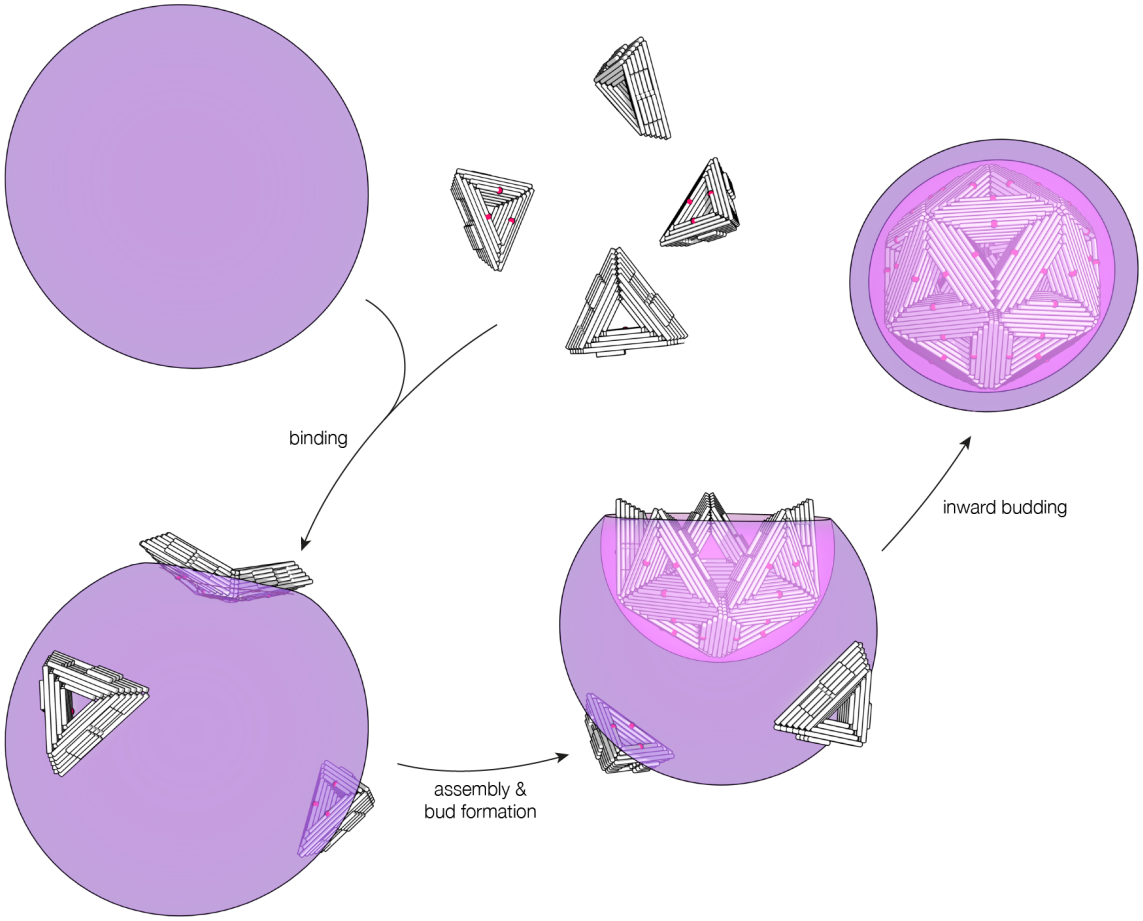

Fig. 4.1: ***Inward budding of DNA origami shells.*** *Triangles for inward budding are functionalised with chol on their top (shell-outward) face. In respect to triangles for outward budding and DCV formation, these triangles bind to lipid vesicles in reversed orientation. Assembly of triangles into shells is triggered by increasing the concentration of $MgCl_2$, which, due to the reversed orientation of the triangles, leads to the formation of inward-facing membrane buds. Spontaneous neck scission finally released a vesicle-coated DNA shell (VCD) into the lumen of the parent vesicle.*

4.1 General principles of inward budding

Outward budding using DNA origami triangles relies on the assembly of membrane-bound triangles into polyhedral shells. The polyhedral assembly product is programmed into the structure of the origami triangle, which features stacking contacts for oligomerisation strategically placed onto its bevelled sides (refer to section 2.1 for details). When two triangles form a dimer, their bottom (shell-inward) faces are angled relative to one another. As more triangles join the assembly, the particle begins to resemble a claw before finally forming a closed shell. In the case of membrane-bound triangles for DCV budding, the claw-like intermediate stage visually conveys outward budding in a very intuitive way (see Fig. 3.5 on page 44). For inward budding, this principle must be reversed. Instead of a claw pulling away membrane material, the origami shell looks more like a clenched fist punching

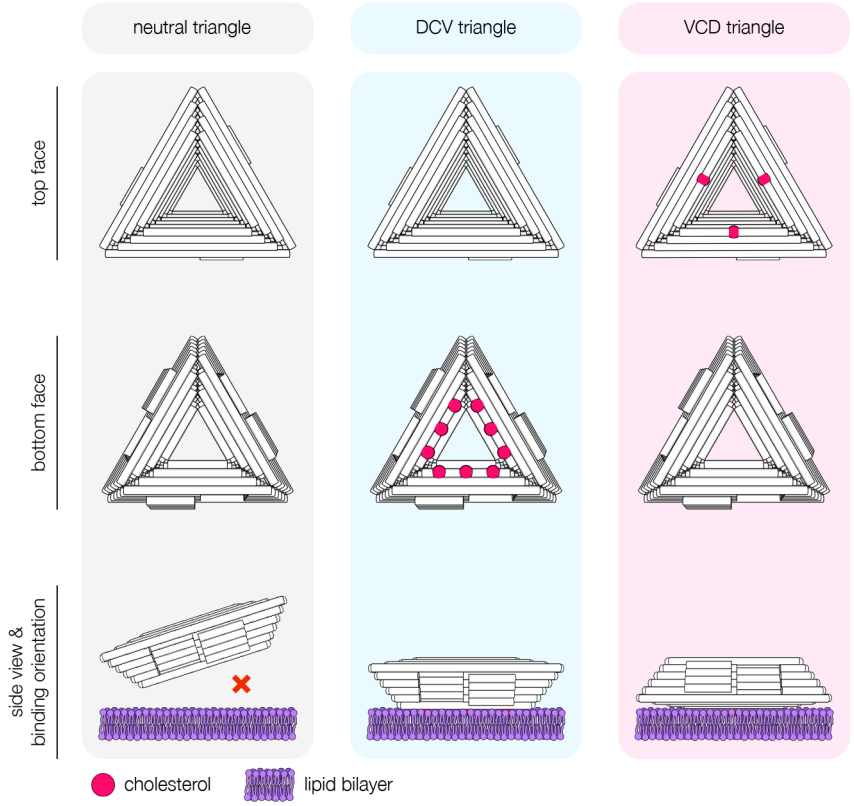

Fig. 4.2: ***Triangle variants and their membrane binding behaviour.*** *Neutral triangles (left) carry no chol-oligos and do not interact with lipid membranes specifically. DCV triangles (middle) carry chol-oligos on their bottom face by which they attach to lipid membranes. VCD triangles (right) have chol-oligos placed on their top faces, and their orientation on the membrane is therefore reversed in respect to DCV triangles. The number of cholesterol on the triangles shown represents commonly used variants chosen to balance out aggregation and stable membrane attachment. When necessary or desirable, the cholesterol count was adjusted within the range of 1–3 cholesterols per side.*

into a vesicle (Fig. 4.1). Despite striking visual differences, physically both processes are governed by the same underlying principles where the free energy of triangle assembly induces curvature on the membrane. Whether positive or negative curvature is induced depends solely on the orientation of the triangle on the membrane. For DCVs, triangles were bound to lipid vesicles by functionalising the bottom (shell-inward) face of the triangle with cholesterol. To reverse the budding direction, the placement of cholesterols on the triangle must be shifted to the top (shell-outward) face (Fig. 4.2). This results in a flipped orientation of VCD triangles on the bilayer in respect to DCV triangles. Dimerisation of VCD triangles therefore forms a dent in the vesicle membrane (as shown in step 2 in Fig. 4.1), in contrast to DCV triangle dimers which induce a bump. As more triangles join the assembly, the dent becomes more and more pronounced, forming a bud. The main difference between inward and outward budding is neck scission. As triangles bind to the outer leaflet of the vesicles, outward-oriented buds may have their necks lined with

triangles from the outside. In this case, the neck sterically hinders the origami shell from closing which is reflected by the occasional appearance of scars on DCVs (see section 3.3). During inward budding, closure of the origami shell requires bridging the width of the neck with a triangle. The high curvature at the neck may pose a kinetic bottleneck as the angle between triangles inside the neck and those already part of the assembling shell could be greater than 180°. Neck scission is reliant on thermal fluctuations in both budding directions, and the whole process may thus share more similarities than apparent on first sight.

An important difference between DCVs and VCDs lies in the methodological toolkit available to study both particles in more detail. DCVs are easier to study than VCDs as all components are addressable. In VCDs, however, the DNA shell is entrapped within two vesicles (or one if the parent vesicle collapsed). Agarose gel electrophoresis for analysis of DNA exploits the negatively charged backbone to separate DNA fragments by size. However, electric fields interact with GVs, deforming them or creating transient holes in the membrane (electroporation) [133]. These effects may distort results with apparent VCD yields differing from actual VCD yields before an electric field was applied. Another potential problem is that commonly used DNA stains like ethidium bromide cannot be used with VCDs, as the dye must pass through the lipid membrane to stain the encapsulated DNA shell. While this is not unimaginable particularly due to electroporation, staining may be too low and uneven to draw conclusions from it. As a workaround, the origami triangles must be labelled using fluorescently labelled oligonucleotides hybridised to an additional set of linker handles on the origami. However, all of these considerations assume that the majority of VCDs are able to enter the gel. As was shown in Fig. 4.1, the inward-oriented budding direction inevitably traps VCDs within the lumen of their parent vesicles. It is furthermore unclear if VCDs whose parent vesicle collapsed and which are therefore freely dispersed in the sample solution can enter the gel. The lipid envelope not only increases the size of the overall particle, but it may also retard particle migration by other effects such as electrofusion of two VCDs, in which two vesicles are fused by exposure to an electric field [133]. As this increases the size of the overall particle, the particle may become too laFrge to migrate deeper into the gel. For all of these reasons, gel electrophoresis is not a suitable method to study VCD formation. Aside from gel electrophoresis, TEM is another useful method to study nanoscopic particles. To increase the contrast of biological samples, samples are frequently stained using heavy metal salts prior to imaging (detailed in section 1.4). The advantage of negative staining TEM (ns-TEM) lies in its simplicity and good contrast, but the staining procedure and subsequent drying is known to damage and alter the appearance of lipid vesicles. For this reason, membrane deformation upon DCV-triangle assembly was studied by cryoEM of vitrified samples (section 3.3). While this method allows imaging of samples in their native state, sample preparation is more

time consuming and technically challenging. The particular structure of VCDs, however, necessitates analysis by cryoEM. The lipid envelope acts as a protective barrier shielding the DNA shell on the inside from the heavy metal stain used for negative staining. As a result, the particle as a whole is stained but not its internal structure, thus VCDs become virtually indistinguishable from empty SUVs.

In summary, VCDs and DCVs share many similarities. Despite the reversal of the budding direction, the induction of curvature, shaping of a membrane bud and the overall energetic cost of the process on DOPC model membranes are very similar between both budding processes. A major difference between VCDs and DCVs is that the DNA shell of VCDs is fully engulfed within a lipid vesicle, and thus its origami components are no longer addressable from the outside. Furthermore, unless the parent vesicle is damaged, VCDs can be assumed to accumulate in its lumen, further complicating their detection. As a label-free method, cryoEM is the method of choice to study inward budding by DNA origami triangles.

4.2 Generation of vesicle-coated DNA shells

As was outlined in section 4.1, DNA origami-mediated inward budding can be considered to proceed analogous to outward budding, requiring only a change in the placement of membrane anchors on the surface of the triangles. Outward budding itself presented itself as a robust mechanism relying mostly on stable membrane tethering and triangle assembly, and the number of cholesterols on the triangle did not seem to play a major role. To reduce the likelihood of aggregation, I placed only three linker handles for chol-oligos on the top (shell-outward) surface of the triangles to be used for inward budding (as depicted in Fig. 4.2, p. 65). Following hybridisation of the linker handles to the chol-oligos, the triangles were mixed with LVs to attach them to the vesicle surface. The LVs were produced by pushing GVs through a porous membrane with an average hole diameter of approx. 200 nm. This ensures that the vesicles are large enough to contain a VCD with a putative size of a bit more than 100 nm in their lumen, but small enough for analysis by cryoEM. The remaining steps are identical to those of outward budding reactions: The concentration of $MgCl_2$ was increased to trigger shell assembly, the sample was then incubated at 37 °C for up to 3 d and finally it was vitrified on a TEM grid for subsequent analysis by cryoEM. As is shown in fig. 4.3A, this procedure indeed yielded VCDs with the expected morphology. Interestingly, some VCDs display scars similar to DCVs (see fig. 3.5, p. 44), implying neck closure across the (occasionally large) gap in the origami shell. Possible explanations may involve non-specific attraction between the origami and the bilayer (similar to that discussed in section 2.2.6) or triangles not participating in the shell assembly acting as bridges across the gap, but the exact mechanism remains elusive.

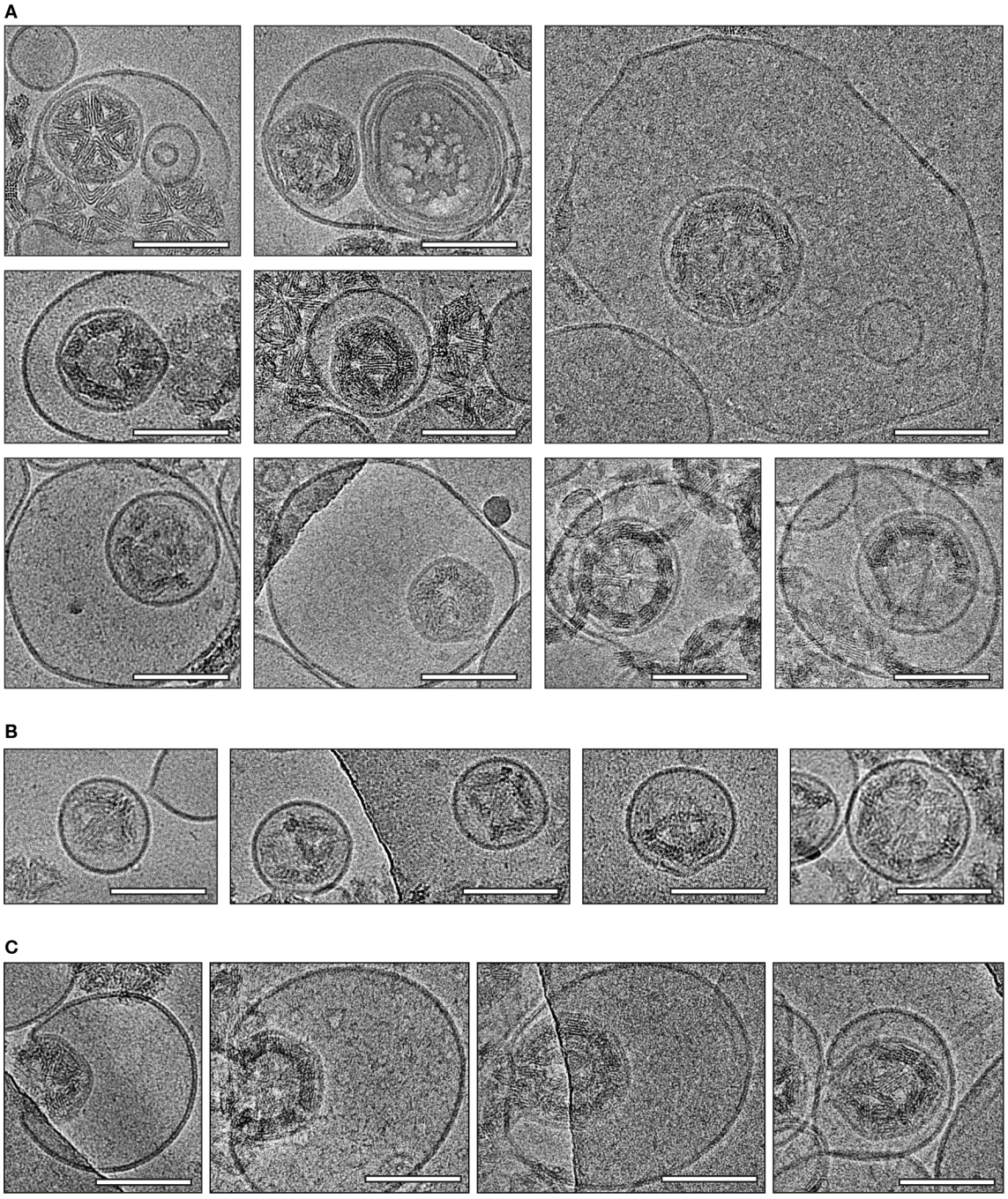

Fig. 4.3: ***VCDs are formed by budding into a parent vesicle.*** ***(A)*** *CryoEM micrographs of VCDs trapped within their parent vesicle.* ***(B)*** *CryoEM micrographs of free VCDs no longer entrapped within their parent vesicle. Shown are octahedral and icosahedral shells, some of which are not complete.* ***(C)*** *CryoEM micrographs of LVs deformed by assembly of membrane-tethered triangles. The degree of induced curvature increases from left to right, ranging from inward-oriented bumps to membrane buds with almost fully-engulfed DNA shells connected to the parent vesicle by a narrow neck. All scale bars: 100 nm.*

The geometry of the DNA shell inside VCDs is typically icosahedral. While octahedral DNA shells can also be found, they are rarer than icosahedral shells which contrasts with typically octahedral shape of DCVs. As discussed in section 2.2.5, this morphological shift occurred only when triangles were assembled on the vesicle membrane and not in samples barring any lipid membranes, suggesting interactions between the triangles and the membrane as the cause. For the triangles to assemble into octahedra instead of icosahedra, the dihedral angle between the bottom (shell-inner) faces of two triangles must be steeper (i.e. two planar triangles must be tilted more towards one another) than designed. In DCVs, placement of cholesterols on the triangles is such that the bottom faces interact with the membrane, which may thus mediate the necessary changes in the dihedral angle. The triangles used for VCDs bind to the membrane with their top (shell-outer) faces which might explain why a lot fewer octahedra form. However, the same principles that promote formation of octahedral DCVs may also alter the shape of the DNA shells within VCDs. By orienting the top (shell-outer) face of the triangles towards the membrane, membrane interference may result in a shallower dihedral angle and thus shells that are larger than a typical icosahedron. Indeed, the large panel in fig. 4.3A shows a VCD with an enlarged DNA shell, supporting this hypothesis. In addition to VCDs entrapped within their parent vesicles, cryoEM analysis also revealed the existence of free VCDs (Fig. 4.3B). Their morphology does not differ from that of any other VCD, but they are not entrapped within a parent vesicle. It is likely that these VCDs formed by budding into a parent vesicle, but were freed when the parent vesicle burst.

The particular appearance of VCDs and their (usual) entrapment within a larger vesicle immediately suggests formation by budding through the parent membrane. Analogous to DCVs, I studied the formation of VCDs by cryoEM, aiming to capture intermediate steps of the budding process. While the kinetics of VCD budding are unknown, DCVs form with rapid kinetics within minutes (see section 3.7). Nevertheless, intermediate steps of DCV budding could be captured by reducing the incubation time to just a couple of hours instead of days. For VCDs, triangle assembly times were shortened to approx. 5 hours or one night before vitrification. As before, LVs (prepared by extrusion through a 200 nm pore membrane) were used as model membranes, and the number of cholesterols per triangle remained at 3 moieties to reduce sample aggregation. As for DCVs, these conditions enabled the acquisition of micrographs showing membrane deformation and bud formation, proving budding as the underlying mechanism behind VCD formation (Fig. 4.3C).

4.3 Bivesicular shell systems

The work presented thus far shows that assembly of membrane-bound DNA origami triangles can induce curvature and budding with programmable directionality. Just by changing

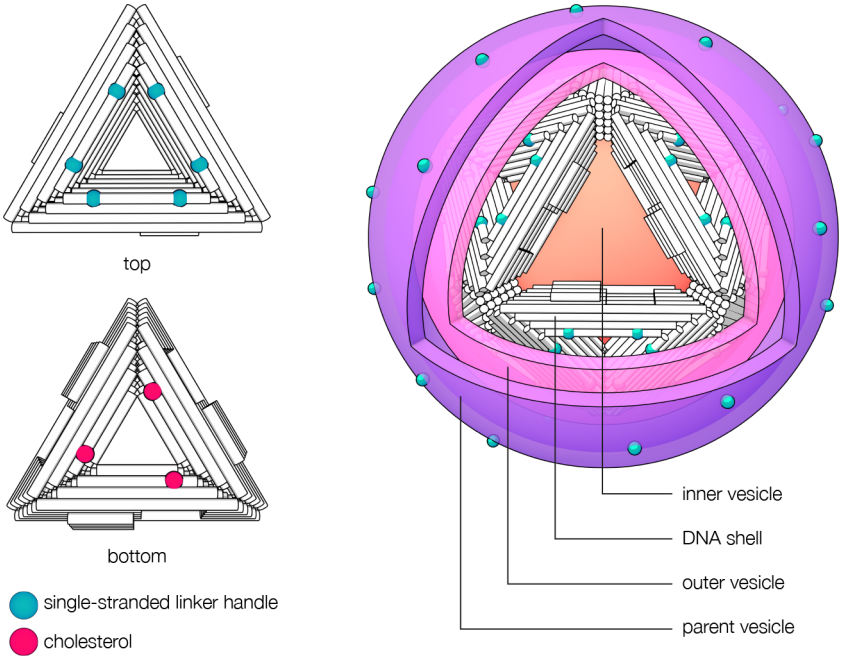

Fig. 4.4: ***Schematic representation of VCDCVs and the triangle used in this experiment.*** *VCDCVs combine features of both DCVs and VCDs. As such, the DNA origami shell engulfs a vesicle and is itself engulfed by another vesicle. As VCDs, VCDCVs are trapped within their parent vesicle. Two sets of linker handles with orthogonal sequences allow splitting up the the entire process into two separate budding reactions.*

the position of cholesterol moieties on the triangle surface, the budding direction can be altered, giving rise to DCVs or VCDs. As the vesicle of DCVs is coated with DNA origami triangles, these remain addressable and their unchanged size in comparison to empty shells of the same geometry allows for easy quantification and comparison by agarose gel electrophoresis. An interesting consequence of the conserved addressability or accessibility of the origami shells of DCVs is that the triangles of DCVs can, in principle, be redesigned to feature unpaired linker handles on their outer faces. This would enable DCVs themselves to induce curvature on a fresh batch of vesicles that culminates into inward budding. The resulting structure would be a crossover between DCVs due to engulfing a vesicle, and VCDs because of the vesicle surrounding the origami shell (Fig. FIG). Like other VCDs, most of these crossover structures would be trapped inside their respective parent vesicle. To distinguish these particles from ordinary VCDs, they will be called vesicle-coated, DNA shell-coated vesicles (VCDCVs) to emphasise their similarity to both VCDs and DCVs.

DCVs and VCDs were assembled by first tethering triangles onto a vesicle choosing either the bottom (DCVs) or top (VCDs) triangle faces to carry cholesterol anchors. Next, the concentration of $MgCl_2$ was increased to trigger triangle assembly, and after an incubation period at 37 °C, the samples were analysed. Given the complexity of the origami structures and budding processes in general, the experimental setup is surprisingly easy and

was generally conducted in a one-pot reaction. This is possible owing to the programmability of DNA nanostructures, which enables precise placement of membrane anchors on the origami surface. As a consequence, all triangles that bind to the vesicle membrane in a specific manner have the same orientation and can thus, in principle, form dimers. Triangles for the assembly of VCDCVs must, in contrast, carry linker handles for membrane anchors on both of their faces. In one pot reactions where all linker handles on both faces are hybridised to chol-oligos in the same step, the orientation of membrane-bound triangles would appear random. Moreover, when the cholesterols on one triangle face are inserted into the membrane of a lipid vesicle, the cholesterols on the opposing face might aggregate with other triangles or bind to another vesicle, forming aggregates of vesicles with interspersed triangles. As a result, the yields of DCVs and VCDs would not only be extremely low, but VCDCVs are unlikely to form at all. For this reason, I decided to split up the assay into a two-step reaction. In the first step, only the bottom (shell-inner) face would be hybridised to chol-oligos to promote the specific formation of DCVs. Thereafter, in the second step, the outward-facing linker handles would be used to trigger inward budding of the DCVs. The first step does not differ from any other outward budding reaction and thus all the known characteristics such as rapid kinetics would still apply. This is not true for the second step, however, as unlike ordinary inward budding reactions, the molecular scaffold initiating membrane deformation no longer is monomeric triangles but DCVs. This circumstance has a number of important consequences for the experimental design, and two major issues must be addressed: (1) the suitability of vesicles for inward budding of DCVs, and (2) the consecutive dilution of the origami in each step.

Membrane requirements for inward budding using DCVs

Triggering inward budding by hybridising chol-oligos to the outward-oriented linker handles on DCVs has several disadvantages. For DCV budding, chol-oligos are hybridised to the bottom face linker handles at low magnesium concentrations (5 mM). These conditions ensure the stability of the origami structure whilst retaining electrostatic repulsion between individual triangles. Electrostatic repulsion can also be exploited to reduce or virtually prevent cholesterol-mediated aggregation of triangles hybridised to chol-oligos by cleverly positioning cholesterol moieties closer to the "core" of the structure (illustrated in Fig. 2.5, p. 26; for theoretical details on DLVO-theory, refer to section 1.3.2). When the concentration of magnesium cations is increased for shell assembly, the negative charges are screened enough for two triangles to come close enough for dimerisation. This, however, also means that cholesterols hybridised to the free linkers on the outside of the DNA shell may now interact with those on other shells, causing aggregation. At the same time, the $MgCl_2$ concentration cannot be lowered as this may cause shells to fall apart. DCVs must therefore by hybridised to chol-oligos at elevated $MgCl_2$ concentrations. As DCV solutions

also contain lipid vesicles, this may cause several problems: Firstly, cholesterol may not only promote aggregation of vesicles and individual DCVs, but a large fraction of chol-oligos will bind to the vesicles before hybridising to the linker handles with unknown outcomes. To prevent aggregation, chol-oligos can also be mixed with lipid vesicles before adding DCVs to the sample solution. Instead of attaching DCVs to the vesicles by cholesterol insertion, this strategy has DCVs attach to chol-oligos already anchored in the membrane by simple DNA-DNA hybridisation. This strategy also deals with a second problem: without the assembly of membrane-tethered triangles into shells, the free energy to induce curvature on a vesicle must be provided by other means. While it is plausible that insertion of cholesterols into the bilayer may suffice to make curvature induction favourable, this approach may require increasing the number of cholesterol per triangle to guide the membrane to wrap around the DNA shell in small steps. However, the approach chosen here generates energy by DNA-DNA hybridisation, which can easily be enhanced by increasing the length of linker handles and chol-oligos if needed.

As already mentioned above, adding chol-oligos to the DCV solution would result in some chol-oligos hybridising to the DCVs, and others first inserting into a membrane before hybridising to a linker handle. Another potential problem is that any triangles still bound to the vesicles from the first step could interfere with inward budding. It is therefore necessary to mix DCVs with fresh vesicles for inward budding. By mixing these with chol-oligos first, DCVs will bind to the vesicles by hybridising to the chol-oligos already inserted in the vesicle membrane. Like VCDs, VCDCVs require analysis by cryoEM which necessitates the use of LVs instead of GVs. One strategy could involve using GVs in the first step, and LVs in the second step to separate the vesicle ultimately analysed by cryoEM also by size.

The reduction of origami concentration and its consequences

The exact yield of DCVs is difficult to determine, but considering that some triangles will form chol-mediated aggregates while others fail to form sufficiently curved membrane buds, it can be assumed to be well below 100%. Furthermore, by mixing triangles, vesicles and $MgCl_2$ solution, the concentration of triangles is reduced in respect to the stock solution. Finally, assembly into octahedral or icosahedral DCVs lowers the number of individual particles, as 8 or 20 individual triangles form only a single shell. If using the product of a DCV budding reaction like a triangle stock solution for inward budding, the concentration of DNA origami in that step would yet again be lowered for the same reasons just mentioned (non-ideal budding yield, dilution of origami particles by mixing with fresh vesicles etc.). If the particle density in the sample solution is too low, there may not be enough particles for analysis by cryoEM. Because of this, the concentration of DCVs after the first budding step must be increased before the solution can be used for inward budding.

Experimental procedure and results

As outlined above, VCDCVs are produced by inward budding of DCVs. The first step in this process is thus an ordinary outward budding reaction to generate DCVs from DNA origami triangles tethered to GVs as discussed in previous sections. A relatively large volume was prepared to obtain sufficient quantities of DCVs for the subsequent steps, in which partial loss of DCVs is to be expected. The composition of the sample after the first step is a mixture of triangles, empty shells, DCVs and vesicles. As only origami particles (specifically DCVs) are needed for the inward budding reaction, vesicles were removed by low-speed centrifugation. The much larger size of GVs means that at low centrifugation speeds GVs will pellet before the DCVs, and the vesicle-depleted supernatant was then separated from the pellet. The solution was then ultracentrifuged to pellet any other particles, including DCVs. Much of the supernatant was pipetted off from the top and discarded, leaving only the origami concentrate at the bottom in the tube.

LVs to serve as parent vesicles for VCDCVs were mixed with chol-oligos to integrate these into the vesicle membrane. As the DCV concentrate has to be kept at high magnesium concentrations to retain shell stability, the LV suspension was adjusted to the same salt conditions before use. The inward budding reaction was finally started by mixing DCVs and LVs. This is a big difference between VCDCV budding and VCD budding, as in the latter the budding reaction is triggered by increasing the $MgCl_2$ concentration to overcome electrostatic repulsion between the individual triangles. As the VCDCV budding reaction does not involve origami assembly, its kinetics could be even more rapid than that of DCVs. However, as this is purely speculative I nevertheless incubated the budding reaction overnight at 37 °C before vitrification.

CryoEM analysis of samples prepared in this way confirmed the formation of VCDCVs (Fig. 4.5 A). However, the yield of VCDCVs was much smaller than that of DCVs and VCDs, and particles were generally heavily aggregated (Fig. 4.5 B). Because of this aggregation, it is difficult to determine if the low yield is a result of particle aggregation or inefficiency of the experimental setup. Without free cholesterol moieties attached to the origami, the likeliest mediator of aggregation appears to be the yet unpaired linker handles. The linker handle sequences were designed to not form hairpins (non self-complementary), thus on first glance shells may aggregate by bridging two vesicles with linker handles on opposing halves of the shell. On second glance, aggregates do not seem to have any order, and shells appear to also form aggregates with one another indicating a problem with the linker handles themselves. The triangles that were used in this experiment carried, in addition to six linker handles matching the sequence of the chol-oligos inserted into the vesicle membrane, nine linker handles for optional hybridisation with an Atto643 fluorescently labelled oligo (A643-oligo). As detection by fluorescence was not planned in

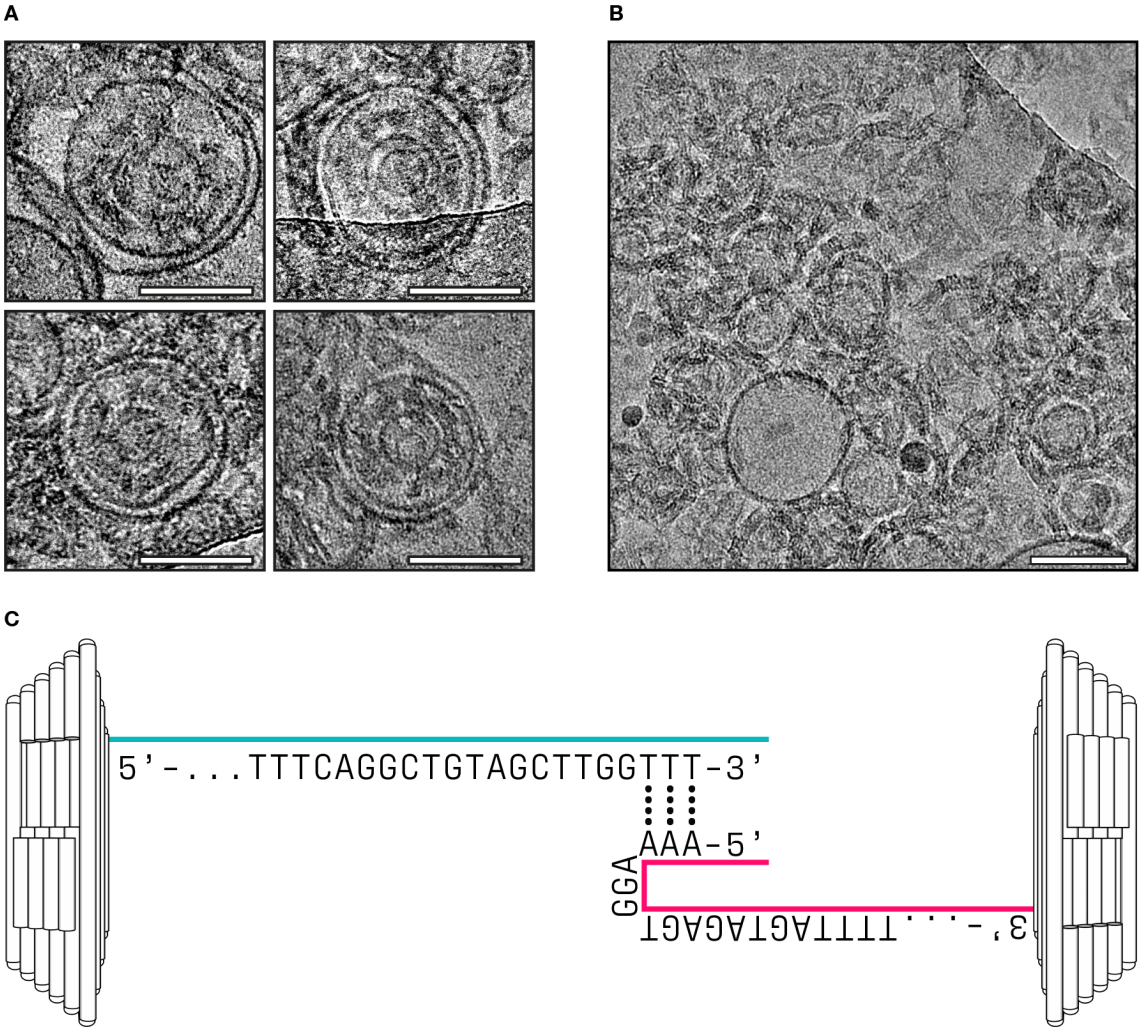

Fig. 4.5: ***VCDCVs and aggregated origami.*** ***(A)*** *CryoEM micrographs of VCDCVs showing characteristic layering. Going from outside to inside,these are the parent vesicle, outer vesicle, origami shell and inner vesicle.* ***(B)*** *CryoEM micrograph showing aggregated DCVs, origami triangles and vesicles.* ***(C)*** *Schematic representation of a potential cause of the observed aggregation mediated by partial complementarity of linker handles. For simplicity, only one interaction is shown, but each triangle carries six linker handles for chol-oligos (red) and nine linkers handles for A643-oligos (teal). All scale bars: 100 nm.*

this experiment, they remained unpaired. Like linker handles for cholesterol, these linker handles were also designed to not interact with one another, but they could nevertheless be causing the aggregation issues. The sequence extending from the origami surface begins and ends with three thymidines. The terminal thymidines are not included in the sequence of A643-oligos and would thus remain unpaired even if the fluorophore had been added. These thymidines are in addition to 4 spacer thymidines on the cholesterol linker handles (refer to Fig. 2.6 on p. 28 for a scheme). Thymidines are a popular choice for single-stranded segments because of their comparably weak interactions [99], but they can

nevertheless form hydrogen bonds with unpaired adenines which must therefore be prevented. However, as the linker handles for cholesterol terminate with four adenines, the linker handles for chol-oligos and A643-oligos could weakly interact, forming at least six A-T pairs (Fig. 4.5 C). The large number of potential interactions (six chol-A643 linker handle interactions per triangle, 8-20 triangles per shell) provide avidity which strengthens the overall bond and promotes aggregation.

In summary, the formation of VCDCVs could be confirmed by cryoEM, but because of heavy particle aggregation most likely mediated by unpaired linker handles, the efficiency of this budding interaction remains unknown. Nevertheless, this data acts as a proof of concept illustrating the versatility of the DNA origami-based budding system.

Chapter 5

Conclusion and outlook

The data presented in this thesis demonstrates the controlled and programmable induction of curvature on lipid vesicles by the self-assembly of membrane-bound DNA origami nanostructures into polyhedral shells. Budding does not occur spontaneously due to a very high energetic penalty (with estimates ranging up to 500 k_BT) and therefore calls for active membrane processes [26]. In the synthetic budding machinery presented here, DNA origami triangles take on the role of a molecular scaffold to remodel the membrane geometry. Previous research established similar hybrids by either coating vesicles with DNA nanostructures [50], growing lipid vesicles around the DNA origami [67] or ripping out membrane material by DNA hybridisation [134]. The main difference to these studies is that the work presented herein provides, to the best of my knowledge, the first example of a fully synthetic membrane budding system not relying on components of natural budding machineries. This claim is supported by visual data in the form of cryoEM micrographs, and by the system's properties which in sum point towards an active membrane process. For example, the finding that DCV yields are strongly enhanced under hypertonic conditions implies that the system benefits from a reduction of membrane tension and the generation of excess membrane area. This fits the narrative of curvature induction preceding DCV formation and is echoed by biological budding machineries such as clathrin-mediated endocytosis [110]. The self-assembly of DNA origami triangles into polyhedral shells mediated by shape-complementary base-stacking interactions provides sufficient free-energy to overcome the energy barrier and guides the budding process (as detailed in section 3.1). In summary, the presented budding system is backed by experimental data, validated by theoretical considerations and integrated into the published scientific literature.

5.1 Parallels and differences between inward and outward budding

According to Helfrich's hamiltonian, the energy required to bend a planar membrane into a spherical vesicle is independent of its radius [103]. In the special case of bilayers composed of a single lipid species, one can deduce that the energetic cost of shaping inward- and outward-oriented membrane buds is extremely similar, if not identical. As a consequence of this I could fairly easily produce VCDs once I had established a robust protocol for outward-directed budding reactions. The most important difference between both types of budding reactions lies in the positioning of cholesterol moieties on the triangle surface. It governs the directionality of the reaction and decides which type of particle is produced. Nevertheless, the theoretical similarities do not mean that the type of triangle variant used in an experiment is the only thing to consider in practice. As the lipid envelope of a VCD lines the DNA shell from the outside, its radius is necessarily larger than that of the vesicle entrapped within a DCV. While it is clear that each budding event removes membrane material from its parent vesicle, the relative amount that is removed is larger for VCDs than DCVs. Experiments probing the influence of osmotic conditions on DCV yields showed that while budding does occur at iso- and hypotonic conditions, it is greatly enhanced at hypertonic conditions. This demonstrates the influence of excess membrane area and membrane tension on the deformation process. The observed relationship between tonicity and DCV yield where greater relative differences to the isotonic baseline translate into greater DCV yields further suggests that the number of DCVs a single vesicle can give rise to is limited. Considering each budding event removes some of the excess membrane material established under hypertonic conditions, one can assume that the membrane tension of the parent vesicle will eventually start to increase until the energetic cost of shaping a bud exceeds the energy that can be supplied by triangle assembly. The slightly larger surface area of VCDs may then translate into fewer possible budding events before membrane tension prohibits further budding. As DCVs often assume octahedral geometries with much smaller cavities than within icosahedral shells, this may further increase the discrepancy of possible budding events between VCDs and DCVs, albeit at the cost of luminal volume. Another practical limitation is the available space within a parent vesicle. As VCDs bud into their parent vesicles, the maximum number of budding events is limited by the volume of a VCD versus the volume of the parent vesicle. Considering the volume of a sphere scales to the cube of the radius whereas its surface area scales to the square, this limit is unlikely to be reached in a GV before membrane tension catches up. However, it may be of relevance in much smaller vesicles such as the LVs that were used for cryoEM analysis of VCDs whose diameter (+/− 200 nm) is insignificantly larger than VCDs (+/− 110 nm). In fact, triangles shaping a membrane bud on a vesicle already containing a VCD with not

enough available space to take up another one may be involved in vesicle rupture, setting the VCD free (as seen in Fig. 4.3, p 68). The lamellarity of the vesicle may influence budding efficiency in a similar way. Multilamellar vesicles reduce the available volume for inward budding to the space in between the two outermost bilayers and may thus limit budding events by volume even in larger vesicles. Similarly, inner lamellae may limit the extent by which the outermost bilayer can shrink by removal of membrane material during DCV budding. The reduced volume in between the outermost lamellae may lead to a more rapid build up of membrane tension, limiting the number of additional budding events that can take place.

5.2 The case of octahedral assembly

An unexpected finding was the altered assembly behaviour of triangles during outward-directed budding assays. Although the triangles should assemble into icosahedra by design, attachment of cholesterol to the bottom face and attachment to membranes both promoted assembly into octahedra instead. For free triangles, the assembly into octahedra directly depended on the reach of cholesterol moieties (detailed in section 2.2.4). This suggests hydrophobic interactions between cholesterols of neighbouring triangles which "pull" both triangles together, making steeper dihedral angles energetically more favourable. Limiting the reach of chol-oligos solved this issue by spatially preventing these interactions to occur. However, chol-mediated aggregation still occurred in the form of "sandwich dimers" where two triangles are stuck on top of one another by their chol-decorated faces. A similar effect occurred when free triangles were assembled with unpaired linker handles (shown in Fig. 3.10 C, p. 53). Depending on the sequence of the linker handles, triangles assembled into either icosahedra or a mixture of icosahedra and octahedra. This suggests that weak interactions between linker handles may stabilise steeper dihedral angles similar to chol-chol interactions, providing further evidence for the proposed mechanism. Octahedral assembly also occurred when triangles were assembled on membranes for outward-directed budding (section 2.2.5). Limiting the reach of chol-oligos did not help here, and since all chol moieties can be assumed to be integrated into the lipid bilayer, hydrophobic interactions are unlikely to play a relevant role here. On the other hand, outward budding using biotin-NeutrAvidin interactions yielded significantly more icosahedral DCVs than cholesterol, implying that the type of membrane anchor does play a role (section 3.5 & Fig. 3.10 B, p. 53). Unlike chol-oligos, b-NAv oligos provide a greater separation between the lipid membrane and the DNA oligo, and no additional lipid species are inserted into the bilayer. The latter may induce curvature and has been named as a potential cause for tubulation of lipid vesicles in response to high-densities of DNA nanostructures tethered to the membrane via cholesterols [54]. On a similar note, certain lipid mixtures appeared to support

assembly into octahedra more than others (Fig. 3.11, p. 57). An interesting example is that (octahedral) DCV yields were much higher in membranes containing 30 mol% cholesterol compared to pure DOPC membranes. This observation directly links cholesterol and formation of octahedral DCVs. The inhomogeneous structure of membranes composed of many lipids may be less prone to alterations in response to cholesterol insertion than more homogenous membranes composed of only one or two lipids. Supporting this hypothesis is the finding that some of the lipid mixtures tested yielded a lot more icosahedral DCVs than others. Furthermore, interactions between the DNA origami and charged lipids and the overall physical properties of the membrane (particularly its bending modulus) are likely to be important variables influencing the geometry of DCVs. The kinetics of DCV budding revealed that octahedral DCVs form very rapidly, whilst icosahedral DCVs take many hours to appear (section 3.7). One reason could be the greater complexity of icosahedra (20 triangles) requiring more time to assemble than octahedra (8 triangles), echoing previously reported kinetics [47]. However, membrane-confined assembly is very different from assembly of free triangles. For example, alterations of membrane properties such as membrane tension or triangle density at later stages of an experiment might explain why icosahedra appear later in the process. The density of triangles on the membrane is a lot higher than in solution, and triangles may thus be pushed by other triangles into steeper angles, promoting the formation of octahedra. Electrostatic effects may also play a role, as higher-than-needed concentrations of $MgCl_2$ promote octahedral assembly even of free triangles in absence of cholesterol (Fig. 3.7, p. 47). In addition, the salt conditions during the assembly stage promote adsorption of triangles onto DOPC membranes, potentially altering the membrane structure. It is known that protein adsorption may alter the membrane shape, and an analogous mechanism may help alter the membrane curvature by DNA origami structures [135]. In the case here, non-specific adsorption would act together with chol-mediated membrane binding, where cholesterol stably binds the structure to the membrane and adsorption effects take place when the triangle surface is in direct contact with the membrane.

Another interesting finding is that while octahedral VCDs exist, they are a lot less common than icosahedral species. Instead, VCDs that are larger than icosahedral shells have been found, suggesting that the same mechanism governing the formation of octahedral DCVs may be at play here. Nevertheless, these atypical shells are a lot less common than octahedral DCVs. This discrepancy, along with the aforementioned differences in geometry between DCVs obtained from vesicles of various lipid compositions, point towards lipid geometry as an influencing variable. The most commonly used lipid in this dissertation, DOPC, is known to favour formation of planar bilayers due to its cylindrical shape [136, 137]. The smaller curvature of lipid vesicles associated with icosahedral DCVs and VCDs should therefore be more favourable. This also means that more curvature must

be induced on the membrane by each dimer, which one would expect to cost more energy, again making the process less favourable than assembly into icosahedral DCVs. Helfrich's widely accepted model, however, states that the energetic cost of bending a planar membrane into a sphere is independent of its radius [103]. Neglecting other influencing factors such as neck scission, the energetic cost of forming octahedral and icosahedral DCVs should be identical. A problem of this reasoning is that in an octahedral DCV, fewer triangles must provide the same energy than icosahedra, and the energy cost per unit area is larger. Nevertheless, my energy estimates detailed in section 3.1 suggest that both octahedral and icosahedral assembly provide more than the theoretical minimum for shaping a vesicle, and thus the question of which polyhedron triangles form may boil down to whichever shell has more favourable kinetics.

5.3 Outlook

DNA origami is a very powerful method to create three-dimensional shapes on the nanoscale, but DNA as a construction material is not without problems. An obvious drawback is that while 3D-renderings suggest DNA nanostructures to be solid objects with smooth surfaces, electrostatic repulsion of neighbouring DNA helices results in small cavities or gaps in between two helices connected by Holliday junctions, resulting in a chickenwire-like pattern [138]. DNA is a great tool to control the position of molecules bound to DNA strands (like cholesterol), but because of these cavities it cannot be used to build containers for small molecules. Nature has solved this problem by building containers out of lipid membranes, giving rise to cells and their membrane-enclosed organelles. DCVs and VCDs combine the advantages of DNA origami and lipid membranes into one particle, leveraging the possibilities of each individual component. An immediate potential application of this system is smart drug delivery vehicles. Whereas the vesicle acts as a container for therapeutic payloads, the DNA origami shell can be used to add targeting or other functions to the particle. An interesting aspect of this system is that the payload is derived from the lumen of the parent vesicle. As DCVs could be obtained from all tested polar extracts of natural origin, obtaining DCVs from living cells is a viable option. In this scenario, the molecular payload would be the cytoplasm, and the process could be seen as some sort of cellular biopsy. Preliminary data from *Escherichia coli* confirms that bacterial cell membranes can be used to form DCVs (5.1A). However,there is no proof that these DCVs were shaped by membrane budding, requiring more research. Nevertheless, these particles show that DNA shells can indeed hold cell membranes also containing non-lipid species such as proteins or carbohydrates, and their formation by a budding mechanism is plausible. The complex structure of biological membranes may require different membrane coupling strategies, potentially using protein components to bind to membrane receptors or other

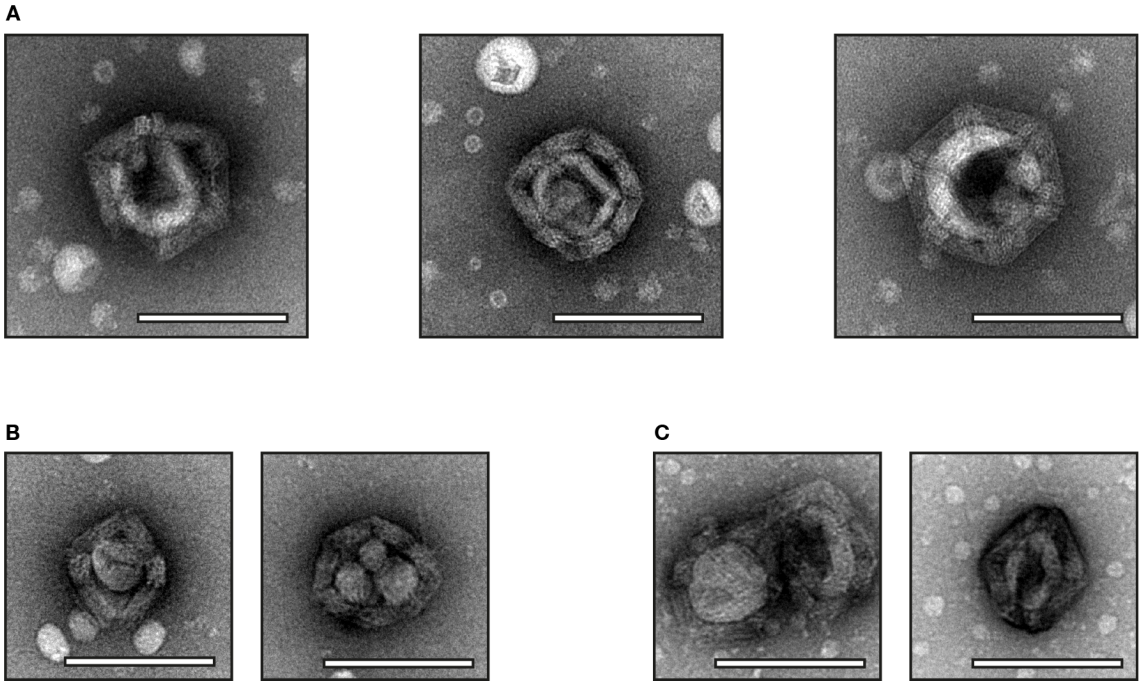

Fig. 5.1: ***DCVs for sampling biological materials.*** ***(A)*** *DCVs obtained from E. coli. Despite their structural similarity to DCVs obtained from synthetic vesicles, definite proof of their formation through membrane budding is missing.* ***(B)*** *DNA-shells containing low-density lipoproteins (LDL).* ***(C)*** *DNA-shells containing high-density lipoproteins (HDL). All scale bars: 100 nm*

structures on the membrane. The data presented in section 3.5 demonstrates that DCV budding does not require insertion of hydrophobic moieties into the membrane and serves as a proof of concept for alternative anchoring strategies.

Surrounding the DNA shells containing *Escherichia coli* membranes are many small structures reminiscent of lipid vesicles. As stated above, it is unclear if these DCVs formed by budding off bacterial cells or by capturing these small structures. However, the latter raises a different question: Can DNA shells lined with hydrophobic moieties be used to capture biological molecules? Previous work demonstrated that the same structures can be used to capture virus-like particles [47], but data for other cargoes is missing. I tested this idea by assembling triangles hybridised to chol-oligos in presence of both low-density and high-density lipoprotein and found that indeed, shells containing both species formed (LDL & HDL, respectively; 5.1B & C). Elevated levels of LDL cholesterol in particular is associated with detrimental health effects, including myocardial infarction and vascular death [139]. Previous studies indicated that DNA origami structures accumulate in the kidneys and are subsequently excreted via urine [140]. DNA shells could therefore potentially be developed into a scavenging system for LDL cholesterol and other harmful substances.

Inward budding of DNA shells may find applications in the delivery of functionalised

DNA nanostructures into cells. DNA origami do not normally pass through the cell membrane, and uptake through vesicular pathways result in its entrapment or degradation within the endosome [141]. However, ionisable lipids like SM-102 have successfully been used to package nucleic acids into lipid nanoparticles for vaccine purposes [142]. The VCDs and bivesicular shell systems discussed in chapter 4 may find applications in delivering DNA origami into cells. Here, VCDs or VCDCVs are produced in vitro, using a suitable ionisable lipid (typically with a pK_a between 6.0 - 7.0 [142]) during the inward budding step. This strategy relies on the spontaneous uptake of the particle into the cell, followed by acidification of the endosome. In response to the pH drop, the ionisable lipid in the vesicle membrane becomes positively charged, upon which it interacts with the negatively charged endosomal membrane allowing entrapped cargo to escape [143]. A potential hurdle is the tight bond between the DNA shell and the vesicle surrounding it, which must be broken for the DNA origami to be released into the cytoplasm. This avenue therefore requires developing alternative membrane anchors that are cleaved upon exposure to the cytoplasm.

5.4 Closing remarks

The application ideas discussed in this chapter demonstrate potential avenues for future research endeavours that may lead to useful products. However, with this dissertation I am hoping to also inspire more curiosity-driven research into nanobiotechnology and synthetic biology to advance our understanding of fundamental natural processes. What started with an ambitious idea led to an exciting journey for me, where every failed experiment was a lesson that ultimately guided me to the results I am now proudly sharing with you.

Over the years, I have presented and defended my data many times, and this thesis contains only a small fraction of my work. I am aiming to present a coherent story, sharing the most compelling data to back up my claims. Nevertheless, many open questions remain: What happens if you lower the concentration of bivalent cations after DCVs have formed? Will they fall apart like free shells, or does the vesicle stabilise the polyhedral shell structure? Can triangles bud off from cells? Can triangles bud into cells, and if so, what happens then? What are the characteristics of VCDs? How can VCD yields be evaluated to optimise the budding process? The list goes on.

Realistically, only a handful of people will ever read these lines, but I do hope that many more will be inspired by my publication in a peer-reviewed journal – once it is out. It represents seven years of passionate research, conference talks, debates... all compressed into 3000 words to meet publisher guidelines. Was it worth it? I have always found it hard to see my research as just a job that I forget about on Friday nights. It feels like a part of me, the product of my creativity and intellect. It is personal. Every success is like a

pat on the back, every failure another reminder that I have not figured it all out just yet. It is humbling. Luckily, I got to meet a lot of people who seemed to feel very similarly. Scientists can be a passionate bunch who may sometimes get lost in details, but do so with a fire in their heart. So maybe, behind the technical details and data to cite, some people will see my manuscript for what it really is:

A love letter to science.

Appendix A

Materials and Methods

The majority of this section was taken from [1].

A.1 Materials

All chemicals were purchased from Sigma Aldrich and Carl Roth unless stated otherwise. 1,2-dioleoyl-sn-glycero-3-phosphocholine (DOPC), 1,2-dipalmitoyl-sn-glycero-3-phosphocholine (DPPC), 1,2-distearoyl-sn-glycero-3-phosphocholine (DSPC), polar lipid extracts (soy, brain, yeast, e. coli), TopFluor cholesterol and Lissamine Rhodamine B-1,2-dioleoyl-sn-glycero-3-phosphoethanolamine (DOPE) were obtained from Avanti Research. Atto488- and Atto643-modified DOPE was obtained from Atto-Tec. NeutrAvidin was purchased from Thermo Scientific. Regular DNA oligonucleotides were purchased from IDT, and modified oligonucleotides were obtained from Biomers. Scaffold DNA was produced biotechnologically in-house. Buffer osmolalities were measured using an Osmomat 3000 freeze point osmometer (Gonotec). Buffer compositions are listed in table A.1.

Table A.1: ***Buffer compositions.*** *All concentrations are in mM. (suc - sucrose; glu - glucose; gly - glycine;)*

Buffer	TRIS	EDTA	$MgCl_2$	NaCl	CsCl	suc	glu	gly	pH
folding	5	1	20	5					8.0
sodium	5	1	5	305					8.0
caesium	5	1	5	5	320				8.0
sucrose	10	1				470			8.0
imaging A	5	1	5	5		280			8.0
imaging B	5	1	5	5			280		8.0
isotonic ass.	5	1	210	5					8.0
glycine	5	1	5					1000	6.8

A.2 DNA origami folding, purification & quantification

DNA origami triangles were folded as described previously21. Briefly, circular scaffold strands of bacteriophage origin (sc8064, 50 nM; B.1) and staple oligonucleotides (200 nM per staple; refer to the supplementary information of [1] for a list of sequences) were mixed in folding buffer and exposed to a thermal annealing ramp (65 °C, 15'; 58-53 °C, 1 h/°C; stored at 20 °C) in a Tetrad2 (Bio-Rad) thermocycler. For some experiments, structures were fluorescently labelled by including Atto643 labelled oligonucleotides in the folding reaction. The folded product was purified by agarose gel electrophoresis by excising the leading band, crushing the gel pieces and centrifuging them in 0.45 µm Costar Spin-X spin columns (Corning) for 10 min at 8 krcf. When needed, the purified structures were washed and concentrated by ultrafiltration (Amicon Ultra 0.5 mL, 100 kDa cut-off, Millipore), exchanging the buffer for sodium buffer. Origami solutions were quantified using a NanoDrop8000 spectrophotometer (Thermo Scientific). For the scaffold & staple routing, refer to fig. B.1, p. 96.

A.3 Vesicle preparation and quantification

Giant vesicles were prepared by gentle swelling of dry lipid films on polyvinyl alcohol gels as described previously24, with slight modifications. A petri dish (⌀ 10 cm) was plasma cleaned in a glow discharge device, and then 1800 µl of a 5% solution of polyvinyl alcohol (Mowiol 28–99, Sigma Aldrich) in ddH2O was evenly distributed across its surface. The dish was incubated for at least 30 min at 50 °C until a dry gel formed. Then, 162 µl of the lipid mixture (typically DOPC with additional 0.5–1% fluorescently labelled DOPE if visualisation by fluorescence was desired, or 0.4% TopFluor cholesterol and LissRhod-PE each for visualisation of lipid phases. Total lipid concentration: 2.54 mM) in chloroform was evenly spread out across the surface using a Drigalski spatula until the chloroform evaporated. Remaining traces of solvent were removed by exposing the dried lipid cake to a vacuum for at least 15 min. Next, 4-5 mL of sodium buffer was added to the petri dish and the solution was left in a humid chamber in the dark at RT for at least 1 h. GVs were detached by gently tapping against the dish and pipetting up and down with a cut pipette tip. The GV suspension was stored at 4 °C in the dark.

When GVs were to be washed and concentrated, the dry lipid film was swollen in caesium buffer or sucrose buffer and, after harvesting, transferred into a falcon tube. The tube was filled up with sodium buffer (isosmotic to the swelling buffers) and centrifuged for at least 30 min at 300 rcf. The supernatant was discarded, and the GV pellet was washed 2-3 more times by adding 900 µl sodium buffer and centrifuging the suspension for 7 min at 300 rcf.

Smaller-sized vesicles were prepared using a mini-extruder (Avanti Research) and polycarbonate membranes with the desired pore size (typically 200 nm; Whatman). GV preparations were pushed back and forth through the membrane 21 times.

Lipids in vesicle preparations were quantified using a colourimetric phospholipid quantification assay kit (Sigma Aldrich CS0001) following the manufacturer's instructions. The absorbance was measured at 570 nm on a Clariostar plus microplate reader (BMG Labtech).

Vesicles used in the lipid mixture screens (section 3.6) were swollen in sucrose buffer at 60 °C to account for differences in lipid charge and melting temperature and washed as described above. Lipid quantity was estimated by measuring the lipid content in sample A (DOPC vesicles) using the colourimetric assay mentioned above. As this assay can only detect choline-containing lipids, the lipid quantity in the remaining samples was estimated based on the fluorescence of Atto643-DOPE species included at equal molar percentages in all lipid mixtures. For this, vesicle preparations were diluted 1:10 and 10 µl aliquots were mixed with 90 µl Triton-X100 (2%) solution in a black 96 well plate. The plate was incubated at 60 °C for 1 h to disintegrate the vesicles and the fluorescence of Atto643-DOPE was measured in a plate reader. The lipid quantity in the other vesicle preparations was finally calculated by normalising the fluorescence readouts in respect to that of sample A, and multiplying the obtained ratio by the colourimetric quantification result for sample A. Images of phase-separated vesicles were obtained using a ThermoFisher EVOS M7000 imaging system.

A.4 Vesicle binding study

Microscope slides and coverslips were washed with ddH2O and incubated in denatured BSA blocking buffer (10 mM TRIS, 150 mM NaCl, 50 µM BSA, pH 8) overnight as described previously [144]. Next, the glassware was thoroughly washed with ddH2O to remove residual blocking buffer and dried at 50 °C for 1 h. 6 µl of GVs (99.95% DOPC, 0.05% DOPE-Atto488; swollen in imaging buffer A) was mixed with origami triangles (+/−cholesterol modified strands; fluorescently labelled with Atto643 modified oligonucleotides; final origami concentration: 7 nM) and topped up to 40 µl with imaging buffer B. 300 mM NaCl was added to samples testing the effect of elevated sodium on the binding behaviour of origami. The samples were pipetted into an imaging chamber formed by sandwiching a silicon isolator (Grace Bio-Labs) between passivated coverslips and microscope slides. The samples were imaged using a Leica TCS SP5 confocal microscope with a Leica HCX PL APO CS 63x/1.40-0.60 oil immersion objective. Intensity profiles were obtained using Fiji [145].

Table A.2: ***Osmolality screen sample compositions.*** *All concentrations are in mM.*

Osmol. diff.	glycine	MgCl2	NaCl	Tot. vol. (µl)
−78%	0	25	26.3	30
−58%	100	30	26.3	30
−42%	200	35	26.3	30
−22%	300	45	26.3	30
−4	400	50	26.3	30
+12%	500	55	26.3	30
+33%	600	65	26.3	30
+54%	700	75	26.3	30

A.5 Budding assays

Vesicles were prepared as described above using 99.0 – 100% DOPC with the remainder being fluorescently labelled DOPE if visualisation by fluorescence was desired. Origami triangles were hybridised to cholesterol-modified oligonucleotides by adding them at a 1.5 x excess with respect to the total amount of compatible linker handles on the origami. The hybridisation reaction was incubated at RT for at least 30 min. For outward budding reactions, 24 µl of untreated GV suspension was mixed with origami triangles with linker handles on the shell-inward face at a final concentration of approx. 2 nM origami. In experiments where lipid quantities in GV preparations were known, 1000 pmol lipid of GVs prepared in caesium buffer, or 350 pmol of GVs prepared in sucrose buffer was mixed with the origami (4.5 µl at 15 nM). The sample was topped up to 30 µl with sodium buffer, and the MgCl2 concentration was adjusted to 65 mM by adding 1 M MgCl2 solution (hypertonic) or to 60 mM by adding isotonic assembly buffer. Budding reactions were incubated at 37 °C for up to 3 d.

For the tonicity screen, undiluted, chol-hybridised triangles were mixed with GVs and diluted using water and glycine buffer. The samples were incubated at RT for 2 h for triangles to bind to the vesicles and for vesicles to adjust to the altered osmotic conditions. Finally, MgCl2 solution was added to trigger assembly and samples were incubated at 37 °C overnight. For detailed sample compositions, refer to table A.2.

The budding kinetics were obtained by mixing samples with gel loading dye (50% Ficoll400, 20 mM MgCl2, Orange G) and freezing them in liquid nitrogen at the indicated time points. Once all time points were taken, the samples were thawed, mixed and used for agarose gel electrophoresis.

For inward budding reactions, origami triangles (3 µl at 20 nM) with linker handles on the shell-outward face were mixed with LVs (1500 pmol lipids; approx. 200 nm diameter) and incubated for up to 3 d.

For bivesicular DNA shells (VCDCVs), triangles with orthogonal linker handles on the

top and bottom face were used, and inward and outward budding reactions were conducted successively. First, DCVs were produced in an outward budding assay (1200 µl in total) using cholesterol-modified oligonucleotides hybridised to the bottom face linker handles. The sample was then centrifuged at 300 rcf for 5–8 min, and the pellet containing residual GVs was discarded. The supernatant was then ultracentrifuged at 55 krpm (avg. 108 krcf) for 30 min in a Beckman Coulter Optima MAX-TL ultracentrifuge equipped with a TLA-110 fixed angle rotor. 80–90% of the supernatant was removed, and the pellet was resuspended in the remaining volume. Meanwhile, LVs (200 nm diameter) were mixed with a second chol-oligo complementary to the linker handles on the top face of the triangles. These oligonucleotides were added at a 50x excess with respect to the total amount of complementary linker handles on the origami, and the solution was incubated at RT for 15-30 min. Then, the magnesium concentration in the LV solution was adjusted to 60 mM MgCl2 by adding isotonic assembly buffer. Finally, LVs (1500 pmol lipids) were mixed with the DCV concentrate (to a final concentration of 1-5 nM DNA), and the samples were incubated at 37 °C for 1–3 d.

A.6 Budding using biotin-NeutrAvidin

For budding reactions using biotin-NeutrAvidin interactions to anchor triangles to the membranes, GVs containing 3% biotinylated DOPE, 1% fluorescently labelled DOPE and 96% DOPC were prepared. Origami triangles were folded with linker handles complementary to biotinylated oligonucleotides and linker handles for purification using magnetic beads. Biotinylated oligonucleotides were already included in the folding reaction to remove unbound strands and excess staples by gel extraction. The triangles were then mixed with a 500-fold excess of NeutrAvidin and incubated for 1 h at 37 °C on an orbital shaker. Next, the sample was transferred into a tube previously passivated with denatured BSA blocking buffer and mixed with magnetic beads (Dynabeads M-270 Streptavidin, Invitrogen) coated with dual-biotinylated DNA linker handles complementary to the linkers on the origami. The sample was incubated for 1 h at RT on a rotary shaker, and the beads now carrying the origami triangles were washed 3–4 times with sodium buffer. Finally, an invader strand complementary to the full length of the purification linker handles was added in great excess, and the solution was incubated at 37 °C for 1 h to uncouple the origami from the magnetic beads by strand displacement. The NeutrAvidin bearing triangles were then mixed with biotinylated GVs, and the MgCl2 concentration was adjusted to 60 mM by adding isotonic assembly buffer. The sample was incubated at 37 °C for 2.5 d.

A.7 Negative stain transmission electron microscopy

Sample solutions were incubated on glow-discharged copper grids (400 mesh) with a carbon support film (Science Services) for 4–8 minutes, depending on the sample concentration. The solution was then blotted off using filter paper (Whatman). Then, the grid was washed once using stain solution (2% aqueous uranyl formate + 25 mM NaOH), followed by incubating another stain droplet on the grid for 30 s. Excess stain was blotted off using filter paper, and the grid was air-dried before imaging.

Grids were typically imaged at x26–30k magnification using SerialEM with an FEI Tecnai T12 electron microscope operated at 120 kV and a Tietz TEMCAM-F416 camera. Image contrast was auto-levelled using Fiji. For tomography, one-directional tilt series were acquired from −50° to +50° in steps of 2° using SerialEM. The resulting image stacks were imported into Etomo (IMOD [146]), and images were aligned without fiducials by cross-correlation with cumulative correlation switched on. Tomograms were generated by filtered back-projection (gaussian filter cut-off: 0.35; fall-off: 0.035;). For visualisation, the z-stacks thus generated were imported into Fiji and z-projected by summing up z-slices corresponding to the top, middle and bottom sections of the respective particle of interest.

A.8 Cryogenic electron microscopy

Sample grids for cryoEM were prepared using an automated vitrification system (FEI Vitrobot Mark V). First, grids (Quantifoil R1.2/1.3, Cu 200 mesh, 100 holey carbon films, 2 nm carbon support film; for images of DCVs: Ted Pella, Cu 400 mesh, lacey carbon, <3 nm carbon support film) were glow-discharged and then inserted into the Vitrobot. The conditions inside the device's environmental chamber were kept at either 4 °C or 22 °C and 100% relative humidity. Samples were typically incubated on the grids inside the chamber for 5 min and plunge-frozen in liquid ethane (blot force: −1, 0 or 25; blot time: 2–3 s; blot total: 1; drain time: 0 s;). The grids were imaged with a spherical-aberration (Cs)-corrected Titan Krios G2 electron microscope (Thermo Fisher) operated at 300 kV and equipped with a Falcon III 4k direct electron detector (Thermo Fisher). Samples were imaged at x29k magnification and defocus values between −1 and −4 µm. Images were auto-levelled in Fiji.

A.9 Agarose gel electrophoresis

Agarose gels were cast by dissolving solid agarose powder (Invitrogen) in boiling running buffer followed by water cooling to harden the homogeneous gel mixture. The amount of agarose to weigh in and the composition of running buffer were chosen based on the

expected size and properties of the sample particles to be resolved. Typically, the weight percentage of agarose in the final gel mixture was 1.5% for native DNA and monomeric DNA origami structures, and 0.8% for oligomeric origami assemblies. Likewise, running buffer (0.5 x TBE prepared from a 10 x TBE stock (Carl Roth)) was supplemented with either no, 5.5 mM or 20 mM $MgCl_2$ (Sigma Aldrich) for gels used to resolve native DNA, monomeric origami or oligomeric assemblies, respectively. If mixed sample types were to be loaded onto a gel, the samples with the most constraining agarose and magnesium requirements dictated the overall amount of each added to the gel mixture. Unless all the nucleic acid samples were hybridised to a fluorophore bearing oligonucleotide (pre-staining), ethidium bromide solution (0.025%, Carl Roth) was added to the gel mixture up to a final concentration of 0.001% (in-gel staining) for visualisation purposes. The gel mixture was finally poured into a gel tray, air bubbles were removed and a comb was inserted into the molten gel until the gel cooled and solidified completely. Next, the comb was removed and the gel was placed into an electrophoresis tank with its pockets oriented towards the cathode. After fully immersing the gel in running buffer, the samples were mixed with 11 x loading dye (50% Ficoll400 + Orange G in ddH_2O, supplemented with 20 mM $MgCl_2$ if used for oligomeric assemblies) and carefully loaded into the pockets of the gel. Samples to be loaded onto a gel were mixed with 11 x loading dye (50% Ficoll400 + Orange G in ddH_2O, supplemented with 20 mM $MgCl_2$ if used for oligomeric assemblies) and carefully pipetted into the pockets. A constant voltage of 90 V was applied for approx. 1.5–2 h before analysing the gel using a Typhoon FLA 9500 laser scanner (GE healthcare). If high $MgCl_2$ concentrations above 10 mM were used, the gel tank was cooled by placing it into an ice-water bath and the running buffer was exchanged every 45 minutes to prevent sample damage by magnesium depletion.

Appendix B

Supporting information

The majority of this section was taken from [1].

B.1 Scaffold sc8064 sequence

GGCAATGACCTGATAGCCTTTGTAGATCTCTCAAAAATAGCTACCCTCTCCGGCATTAATTTATCAGCTAGAACGGTTGAATATCATATTGATGGTGATT
TGACTGTCTCCGGCCTTTCTCACCCTTTTGAATCTTTACCTACACATTACTCAGGCATTGCATTTAAAATATATGAGGGTTCTAAAAATTTTTATCCTTG
CGTTGAAATAAAGGCTTCTCCCGCAAAAGTATTACAGGGTCATAATGTTTTTGGTACAACCGATTTAGCTTTATGCTCTGAGGCTTTATTGCTTAATTTT
GCTAATTCTTTGCCTTGCCTGTATGATTTATTGGATGTTAATGCTACTACTATTAGTAGAATTGATGCCACCTTTTCAGCTCGCGCCCCAAATGAAAATA
TAGCTAAACAGGTTATTGACCATTTGCGAAATGTATCTAATGGTCAAACTAAATCTACTCGTTCGCAGAATTGGGAATCAACTGTTATATGGAATGAAAC
TTCCAGACACCGTACTTTAGTTGCATATTTAAAACATGTTGAGCTACAGCATTATATTCAGCAATTAAGCTCTAAGCCATCCGCAAAAATGACCTCTTAT
CAAAAGGAGCAATTAAAGGTACTCTCTAATCCTGACCTGTTGGAGTTTGCTTCCGGTCTGGTTCGCTTTGAAGCTCGAATTAAAACGCGATATTTGAAGT
CTTTCGGGCTTCCTCTTAATCTTTTTGATGCAATCCGCTTTGCTTCTGACTATAATAGTCAGGGTAAAGACCTGATTTTTGATTTATGGTCATTCTCGTT
TTCTGAACTGTTTAAAGCATTTGAGGGGGATTCAATGAATATTTATGACGATTCCGCAGTATTGGACGCTATCCAGTCTAAACATTTTACTATTACCCCC
TCTGGCAAAACTTCTTTTGCAAAAGCCTCTCGCTATTTTGGTTTTTATCGTCGTCTGGTAAACGAGGGTTATGATAGTGTTGCTCTTACTATGCCTCGTA
ATTCCTTTTGGCGTTATGTATCTGCATTAGTTGAATGTGGTATTCCTAAATCTCAACTGATGAATCTTTCTACCTGTAATAATGTTGTTCCGTTAGTTCG
TTTTATTAACGTAGATTTTTCTTCCCAACGTCCTGACTGGTATAATGAGCCAGTTCTTAAAATCGCATAAGGTAATTCACAATGATTAAAGTTGAAATTA
AACCATCTCAAGCCCAATTTACTACTCGTTCTGGTGTTTCTCGTCAGGGCAAGCCTTATTCACTGAATGAGCAGCTTTGTTACGTTGATTTGGGTAATGA
ATATCCGGTTCTTGTCAAGATTACTCTTGATGAAGGTCAGCCAGCCTATGCGCCTGGTCTGTACACCGTTCATCTGTCCTCTTTCAAAGTTGGTCAGTTC
GGTTCCCTTATGATTGACCGTCTGCGCCTCGTTCCGGCTAAGTAACATGGAGCAGGTCGCGGATTTCGACACAATTTATCAGGCGATGATACAAATCTCC
GTTGTACTTTGTTTCGCGCTTGGTATAATCGCTGGGGGTCAAAGATGAGTGTTTTAGTGTATTCTTTTGCCTCTTTCGTTTTAGGTTGGTGCCTTCGTAG
TGGCATTACGTATTTTACCCGTTTAATGGAAACTTCCTCATGAAAAAGTCTTTAGTCCTCAAAGCCTCTGTAGCCGTTGCTACCCTCGTTCCGATGCTGT
CTTTCGCTGCTGAGGGTGACGATCCCGCAAAAGCGGCCTTTAACTCCCTGCAAGCCTCAGCGACCGAATATATCGGTTATGCGTGGGCGATGGTTGTTGT
CATTGTCGGCGCAACTATCGGTATCAAGCTGTTTAAGAAATTCACCTCGAAAGCAAGCTGATAAACCGATACAATTAAAGGCTCCTTTTGGAGCCTTTTT
TTTGGAGATTTTCAACGTGAAAAAATTATTATTCGCAATTCCTTTAGTTGTTCCTTTCTATTCTCACTCCGCTGAAACTGTTGAAAGTTGTTTAGCAAAA
TCCCATACAGAAAATTCATTTACTAACGTCTGGAAAGACGACAAAACTTTAGATCGTTACGCTAACTATGAGGGCTGTCTGTGGAATGCTACAGGCGTTG
TAGTTTGTACTGGTGACGAAACTCAGTGTTACGGTACATGGGTTCCTATTGGGCTTGCTATCCCTGAAAATGAGGGTGGTGGCTCTGAGGGTGGCGGTTC
TGAGGGTGGCGGTTCTGAGGGTGGCGGTACTAAACCTCCTGAGTACGGTGATACACCTATTCCGGGCTATACTTATATCAACCCTCTCGACGGCACTTAT
CCGCCTGGTACTGAGCAAAACCCCGCTAATCCTAATCCTTCTCTTGAGGAGTCTCAGCCTCTTAATACTTTCATGTTTCAGAATAATAGGTTCCGAAATA
GGCAGGGGGCATTAACTGTTTATACGGGCACTGTTACTCAAGGCACTGACCCCGTTAAAACTTATTACCAGTACACTCCTGTATCATCAAAAGCCATGTA
TGACGCTTACTGGAACGGTAAATTCAGAGACTGCGCTTTCCATTCTGGCTTTAATGAGGATTTATTTGTTTGTGAATATCAAGGCCAATCGTCTGACCTG
CCTCAACCTCCTGTCAATGCTGGCGGCGGCTCTGGTGGTGGTTCTGGTGGCGGCTCTGAGGGTGGTGGCTCTGAGGGTGGCGGTTCTGAGGGTGGCGGCT
CTGAGGGAGGCGGTTCCGGTGGTGGCTCTGGTTCCGGTGATTTTGATTATGAAAAGATGGCAAACGCTAATAAGGGGGCTATGACCGAAAATGCCGATGA
AAACGCGCTACAGTCTGACGCTAAAGGCAAACTTGATTCTGTCGCTACTGATTACGGTGCTGCTATCGATGGTTTCATTGGTGACGTTTCCGGCCTTGCT
AATGGTAATGGTGCTACTGGTGATTTTGCTGGCTCTAATTCCCAAATGGCTCAAGTCGGTGACGGTGATAATTCACCTTTAATGAATAATTTCCGTCAAT
ATTTACCTTCCCTCCCTCAATCGGTTGAATGTCGCCCTTTTGTCTTTGGCGCTGGTAAACCATATGAATTTTCTATTGATTGTGACAAAATAAACTTATT
CCGTGGTGTCTTTGCGTTTCTTTTATATGTTGCCACCTTTATGTATGTATTTTCTACGTTTGCTAACATACTGCGTAATAAGGAGTCTTAATCATGCCAG
TTCTTTTGGGTATTCCGTTATTATTGCGTTTCCTCGGTTTCCTTCTGGTAACTTTGTTCGGCTATCTGCTTACTTTTCTTAAAAAGGGCTTCGGTAAGAT
AGCTATTGCTATTTCATTGTTTCTTGCTCTTATTATTGGGCTTAACTCAATTCTTGTGGGTTATCTCTCTGATATTAGCGCTCAATTACCCTCTGACTTT
GTTCAGGGTGTTCAGTTAATTCTCCCGTCTAATGCGCTTCCCTGTTTTTATGTTATTCTCTCTGTAAAGGCTGCTATTTTCATTTTTGACGTTAAACAAA
AAATCGTTTCTTATTTGGATTGGGATAAATAATATGGCTGTTTATTTTGTAACTGGCAAATTAGGCTCTGGAAAGACGCTCGTTAGCGTTGGTAAGATTC
AGGATAAAATTGTAGCTGGGTGCAAAATAGCAACTAATCTTGATTTAAGGCTTCAAAACCTCCCGCAAGTCGGGAGGTTCGCTAAAACGCCTCGCGTTCT
TAGAATACCGGATAAGCCTTCTATATCTGATTTGCTTGCTATTGGGCGCGGTAATGATTCCTACGATGAAAATAAAAACGGCTTGCTTGTTCTCGATGAG
TGCGGTACTTGGTTTAATACCCGTTCTTGGAATGATAAGGAAAGACAGCCGATTATTGATTGGTTTCTACATGCTCGTAAATTAGGATGGGATATTATTT
TTCTTGTTCAGGACTTATCTATTGTTGATAAACAGGCGCGTTCTGCATTAGCTGAACATGTTGTTTATTGTCGTCGTCTGGACAGAATTACTTTACCTTT
TGTCGGTACTTTATATTCTCTTATTACTGGCTCGAAAATGCCTCTGCCTAAATTACATGTTGGCGTTGTTAAATATGGCGATTCTCAATTAAGCCCTACT
GTTGAGCGTTGGCTTTATACTGGTAAGAATTTGTATAACGCATATGATACTAAACAGGCTTTTTCTAGTAATTATGATTCCGGTGTTTATTCTTATTTAA
CGCCTTATTTATCACACGGTCGGTATTTCAAACCATTAAATTTAGGTCAGAAGATGAAATTAACTAAAATATATTTGAAAAAGTTTTCTCGCGTTCTTTG
TCTTGCGATTGGATTTGCATCAGCATTTACATATAGTTATATAACCCAACCTAAGCCGGAGGTTAAAAAGGTAGTCTCTCAGACCTATGATTTTGATAAA
TTCACTATTGACTCTTCTCAGCGTCTTAATCTAAGCTATCGCTATGTTTTCAAGGATTCTAAGGGAAAATTAATTAATAGCGACGATTTACAGAAGCAAG

GTTATTCACTCACATATATTGATTTATGTACTGTTTCCATTAAAAAAGGTAATTCAAATGAAATTGTTAAATGTAATTAATTTTGTTTTCTTGATGTTTG
TTTCATCATCTTCTTTTGCTCAGGTAATTGAAATGAATAATTCGCCTCTGCGCGATTTTGTAACTTGGTATTCAAAGCAATCAGGCGAATCCGTTATTGT
TTCTCCCGATGTAAAAGGTACTGTTACTGTATATTCATCTGACGTTAAACCTGAAAATCTACGCAATTTCTTTATTTCTGTTTTACGTGCAAATAATTTT
GATATGGTAGGTTCTAACCCTTCCATTATTCAGAAGTATAATCCAAACAATCAGGATTATATTGATGAATTGCCATCATCTGATAATCAGGAATATGATG
ATAATTCCGCTCCTTCTGGTGGTTTCTTTGTTCCGCAAAATGATAATGTTACTCAAACTTTTAAAATTAATAACGTTCGGGCAAAGGATTTAATACGAGT
TGTCGAATTGTTTGTAAAGTCTAATACTTCTAAATCCTCAAATGTATTATCTATTGACGGCTCTAATCTATTAGTTGTTAGTGCTCCTAAAGATATTTTA
GATAACCTTCCTCAATTCCTTTCAACTGTTGATTTGCCAACTGACCAGATATTGATTGAGGGTTTGATATTTGAGGTTCAGCAAGGTGATGCTTTAGATT
TTTCATTTGCTGCTGGCTCTCAGCGTGGCACTGTTGCAGGCGGTGTTAATACTGACCGCCTCACCTCTGTTTTATCTTCTGCTGGTGGTTCGTTCGGTAT
TTTTAATGGCGATGTTTTAGGGCTATCAGTTCGCGCATTAAAGACTAATAGCCATTCAAAAATATTGTCTGTGCCACGTATTCTTACGCTTTCAGGTCAG
AAGGGTTCTATCTCTGTTGGCCAGAATGTCCCTTTTATTACTGGTCGTGTGACTGGTGAATCTGCCAATGTAAATAATCCATTTCAGACGATTGAGCGTC
AAAATGTAGGTATTTCCATGAGCGTTTTTCCTGTTGCAATGGCTGGCGGTAATATTGTTCTGGATATTACCAGCAAGGCCGATAGTTTGAGTTCTTCTAC
TCAGGCAAGTGATGTTATTACTAATCAAAGAAGTATTGCTACAACGGTTAATTTGCGTGATGGACAGACTCTTTTACTCGGTGGCCTCACTGATTATAAA
AACACTTCTCAGGATTCTGGCGTACCGTTCCTGTCTAAAATCCCTTTAATCGGCCTCCTGTTTAGCTCCCGCTCTGATTCTAACGAGGAAAGCACGTTAT
ACGTGCTCGTCAAAGCAACCATAGTACGCGCCCTGTAGCGGCGCATTAAGCGCGGCGGGTGTGGTGGTTACGCGCAGCGTGACCGCTACACTTGCCAGCG
CCCTAGCGCCCGCTCCTTTCGCTTTCTTCCCTTCCTTTCTCGCCACGTTCGCCGGCTTTCCCCGTCAAGCTCTAAATCGGGGGCTCCCTTTAGGGTTCCG
ATTTAGTGCTTTACGGCACCTCGACCCCAAAAAACTTGATTTGGGTGATGGTTCACGTAGTGGGCCATCGCCCTGATAGACGGTTTTTCGCCCTTTGACG
TTGGAGTCCACGTTCTTTAATAGTGGACTCTTGTTCCAAACTGGAACAACACTCAACCCTATCTCGGGCTATTCTTTTGATTTATAAGGGATTTTGCCGA
TTTCGGAACCACCATCAAACAGGATTTTCGCCTGCTGGGGCAAACCAGCGTGGACCGCTTGCTGCAACTCTCTCAGGGCCAGGCGGTGAAGGGCAATCAG
CTGTTGCCCGTCTCACTGGTGAAAAGAAAAACCACCCTGGCGCCCAATACGCAAACCGCCTCTCCCCGCGCGTTGGCCGATTCATTAATGCAGCTGGCAC
GACAGGTTTCCCGACTGGAAAGCGGGCAGTGAGCGCAACGCAATTAATGTGAGTTAGCTCACTCATTAGGCACCCCAGGCTTTACACTTTATGCTTCCGG
CTCGTATGTTGTGTGGAATTGTGAGCGGATAACAATTTCACACAGGAAACAGCTATGACCATGATTACGAATTCGAGCTCGGTACCCGGGGATCCTCAAC
TGTGAGGAGGCTCACGGACGCGAAGAACAGGCACGCGTGCTGGCAGAAACCCCCGGTATGACCGTGAAAACGGCCCGCCGCATTCTGGCCGCAGCACCAC
AGAGTGCACAGGCGCGCAGTGACACTGCGCTGGATCGTCTGATGCAGGGGGCACCGGCACCGCTGGCTGCAGGTAACCCGGCATCTGATGCCGTTAACGA
TTTGCTGAACACACCAGTGTAAGGGATGTTTATGACGAGCAAAGAAACCTTTACCCATTACCAGCCGCAGGGCAACAGTGACCCGGCTCATACCGCAACC
GCGCCCGGCGGATTGAGTGCGAAAGCGCCTGCAATGACCCCGCTGATGCTGGACACCTCCAGCCGTAAGCTGGTTGCGTGGGATGGCACCACCGACGGTG
CTGCCGTTGGCATTCTTGCGGTTGCTGCTGACCAGACCAGCACCACGCTGACGTTCTACAAGTCCGGCACGTTCCGTTATGAGGATGTGCTCTGGCCGGA
GGCTGCCAGCGACGAGACGAAAAAACGGACCGCGTTTGCCGGAACGGCAATCAGCATCGTTTAACTTTACCCTTCATCACTAAAGGCCGCCTGTGCGGCT
TTTTTTACGGGATTTTTTTATGTCGATGTACACAACCGCCCAACTGCTGGCGGCAAATGAGCAGAAATTTAAGTTTGATCCGCTGTTTCTGCGTCTCTTT
TTCCGTGAGAGCTATCCCTTCACCACGGAGAAAGTCTATCTCTCACAAATTCCGGGACTGGTAAACATGGCGCTGTACGTTTCGCCGATTGTTTCCGGTG
AGGTTATCCGTTCCCGTGGCGGCTCCACCTCTGAAAGCTTGGCACTGGCCGTCGTTTTACAACGTCGTGACTGGGAAAACCCTGGCGTTACCCAACTTAA
TCGCCTTGCAGCACATCCCCCTTTCGCCAGCTGGCGTAATAGCGAAGAGGCCCGCACCGATCGCCCTTCCCAACAGTTGCGCAGCCTGAATGGCGAATGG
CGCTTTGCCTGGTTTCCGGCACCAGAAGCGGTGCCGGAAAGCTGGCTGGAGTGCGATCTTCCTGAGGCCGATACTGTCGTCGTCCCCTCAAACTGGCAGA
TGCACGGTTACGATGCGCCCATCTACACCAACGTGACCTATCCCATTACGGTCAATCCGCCGTTTGTTCCCACGGAGAATCCGACGGGTTGTTACTCGCT
CACATTTAATGTTGATGAAAGCTGGCTACAGGAAGGCCAGACGCGAATTATTTTTGATGGCGTTCCTATTGGTTAAAAAATGAGCTGATTTAACAAAAAT
TTAATGCGAATTTTAACAAAATATTAACGTTTACAATTTAAATATTTGCTTATACAATCTTCCTGTTTTTGGGGCTTTTCTGATTATCAACCGGGGTACA
TATGATTGACATGCTAGTTTTACGATTACCGTTCATCGATTCTCTTGTTTGCTCCAGACTCTCA

B.2 Triangle scaffold & staple routing

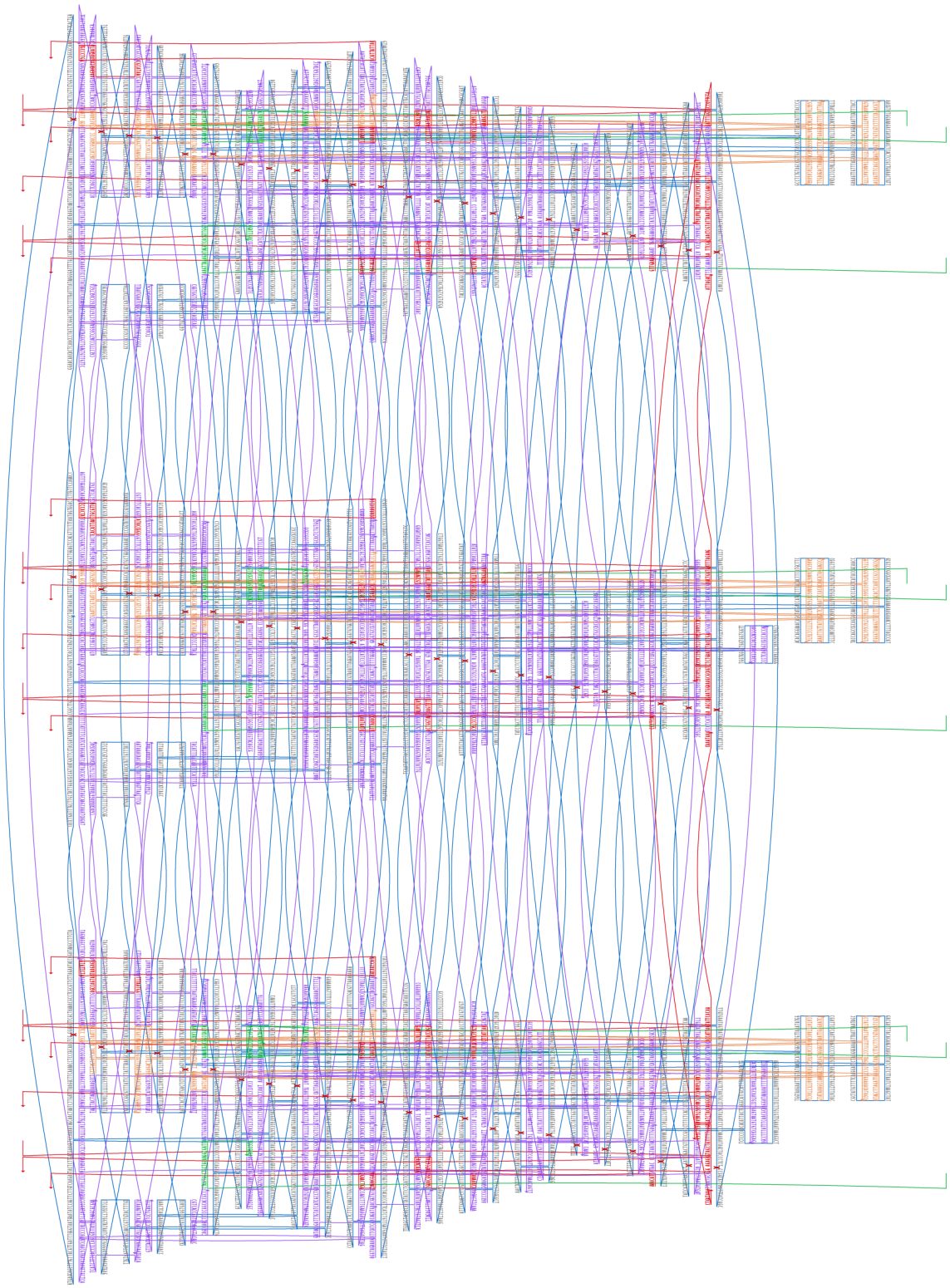

Fig. B.1: ***Triangle design map.*** *Exemplary linker handles extending from the origami surface are shown in red (shell-outer face) and green (shell-inner face). The three main domains represent the three sides comprising the triangle. Protrusions used for triangle assembly are highlighted in orange, the shape-complementary recesses are visible as holes in the design.*

Bibliography

[1] Pinner, M. T. & Dietz, H. Programmable DNA shell scaffolds for directional membrane budding (2024).

[2] Votteler, J. & Sundquist, W. I. Virus Budding and the ESCRT Pathway. *Cell Host & Microbe* **14**, 232–241 (2013).

[3] Rideau, E., Dimova, R., Schwille, P., R. Wurm, F. & Landfester, K. Liposomes and polymersomes: A comparative review towards cell mimicking. *Chemical Society Reviews* **47**, 8572–8610 (2018).

[4] Harayama, T. & Riezman, H. Understanding the diversity of membrane lipid composition. *Nat Rev Mol Cell Biol* **19**, 281–296 (2018).

[5] Casares, D., Escribá, P. V. & Rosselló, C. A. Membrane Lipid Composition: Effect on Membrane and Organelle Structure, Function and Compartmentalization and Therapeutic Avenues. *International Journal of Molecular Sciences* **20**, 2167 (2019).

[6] Kaksonen, M. & Roux, A. Mechanisms of clathrin-mediated endocytosis. *Nat Rev Mol Cell Biol* **19**, 313–326 (2018).

[7] McMahon, H. T. & Boucrot, E. Membrane curvature at a glance. *Journal of Cell Science* **128**, 1065–1070 (2015).

[8] Van Meer, G., Voelker, D. R. & Feigenson, G. W. Membrane lipids: Where they are and how they behave. *Nat Rev Mol Cell Biol* **9**, 112–124 (2008).

[9] Wehman, A. M., Poggioli, C., Schweinsberg, P., Grant, B. D. & Nance, J. The P4-ATPase TAT-5 Inhibits the Budding of Extracellular Vesicles in C. elegans Embryos. *Current Biology* **21**, 1951–1959 (2011).

[10] Bremser, M. *et al.* Coupling of Coat Assembly and Vesicle Budding to Packaging of Putative Cargo Receptors. *Cell* **96**, 495–506 (1999).

[11] Beck, R. *et al.* Membrane curvature induced by Arf1-GTP is essential for vesicle formation. *Proc Natl Acad Sci U S A* **105**, 11731–11736 (2008).

[12] McMahon, H. T. & Boucrot, E. Molecular mechanism and physiological functions of clathrin-mediated endocytosis. *Nat Rev Mol Cell Biol* **12**, 517–533 (2011).

[13] Kirchhausen, T. & Harrison, S. C. Protein organization in clathrin trimers. *Cell* **23**, 755–761 (1981).

[14] Ungewickell, E. & Branton, D. Assembly units of clathrin coats. *Nature* **289**, 420–422 (1981).

[15] Fotin, A. *et al.* Molecular model for a complete clathrin lattice from electron cryomicroscopy. *Nature* **432**, 573–579 (2004).

[16] Dannhauser, P. N. & Ungewickell, E. J. Reconstitution of clathrin-coated bud and vesicle formation with minimal components. *Nat Cell Biol* **14**, 634–639 (2012).

[17] Cail, R. C., Shirazinejad, C. R. & Drubin, D. G. Induced nanoscale membrane curvature bypasses the essential endocytic function of clathrin. *Journal of Cell Biology* **221**, e202109013 (2022).

[18] Fujimoto, L. M., Roth, R., Heuser, J. E. & Schmid, S. L. Actin Assembly Plays a Variable, but not Obligatory Role in Receptor-Mediated Endocytosis. *Traffic* **1**, 161–171 (2000).

[19] Katzmann, D. J., Babst, M. & Emr, S. D. Ubiquitin-Dependent Sorting into the Multivesicular Body Pathway Requires the Function of a Conserved Endosomal Protein Sorting Complex, ESCRT-I. *Cell* **106**, 145–155 (2001).

[20] Schöneberg, J., Lee, I.-H., Iwasa, J. H. & Hurley, J. H. Reverse-topology membrane scission by the ESCRT proteins. *Nat Rev Mol Cell Biol* **18**, 5–17 (2017).

[21] Henne, W. M., Buchkovich, N. J. & Emr, S. D. The ESCRT Pathway. *Developmental Cell* **21**, 77–91 (2011).

[22] Wollert, T. & Hurley, J. H. Molecular Mechanism of Multivesicular Body Biogenesis by ESCRT Complexes. *Nature* **464**, 864–869 (2010).

[23] Chiaruttini, N. *et al.* Relaxation of Loaded ESCRT-III Spiral Springs Drives Membrane Deformation. *Cell* **163**, 866–879 (2015).

[24] Buchkovich, N. J., Henne, W. M., Tang, S. & Emr, S. D. Essential N-Terminal Insertion Motif Anchors the ESCRT-III Filament during MVB Vesicle Formation. *Developmental Cell* **27**, 201–214 (2013).

[25] Bodon, G. *et al.* Charged Multivesicular Body Protein 2B (CHMP2B) of the Endosomal Sorting Complex Required for Transport-III (ESCRT-III) Polymerizes into Helical Structures Deforming the Plasma Membrane *. *Journal of Biological Chemistry* **286**, 40276–40286 (2011).

[26] Ryu, Y.-S. *et al.* Reconstituting ring-rafts in bud-mimicking topography of model membranes. *Nat Commun* **5**, 4507 (2014).

[27] Ford, M. G. J. *et al.* Curvature of clathrin-coated pits driven by epsin. *Nature* **419**, 361–366 (2002).

[28] Frost, A., Unger, V. M. & Camilli, P. D. The BAR Domain Superfamily: Membrane-Molding Macromolecules. *Cell* **137**, 191–196 (2009).

[29] Watson, J. D. & Crick, F. H. C. Molecular Structure of Nucleic Acids: A Structure for Deoxyribose Nucleic Acid. *Nature* **171**, 737–738 (1953).

[30] Holliday, R. A mechanism for gene conversion in fungi. *Genetics Research* **5**, 282–304 (1964).

[31] Seeman, N. C. Nucleic acid junctions and lattices. *Journal of Theoretical Biology* **99**, 237–247 (1982).

[32] Rothemund, P. W. K. Folding DNA to create nanoscale shapes and patterns. *Nature* **440**, 297–302 (2006).

[33] Dey, S. *et al.* DNA origami. *Nat Rev Methods Primers* **1**, 1–24 (2021).

[34] Douglas, S. M. *et al.* Self-assembly of DNA into nanoscale three-dimensional shapes. *Nature* **459**, 414–418 (2009).

[35] Schneider, F., Möritz, N. & Dietz, H. The sequence of events during folding of a DNA origami. *Science Advances* **5**, eaaw1412 (2019).

[36] Martin, T. G. & Dietz, H. Magnesium-free self-assembly of multi-layer DNA objects. *Nat Commun* **3**, 1103 (2012).

[37] Ke, Y. *et al.* Multilayer DNA Origami Packed on a Square Lattice. *J. Am. Chem. Soc.* **131**, 15903–15908 (2009).

[38] Kube, M. *et al.* Revealing the structures of megadalton-scale DNA complexes with nucleotide resolution. *Nat Commun* **11**, 6229 (2020).

[39] Dietz, H., Douglas, S. M. & Shih, W. M. Folding DNA into Twisted and Curved Nanoscale Shapes. *Science* **325**, 725–730 (2009).

[40] Gerling, T., Wagenbauer, K. F., Neuner, A. M. & Dietz, H. Dynamic DNA devices and assemblies formed by shape-complementary, non–base pairing 3D components. *Science* **347**, 1446–1452 (2015).

[41] Kool, E. T. Hydrogen Bonding, Base Stacking, and Steric Effects in DNA Replication. *Annual Review of Biophysics and Biomolecular Structure* **30**, 1–22 (2001).

[42] Yakovchuk, P., Protozanova, E. & Frank-Kamenetskii, M. D. Base-stacking and base-pairing contributions into thermal stability of the DNA double helix. *Nucleic Acids Res* **34**, 564–574 (2006).

[43] Lekkerkerker, H. N. W., Tuinier, R. & Vis, M. Introduction. In Lekkerkerker, H. N., Tuinier, R. & Vis, M. (eds.) *Colloids and the Depletion Interaction*, 1–65 (Springer International Publishing, Cham, 2024).

[44] Electrostatic Forces between Surfaces in Liquids. In Israelachvili, J. N. (ed.) *Intermolecular and Surface Forces (Third Edition)*, iii (Academic Press, San Diego, 2011).

[45] Agmo Hernández, V. An overview of surface forces and the DLVO theory. *ChemTexts* **9**, 10 (2023).

[46] Wagenbauer, K. F., Sigl, C. & Dietz, H. Gigadalton-scale shape-programmable DNA assemblies. *Nature* **552**, 78–83 (2017).

[47] Sigl, C. *et al.* Programmable icosahedral shell system for virus trapping. *Nat. Mater.* **20**, 1281–1289 (2021).

[48] Langecker, M., Arnaut, V., List, J. & Simmel, F. C. DNA Nanostructures Interacting with Lipid Bilayer Membranes. *Acc. Chem. Res.* **47**, 1807–1815 (2014).

[49] Khmelinskaia, A., Mücksch, J., Petrov, E. P., Franquelim, H. G. & Schwille, P. Control of Membrane Binding and Diffusion of Cholesteryl-Modified DNA Origami Nanostructures by DNA Spacers. *Langmuir* **34**, 14921–14931 (2018).

[50] Kocabey, S. *et al.* Membrane-Assisted Growth of DNA Origami Nanostructure Arrays. *ACS Nano* **9**, 3530–3539 (2015).

[51] Singer, S. J. & Nicolson, G. L. The Fluid Mosaic Model of the Structure of Cell Membranes. *Science* **175**, 720–731 (1972).

[52] Baumann, K. N. *et al.* Coating and Stabilization of Liposomes by Clathrin-Inspired DNA Self-Assembly. *ACS Nano* **14**, 2316–2323 (2020).

[53] Franquelim, H. G., Khmelinskaia, A., Sobczak, J.-P., Dietz, H. & Schwille, P. Membrane sculpting by curved DNA origami scaffolds. *Nat Commun* **9**, 811 (2018).

[54] Grome, M. W., Zhang, Z., Pincet, F. & Lin, C. Vesicle Tubulation with Self-Assembling DNA Nanosprings. *Angewandte Chemie International Edition* **57**, 5330–5334 (2018).

[55] Liu, L., Xiong, Q., Xie, C., Pincet, F. & Lin, C. Actuating tension-loaded DNA clamps drives membrane tubulation. *Science Advances* **8**, eadd1830 (2022).

[56] Burns, J. R., Seifert, A., Fertig, N. & Howorka, S. A biomimetic DNA-based channel for the ligand-controlled transport of charged molecular cargo across a biological membrane. *Nature Nanotech* **11**, 152–156 (2016).

[57] Burns, J. R. *et al.* Lipid-Bilayer-Spanning DNA Nanopores with a Bifunctional Porphyrin Anchor. *Angewandte Chemie International Edition* **52**, 12069–12072 (2013).

[58] Burns, J. R., Stulz, E. & Howorka, S. Self-Assembled DNA Nanopores That Span Lipid Bilayers. *Nano Lett.* **13**, 2351–2356 (2013).

[59] Diederichs, T. *et al.* Synthetic protein-conductive membrane nanopores built with DNA. *Nat Commun* **10**, 5018 (2019).

[60] Göpfrich, K. *et al.* DNA-Tile Structures Induce Ionic Currents through Lipid Membranes. *Nano Lett.* **15**, 3134–3138 (2015).

[61] Krishnan, S. *et al.* Molecular transport through large-diameter DNA nanopores. *Nat Commun* **7**, 12787 (2016).

[62] Langecker, M. *et al.* Synthetic lipid membrane channels formed by designed DNA nanostructures. *Science* **338**, 932–936 (2012).

[63] Thomsen, R. P. *et al.* A large size-selective DNA nanopore with sensing applications. *Nat Commun* **10**, 5655 (2019).

[64] Xing, Y., Dorey, A., Jayasinghe, L. & Howorka, S. Highly shape- and size-tunable membrane nanopores made with DNA. *Nat. Nanotechnol.* **17**, 708–713 (2022).

[65] Fragasso, A. *et al.* Reconstitution of Ultrawide DNA Origami Pores in Liposomes for Transmembrane Transport of Macromolecules. *ACS Nano* **15**, 12768–12779 (2021).

[66] Ohmann, A. *et al.* A synthetic enzyme built from DNA flips 107 lipids per second in biological membranes. *Nat Commun* **9**, 2426 (2018).

[67] Perrault, S. D. & Shih, W. M. Virus-Inspired Membrane Encapsulation of DNA Nanostructures To Achieve In Vivo Stability. *ACS Nano* **8**, 5132–5140 (2014).

[68] Dong, Y. *et al.* Cuboid Vesicles Formed by Frame-Guided Assembly on DNA Origami Scaffolds. *Angewandte Chemie International Edition* **56**, 1586–1589 (2017).

[69] Xu, W. *et al.* A Programmable DNA Origami Platform to Organize SNAREs for Membrane Fusion. *J. Am. Chem. Soc.* **138**, 4439–4447 (2016).

[70] Williams, D. B. & Carter, C. B. *Transmission Electron Microscopy* (Springer US, Boston, MA, 2009).

[71] Broglie, L. D. Recherches sur la théorie des Quanta. *Ann. Phys.* **10**, 22–128 (1925).

[72] Douglas, S. M. *et al.* Rapid prototyping of 3D DNA-origami shapes with caDNAno. *Nucleic Acids Res* **37**, 5001–5006 (2009).

[73] Castro, C. E. *et al.* A primer to scaffolded DNA origami. *Nat Methods* **8**, 221–229 (2011).

[74] Kim, D.-N., Kilchherr, F., Dietz, H. & Bathe, M. Quantitative prediction of 3D solution shape and flexibility of nucleic acid nanostructures. *Nucleic Acids Res* **40**, 2862–2868 (2012).

[75] Robson, A.-L. *et al.* Advantages and Limitations of Current Imaging Techniques for Characterizing Liposome Morphology. *Front Pharmacol* **9**, 80 (2018).

[76] Adrian, M., Dubochet, J., Lepault, J. & McDowall, A. W. Cryo-electron microscopy of viruses. *Nature* **308**, 32–36 (1984).

[77] Brüggeller, P. & Mayer, E. Complete vitrification in pure liquid water and dilute aqueous solutions. *Nature* **288**, 569–571 (1980).

[78] Bhella, D. Cryo-electron microscopy: An introduction to the technique, and considerations when working to establish a national facility. *Biophys Rev* **11**, 515–519 (2019).

[79] Xiao, C. *et al.* Cryo-electron Microscopy of the Giant Mimivirus. *Journal of Molecular Biology* **353**, 493–496 (2005).

[80] Hassinger, J. E., Oster, G., Drubin, D. G. & Rangamani, P. Design principles for robust vesiculation in clathrin-mediated endocytosis. *Proceedings of the National Academy of Sciences* **114**, E1118–E1127 (2017).

[81] Kirchhausen, T. Three ways to make a vesicle. *Nat Rev Mol Cell Biol* **1**, 187–198 (2000).

[82] Lee, C. & Goldberg, J. Structure of Coatomer Cage Proteins and the Relationship among COPI, COPII, and Clathrin Vesicle Coats. *Cell* **142**, 123–132 (2010).

[83] Dodonova, S. O. *et al.* A structure of the COPI coat and the role of coat proteins in membrane vesicle assembly. *Science* **349**, 195–198 (2015).

[84] Fath, S., Mancias, J. D., Bi, X. & Goldberg, J. Structure and Organization of Coat Proteins in the COPII Cage. *Cell* **129**, 1325–1336 (2007).

[85] Saleem, M. *et al.* A balance between membrane elasticity and polymerization energy sets the shape of spherical clathrin coats. *Nat Commun* **6**, 6249 (2015).

[86] Ogunkoya, Y., Nickel, BM., Gay, VL. & Murray, SA. Using quantum dots to visualize clathrin associations. *Biotechnic & Histochemistry* **84**, 109–115 (2009).

[87] Stoorvogel, W., Oorschot, V. & Geuze, H. J. A novel class of clathrin-coated vesicles budding from endosomes. *Journal of Cell Biology* **132**, 21–33 (1996).

[88] Boucrot, E. *et al.* Membrane Fission Is Promoted by Insertion of Amphipathic Helices and Is Restricted by Crescent BAR Domains. *Cell* **149**, 124–136 (2012).

[89] Rossman, J. S., Jing, X., Leser, G. P. & Lamb, R. A. Influenza Virus M2 Protein Mediates ESCRT-Independent Membrane Scission. *Cell* **142**, 902–913 (2010).

[90] List, J., Weber, M. & Simmel, F. C. Hydrophobic Actuation of a DNA Origami Bilayer Structure. *Angewandte Chemie International Edition* **53**, 4236–4239 (2014).

[91] Roth, E., Glick Azaria, A., Girshevitz, O., Bitler, A. & Garini, Y. Measuring the Conformation and Persistence Length of Single-Stranded DNA Using a DNA Origami Structure. *Nano Lett.* **18**, 6703–6709 (2018).

[92] Shon, M. J., Rah, S.-H. & Yoon, T.-Y. Submicrometer elasticity of double-stranded DNA revealed by precision force-extension measurements with magnetic tweezers. *Science Advances* **5**, eaav1697 (2019).

[93] Patist, A., Bhagwat, S. S., Penfield, K. W., Aikens, P. & Shah, D. O. On the measurement of critical micelle concentrations of pure and technical-grade nonionic surfactants. *J Surfact Deterg* **3**, 53–58 (2000).

[94] Kameyama, K. & Takagi, T. Micellar properties of octylglucoside in aqueous solutions. *Journal of Colloid and Interface Science* **137**, 1–10 (1990).

[95] Haberland, M. E. & Reynolds, J. A. Self-association of Cholesterol in Aqueous Solution. *Proc Natl Acad Sci U S A* **70**, 2313–2316 (1973).

[96] Heerklotz, H. Interactions of surfactants with lipid membranes. *Quarterly Reviews of Biophysics* **41**, 205–264 (2008).

[97] Fischer, S. *et al.* Shape and inter-helical spacing of DNA origami nanostructures studied by small angle X-ray scattering. *Nano Lett* **16**, 4282–4287 (2016).

[98] Charmainne, C. & Chithrani, D. B. Polyethylene Glycol Density and Length Affects Nanoparticle Uptake by Cancer Cells. *Journal of Nanomedicine Research* **Volume 1** (2014).

[99] Ohmann, A. *et al.* Controlling aggregation of cholesterol-modified DNA nanostructures. *Nucleic Acids Res* **47**, 11441–11451 (2019).

[100] Morzy, D. *et al.* Cations Regulate Membrane Attachment and Functionality of DNA Nanostructures. *J Am Chem Soc* **143**, 7358–7367 (2021).

[101] Pfeiffer, I. & Höök, F. Bivalent Cholesterol-Based Coupling of Oligonucletides to Lipid Membrane Assemblies. *J. Am. Chem. Soc.* **126**, 10224–10225 (2004).

[102] McMahon, H. T. & Gallop, J. L. Membrane curvature and mechanisms of dynamic cell membrane remodelling. *Nature* **438**, 590–596 (2005).

[103] Helfrich, W. Elastic properties of lipid bilayers: Theory and possible experiments. *Z Naturforsch C* **28**, 693–703 (1973).

[104] Campelo, F., Arnarez, C., Marrink, S. J. & Kozlov, M. M. Helfrich model of membrane bending: From Gibbs theory of liquid interfaces to membranes as thick anisotropic elastic layers. *Advances in Colloid and Interface Science* **208**, 25–33 (2014).

[105] Hurley, J. H., Boura, E., Carlson, L.-A. & Różycki, B. Membrane Budding. *Cell* **143**, 875–887 (2010).

[106] Stachowiak, J. C., Brodsky, F. M. & Miller, E. A. A cost-benefit analysis of the physical mechanisms of membrane curvature. *Nat Cell Biol* **15**, 10.1038/ncb2832 (2013).

[107] Kilchherr, F. *et al.* Single-molecule dissection of stacking forces in DNA. *Science* **353**, aaf5508 (2016).

[108] Protozanova, E., Yakovchuk, P. & Frank-Kamenetskii, M. D. Stacked–Unstacked Equilibrium at the Nick Site of DNA. *Journal of Molecular Biology* **342**, 775–785 (2004).

[109] Bhella, D. Cryo-electron microscopy: An introduction to the technique, and considerations when working to establish a national facility. *Biophys Rev* **11**, 515–519 (2019).

[110] Boulant, S., Kural, C., Zeeh, J.-C., Ubelmann, F. & Kirchhausen, T. Actin dynamics counteract membrane tension during clathrin-mediated endocytosis. *Nat Cell Biol* **13**, 1124–1131 (2011).

[111] Malek, A. M., Goss, G. G., Jiang, L., Izumo, S. & Alper, S. L. Mannitol at Clinical Concentrations Activates Multiple Signaling Pathways and Induces Apoptosis in Endothelial Cells. *Stroke* **29**, 2631–2640 (1998).

[112] Yamabe, S., Ono, N. & Tsuchida, N. Molecular Interactions between Glycine and H2O Affording the Zwitterion. *J. Phys. Chem. A* **107**, 7915–7922 (2003).

[113] Singh, J. K. D. *et al.* Binding of DNA origami to lipids: Maximizing yield and switching via strand displacement. *Nucleic Acids Res* **49**, 10835–10850 (2021).

[114] Svetina, S. & Žekš, B. Membrane bending energy and shape determination of phospholipid vesicles and red blood cells. *Eur Biophys J* **17**, 101–111 (1989).

[115] Markvoort, A. J. *et al.* Vesicle Deformation by Draining: Geometrical and Topological Shape Changes. *J. Phys. Chem. B* **113**, 8731–8737 (2009).

[116] Alwarawrah, M., Dai, J. & Huang, J. A Molecular View of the Cholesterol Condensing Effect in DOPC Lipid Bilayers. *J Phys Chem B* **114**, 7516–7523 (2010).

[117] Beck, J. S. Relations between membrane monolayers in some red cell shape transformations. *Journal of Theoretical Biology* **75**, 487–501 (1978).

[118] General, I. J., Dragomirova, R. & Meirovitch, H. The Absolute Free Energy of Binding of Avidin/Biotin Revisited. *J Phys Chem B* **116**, 6628–6636 (2012).

[119] Chakraborty, S. *et al.* How cholesterol stiffens unsaturated lipid membranes. *Proceedings of the National Academy of Sciences* **117**, 21896–21905 (2020).

[120] Johnson, D. H., Kou, O. H., Bouzos, N. & Zeno, W. F. Protein–membrane interactions: Sensing and generating curvature. *Trends in Biochemical Sciences* **49**, 401–416 (2024).

[121] Doktorova, M., Harries, D. & Khelashvili, G. Determination of bending rigidity and tilt modulus of lipid membranes from real-space fluctuation analysis of molecular dynamics simulations. *Phys Chem Chem Phys* **19**, 16806–16818 (2017).

[122] Janmey, P. A. & Kinnunen, P. K. J. Biophysical properties of lipids and dynamic membranes. *Trends in Cell Biology* **16**, 538–546 (2006).

[123] Koynova, R. & Tenchov, B. Lipids: Phase Transitions. In *Wiley Encyclopedia of Chemical Biology*, 1–15 (John Wiley & Sons, Ltd, 2008).

[124] Dimova, R. Recent developments in the field of bending rigidity measurements on membranes. *Advances in Colloid and Interface Science* **208**, 225–234 (2014).

[125] Subczynski, W. K., Pasenkiewicz-Gierula, M., Widomska, J., Mainali, L. & Raguz, M. High Cholesterol/Low Cholesterol: Effects in Biological Membranes: A Review. *Cell Biochem Biophys* **75**, 369–385 (2017).

[126] Baumgart, T., Hess, S. T. & Webb, W. W. Imaging coexisting fluid domains in biomembrane models coupling curvature and line tension. *Nature* **425**, 821–824 (2003).

[127] Cooke, I. R. & Deserno, M. Coupling between Lipid Shape and Membrane Curvature. *Biophysical Journal* **91**, 487–495 (2006).

[128] Veatch, S. L. & Keller, S. L. Separation of Liquid Phases in Giant Vesicles of Ternary Mixtures of Phospholipids and Cholesterol. *Biophysical Journal* **85**, 3074–3083 (2003).

[129] Jülicher, F. & Lipowsky, R. Domain-induced budding of vesicles. *Phys. Rev. Lett.* **70**, 2964–2967 (1993).

[130] Banerjee, A., Berezhkovskii, A. & Nossal, R. Kinetics of cellular uptake of viruses and nanoparticles via clathrin-mediated endocytosis. *Phys Biol* **13**, 016005 (2016).

[131] Li, Y. *et al.* Dynamic Dissection of the Endocytosis of Porcine Epidemic Diarrhea Coronavirus Cooperatively Mediated by Clathrin and Caveolae as Visualized by Single-Virus Tracking. *mBio* **12**, e00256–21 (2021).

[132] Puthenveedu, M. A. & von Zastrow, M. Cargo Regulates Clathrin-Coated Pit Dynamics. *Cell* **127**, 113–124 (2006).

[133] Perrier, D. L., Rems, L. & Boukany, P. E. Lipid vesicles in pulsed electric fields: Fundamental principles of the membrane response and its biomedical applications. *Advances in Colloid and Interface Science* **249**, 248–271 (2017).

[134] Zhan, P. *et al.* 3D DNA origami pincers that multitask on giant unilamellar vesicles. *Science Advances* **10**, eadn8903 (2024).

[135] Rangamani, P., Mandadap, K. K. & Oster, G. Protein-Induced Membrane Curvature Alters Local Membrane Tension. *Biophys J* **107**, 751–762 (2014).

[136] Corin, K. & Bowie, J. U. How bilayer properties influence membrane protein folding. *Protein Sci* **29**, 2348–2362 (2020).

[137] Hamai, C., Yang, T., Kataoka, S., Cremer, P. S. & Musser, S. M. Effect of Average Phospholipid Curvature on Supported Bilayer Formation on Glass by Vesicle Fusion. *Biophys J* **90**, 1241–1248 (2006).

[138] Bai, X.-c., Martin, T. G., Scheres, S. H. W. & Dietz, H. Cryo-EM structure of a 3D DNA-origami object. *Proceedings of the National Academy of Sciences* **109**, 20012–20017 (2012).

[139] Ridker, P. M. LDL cholesterol: Controversies and future therapeutic directions. *The Lancet* **384**, 607–617 (2014).

[140] Jiang, D. *et al.* DNA origami nanostructures can exhibit preferential renal uptake and alleviate acute kidney injury. *Nat Biomed Eng* **2**, 865–877 (2018).

[141] Wang, P. *et al.* Visualization of the Cellular Uptake and Trafficking of DNA Origami Nanostructures in Cancer Cells. *J Am Chem Soc* **140**, 2478–2484 (2018).

[142] Mrksich, K., Padilla, M. S. & Mitchell, M. J. Breaking the final barrier: Evolution of cationic and ionizable lipid structure in lipid nanoparticles to escape the endosome. *Advanced Drug Delivery Reviews* **214**, 115446 (2024).

[143] Schlich, M. *et al.* Cytosolic delivery of nucleic acids: The case of ionizable lipid nanoparticles. *Bioeng Transl Med* **6**, e10213 (2021).

[144] Park, J. H. *et al.* Temperature-Induced Denaturation of BSA Protein Molecules for Improved Surface Passivation Coatings. *ACS Appl. Mater. Interfaces* **10**, 32047–32057 (2018).

[145] Schindelin, J. *et al.* Fiji: An open-source platform for biological-image analysis. *Nat Methods* **9**, 676–682 (2012).

[146] Kremer, J. R., Mastronarde, D. N. & McIntosh, J. R. Computer Visualization of Three-Dimensional Image Data Using IMOD. *Journal of Structural Biology* **116**, 71–76 (1996).

Appendix C

Acknowledgements

My PhD journey was one hell of a ride – as it should be! It's a bit of a cliché, but the many ups and downs are what finally shaped me to become the scientist I am today. Of course, I mainly mention successful experiments in this thesis, but as every other scientist will know it is the many failed experiments that paved my path – and alongside this path, I have met many fantastic individuals.
I would like to thank all the colleagues at the Dietz lab who have supported me over the years. Be it stimulating discussions or just fun hours enjoying a drink after work: Without you guys, this journey would have been really lonely. It is an honour to work alongside you.

Hendrik: Thank you for your continuous support over the years. You established an atmosphere where everyone can follow their curiosity with nearly no restrictions and seemingly bottomless funds. Many of the struggles other students are facing are unknown in your lab, and I really am grateful for that.

Vova: When I was stressing out before my first conference talk in Rome, you spent your evening making me illustrations that I am using to this day. Thank you for always helping me out whenever I needed something, be it inside or outside the lab. You were my first friend in the lab, and you've been a great friend ever since.

Sam: I have never worked as closely with someone as I have with you, and when you're around, even long evenings in the lab are really fun! With you I've had some of the best brainstorming sessions (and shit talk) of my PhD. Whether it's proofreading my (entire) dissertation, or calming my nerves when reviewer comments felt overwhelming: When it matters, I know I can count on you. Thank you for being as great a coworker as you are a friend!

Throughout my PhD, I also got to work with a lot of talented students who have helped test me a lot of crazy ideas. Thank you for your hard work and for dealing with my chaotic work style: *Hannah, Daniel, Ken, Viktorija, Anastassiya, Alvaro, Nathalie, Paul.*

I have been lucky to be a member of the Marie Curie ITN 'DNA Robotics', through which I got to meet many fantastic individuals. Thank you guys for all the fun times! I am happy that even years after the ITN has ended, we still bump into each other at conferences around the world.

Finally, I would like to thank the special people in my life without whose support living through the challenges of academic research would not have been possible.

Fabi: You've been the foundation of my life for over 11 years now. No matter what, you've always had my back and patiently listened even if I complained about the same challenges over and over again. Thank you for always being there for me.

Zu guter Letzt möchte ich meiner Mutter *Krystyn*a danken. Nach Jahren im Ausland weiß ich: Deine Wärme kennt keine Grenzen. Ohne dich wäre ich nicht hier.